TRACTION MOTOR DRIVE FOR DIESEL LOCOMOTIVE

A Project Report

submitted by

HARIKRISHNAN P

in partial fulfillment of the requirements

for the award of the degree of

MASTER OF TECHNOLOGY

DEPARTMENT OF ELECTRICAL ENGINEERING

INDIAN INSTITUTE OF TECHNOLOGY MADRAS

THESIS CERTIFICATE

This is to certify that the thesis titled **TRACTION MOTOR DRIVE FOR DIESEL LOCOMOTIVE**, submitted by **HARIKRISHNAN P**, to the Indian Institute of Technology Madras, for the award of the degree of **Master of Technology**, is a bona fide record of the project work done by him under my supervision. The contents of this thesis, in full or in parts, have not been submitted to any other Institute or University for the award of any degree or diploma.

Dr. Kamalesh Hatua
(Project Guide)
Asst.Professor
Department of Electrical Engineering
IIT-Madras,600 036

Place: Chennai
Date:

ACKNOWLEDGEMENTS

I feel a great pleasure in expressing my sincere thanks to Dr.Kamalesh Hatua who give me a chance to work under his able guidance. His dedication and keen interest and above all his overwhelming attitude to help his students had been solely and mainly responsible for completing my work. I consider it as an invaluable learning opportunity to work on this exciting project under his guidance.

I am grateful to Dr. Krishna Vasudevan for his excellent lectures on Advanced Motor Control which helped me to understand the subject with good clarity.

I am very thankful to Mr. Jose Titus, for his valuable support during my project. His help was very crucial in solving many problems that I encountered. I am very grateful for the support that I got from my friends Mr. Arun Chithrabhanu and Mr. Sandeep V Nair in discussing about the project.

I would like to express my gratitude to Vamshi Krishna, Aloka Mohapatra, Yash Sukhatme, Veera Balaji , Deepthi Sivadas, Prathibha, Manik Pradhan and Saranya for their continuous support and technical suggestions. I would also extend my thanks to all my M.Tech batch mates for their support during my work.

This work could not have come to this stage without the support and encouragement from my family and friends. My heartfelt thanks to all of them.

Finally I take this opportunity to express my regards to all the teachers in my life.

ABSTRACT

KEYWORDS: Field Oriented Control; Field weakening scheme; Overmodulation

The Field Oriented Control (FOC) of induction machine is a control scheme which enables independent control of torque and speed, similar to that of a DC machine. In FOC based induction machine drive, the operation above base speed is achieved by reducing the flux component of the current. The maximum torque capability of the drive reduces as the speed increases beyond the base speed. In field weakening regions, the developed torque capability of the induction machine mainly depends on control strategy. So the control strategy must ensure that the maximum torque generation is possible in the entire field weakening region.

The PWM signals to the switches of the inverter are generated using space vector modulation. In lower speed operation of the drive, inverter will be operating in the linear region. At higher speeds, in order to maximize the DC- bus utilisation, the inverter should be operated in the overmodulation region. The control algorithm for overmodulation is designed to ensure the linearity between the reference voltage and the output fundamental voltage. A fundamental current estimation algorithm is used for improving the performance of the drive during overmodulation.

The main focus of this project is towards implementing an induction machine drive suitable for traction application. High inertia is the main feature of traction drive, so the required torque during starting is much higher that the steady state full load torque. So an induction machine drive with field weakening scheme is preferred choice for high speed applications.

The simulation studies are done for a 630 kW machine using MATLAB/SIMULINK to verify the control algorithm for field weakening operation and SVPWM based overmodulation scheme of the drive. The TMS320F28335 based DSP board is used for implementing the control algorithm in hardware test set-up. The field weakening algorithm is experimentally validated on a laboratory model of 30 kW induction machine.

TABLE OF CONTENTS

LIST OF TABLES

LIST OF FIGURES

ABBREVIATIONS

FOC	Field Oriented Control
PI	Proportional and Integral
DC	Direct Current
CCS	Code Composer Studio
VSI	Voltage Source Inverter
PWM	Pulse Width Modulation
SVPWM	Space Vector Pulse Width Modulation
PD	Protection and Delay
IM	Induction Motor

NOTATIONS

v_a, v_b, v_c	Instantaneous stator voltages in *abc* frame, *V*
$v_{s\alpha}, v_{s\beta}$	Instantaneous stator voltages in $\alpha\beta$ frame, *V*
v_{sd}, v_{sq}	Instantaneous stator voltages in *dq* frame, *V*
i_a, i_b, i_c	Instantaneous stator current in *abc* frame, *V*
$i_{s\alpha}, i_{s\beta}$	Instantaneous stator currents in $\alpha\beta$ frame, *A*
i_{sd}, i_{sq}	Instantaneous stator currents in *dq* frame, *A*
V_{max}	Maximum stator voltage vector in stationary reference frame, *V*
I_{max}	Maximum stator current vector in stationary reference frame, *A*
L_s	Stator inductance, *H*
L_r	Rotor inductance, *H*
L_m	Magnetising inductance, *H*
L_{ls}	Stator leakage inductance, *H*
L_{lr}	Rotor leakage inductance, *H*
R_s	Stator resistance, Ω
R_r	Rotor resistance, Ω
τ_r	Rotor time constant, *s*
V_{dc}	Inverter DC bus voltage, *V*
ω_e	Rotor flux speed, $elect.rad/s$
θ	Position of rotor flux phasor, *rad*
i^*_{mr}	Rated rotor magnetising current, *A*
ω^*	Reference speed, rad/s
ω_{base}	Base speed, $elect.rad/s$
ω_1	Transition speed between field weakening regions, $elect.rad/s$
K_t	Torque constant , Nm/A^2
T_g	Generated torque, *Nm*
V_{ref}	Reference voltage space vector, *V*
V_p	Applied voltage space vector, *V*
T_s	Sampling time, *s*
σ	Total leakage factor
σ_s	Stator leakage factor
σ_r	Rotor leakage factor

CHAPTER 1

INTRODUCTION

DC motors were widely used for variable speed drive applications in industry owing to simple speed control algorithm and fairly good dynamic response over wide speed range. The flux producing current and the torque producing current exist mutually orthogonal in two separate windings in a DC machine. Because of this arrangement flux and torque can be independently controlled making the speed control of DC machine fairly simple over wide speed ranges. This advantage is not available in an induction machine drive, where there is only a three phase winding supplied by a three phase source. Field Oriented Control (FOC) of induction machine is a control methodology which enable the induction machine be controlled like a DC machine. In FOC of induction machine, the flux producing component and the torque producing component are identified and controlled separately. This is achieved by transforming the instantaneous stator currents to a rotating frame of reference aligned with the rotor flux axis (Rotor flux oriented FOC). The direction along the rotor flux is taken as d-axis and the direction in quadrature to the rotor flux taken as q-axis. The development of field oriented control makes the induction machine drives a preferable choice in industry for high performance applications like traction drive.

A traction drive system is used for the propulsion of vehicles, in which the driving force is obtained from various drives such as diesel engine drives, steam engine drives, electrical motors etc. The traction system is generally classified as non electric and electric system. The non electric traction system does not use electrical energy for the movement of vehicle at any stage. The steam engine drive and the IC engine drive come under this catagory . The electric traction involves the use of electricity at some stages or all the stages of locomotive movement. Straight electric drives, diesel electric and battery operated electric vehicle are typical examples of electric drive system. The electric traction system offers several benefits over other systems, including quick start and stop, high efficiency, pollution free operation and simple speed control. Due to these features, the electric traction system become the best choice for traction drives.

Control of an electric motor in a wide speed range is very important in traction application. Traction system has very large inertia, so the torque required during acceleration is much higher than the torque required during steady state rated speed operation. So it is preferred to use a smaller power rating motor which accelerates at limited constant power level, employing field weakening scheme. The field- oriented induction machine drive is a good choice for this application since the field of the machine is controlled easily by controlling the flux component current at higher speed.

The main focus of this project is towards the development of an induction motor drive for traction application. The power structure of a traction drive is shown in Fig. 1.1. A diesel engine is used to drive the prime mover whose excitation is separately controlled by an exciter. The alternator output is fed to a diode bridge rectifier which provides the required DC-link voltage for VSI. The DC-link voltage is controlled by controlling the excitation system of the alternator. This project mainly focuses on controlling the VSI to drive the induction machine above the base speed through field weakening. Since the system has a limited DC bus, in order to completely utilize the available DC-link voltage, overmodulation scheme is used.

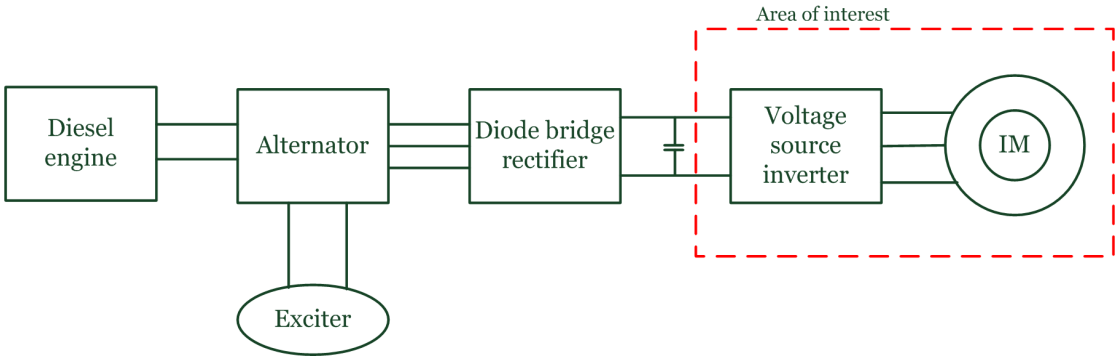

Figure 1.1: Power structure of traction drive

Field weakening

The maximum current flow through the stator winding of an induction machine drive is limited by the thermal rating of the machine and the current rating of inverter switches. The maximum voltage that can be applied to machine is limited by the class of insulation provided and the available DC-link voltage of VSI. For an induction machine drive running at low speeds, the voltage applied to the machine from the VSI will also be low.

As the speed of the machine increases, the machine demands more voltage to reach the required speed. Similarly the current flowing through the winding depends on the load condition of the machine. At light load conditions, the current flowing will be small and as the load increases, current will also increases. At the base speed of the machine, if rated load is applied, the applied voltage to the machine and the current flowing through the winding of the machine will be at maximum allowable values. The machine generate maximum possible torque at this operating condition. For the speed variation from zero to base speed, the flux of the machine is left at rated value. In Field Oriented Control (FOC) of induction machine, this is achieved by keeping the flux component of the current (i_{mr}) constant in below the base speed region. The q-axis current will depends on the load on the machine and the machine can operate from no load to rated load in this speed range.

In the DC machine, operation above the base speed is achieved by reducing the flux of the machine. Similarly in FOC based induction machine drive, the flux component of the current (i_{mr}) is reduced in order to achieve above base speed operation. In the field weakening region, it should be ensured that the voltage applied to the machine and the current flowing through the winding of the machine are within the rated value of the machine. Since the flux of the machine is reducing, the maximum torque capability will also reduces as the speed increases beyond the base speed. In the field weakening region the developed torque capability of the induction machine mainly depends on the control strategy. Therefore it is desirable to use a control scheme considering the voltage and current limit conditions, which can yield the maximum torque over the entire speed range.

In conventional field weakening method, the rotor flux reference of the machine varies inversely with respect to the speed of the machine . The voltage limit and the current limit constraints are not considered in conventional field weakening, so it is impossible to obtain the maximum possible developed torque by this method. A field weakening approach considering both the voltage limit constraint and the current limit constraint, ensuring maximum possible developed torque in the entire speed range is presented in [1].

Based on the speed of the induction machine drive, the whole operating range can be divided in to three regions as specified below.

- *Below base speed region*
- *Field weakening region I*
- *Field weakening region II*

In *Below base speed region*, the conventional rotor flux oriented vector control is used for speed control. The flux reference is constant in this operating region. In *Field weakening region I*, flux of the machine is reduced considering both the voltage limit constraint and the current limit constraint such that the maximum torque development is possible. As the speed increases further, the operating point depends only on the voltage limit constraint, then the *Field weakening region II* starts. In *Field weakening region II*, the flux of the machine is reduced considering the voltage constraint alone, such that the maximum torque development is possible. The base speed of the machine is a critical parameter in the field weakening operation. The base speed is calculated according to the flux level at rated condition and the voltage and current limits. Any miscalculation of base speed will lead to undesired drop in the developed torque.

Linear and overmodulation PWM scheme

The basic function of any pulse width modulation approach, is to generate the 3 phase stator voltages of required fundamental amplitude and frequency for driving the motor. At low speed operation, since the applied voltage is low, the inverter is operated in its linear modulation region. In this region the line side fundamental voltage is proportional to the reference voltage. The number of switchings per fundamental period is constant in the linear operating region. As the speed of the machine increases, the required fundamental amplitude and frequency increases. From a particular value of fundamental voltage onwards it become impossible to maintain the linearity between the reference voltage and the output voltage, which forces the VSI to operate in overmodulation zone. In overmodulation region the number of switchings per fundamental period will decrease and the DC-bus utilisation increases as the fundamental reference increases. If the reference voltage increases further, the VSI will finally enter into the six step operating mode where the highest possible line side voltage can be generated from a given DC bus voltage (V_{dc}). At the six step mode of operation the inverter

switches only 6 times per fundamental time period, so the switching loss will be very less.

The major problem with overmodulation is that the non-linearity in output voltage will cause flow of higher order harmonic rich currents in the machine, since the inverter moves to overmodulation zone at that speed. Stator and rotor leakage inductance controls the harmonic current flow at higher speed. They are relatively higher in magnitude at higher frequency of operation. Hence during high speed operation of the drive, the inverter is operated at six step mode so that maximum DC- link utilisation is possible.

The linearity between the average value of reference voltage and the output voltage is lost in overmodulation region of operation. Therefore a proper compensation algorithm must be used in overmodulation zones to achieve linearity. Based on this compensation algorithm Overmodulation region is classified as given below

- *Overmodulation region I*
- *Overmodulation region II*
- *Six step mode*

At *six step mode* of operation, DC-bus utilisation is maximum and switching losses are minimum. So at a higher speeds of operation, six step mode of operation is preferred.

PWM output voltage will be a pure sine wave if switching frequency is very high and inverter operates in linear modulation. In overmodulation region, since switching frequency is low and the inverter operates in non-linear region of modulation, actual PWM output voltage will have considerable harmonics which will produce larger harmonic current. This distorted current has to be used by the speed estimation block and the current controller. The harmonic current corrupts the actual rotor position information which is essential for rotor flux oriented FOC based induction machine drive. So the system has a very high risk of instability. So the estimation of lower order current ripple is essential in overmodulation region of operation. In this project, lower order current harmonics are estimated to calculate the fundamental component of the current.

Organisation of Thesis

Chapter2 presents a detailed description of field weakening and overmodulation operation with SVPWM in induction machine. The conventional and proposed field weakening methods are compared. The detailed derivation of all the relevant equations in field weakening regions are included in this chapter. Detailed theory of SVPWM in linear modulation and overmodulation zones are also presented. All the equations required for calculation of duty ratios of switches in different modulation zones are derived. The fundamental current estimation algorithm is also explained.

Chapter3 deals with the hardware organisation for the implementation of field weakening method on a 30 kW laboratory prototype. A brief description about Digital Signal Controller (DSC), used for control implementation is included in this chapter. The voltage and current sensors used in the setup and Protection and Delay card (PD card), which act as the interface between the controller and the inverter are also discussed.

Chapter4 discusses the results obtained from the simulation of the 630 kW and 30 kW induction motor drive as well as that from the actual hardware implementation on the 30 kW induction motor.

Chapter5 presents the summary of the work done and the future scope for improving the work.

CHAPTER 2

FIELD WEAKENING AND OVERMODULATION SCHEME

2.1 Introduction

In this chapter the detailed theory of field weakening scheme for a field oriented control based induction machine drive is presented. All the relevant equations for the control are derived and the basic control scheme is presented. The details explanation of linear and overmodulation zone operation of SVPWM inverter is included in this chapter. The control strategy in different operating zones is explained with the diagrams. The fundamental current extraction algorithm is discussed with relevant equations.

2.2 Field Oriented Control of induction machine

The independent control of speed and torque in an induction machine is achieved by separately controlling d-axis component of current (i_{sd}) and q-axis component of current (i_{sq}). The control over torque is achieved by controlling the magnitude of i_{sq}. The rotor flux control is achieved by controlling the magnitude of i_{sd}, which in turn is achieved by controlling the magnitude of flux component of the current (i_{mr}). The structure of a Field Oriented Control based induction machine drive is shown in Fig. 2.1.

The reference value of q-axis current, i^*_{sq} is generated by the torque loop and reference value of d-axis current, i^*_{sd} is generated by the flux loop. The reference values are compared with the actual values and the error values are fed to the respective PI controllers. The d-axis and q-axis current controllers generate the corresponding voltage references, v_{qref} and v_{dref} which are realised using PWM based voltage source inverter. The emf terms, e_{ffd} and e_{ffq} can be fed forward to improve the transient response of i_{sd} and i_{sq}, where e_{ffd} and e_{ffq} are the d-axis fed forward voltage and q-axis fed forward

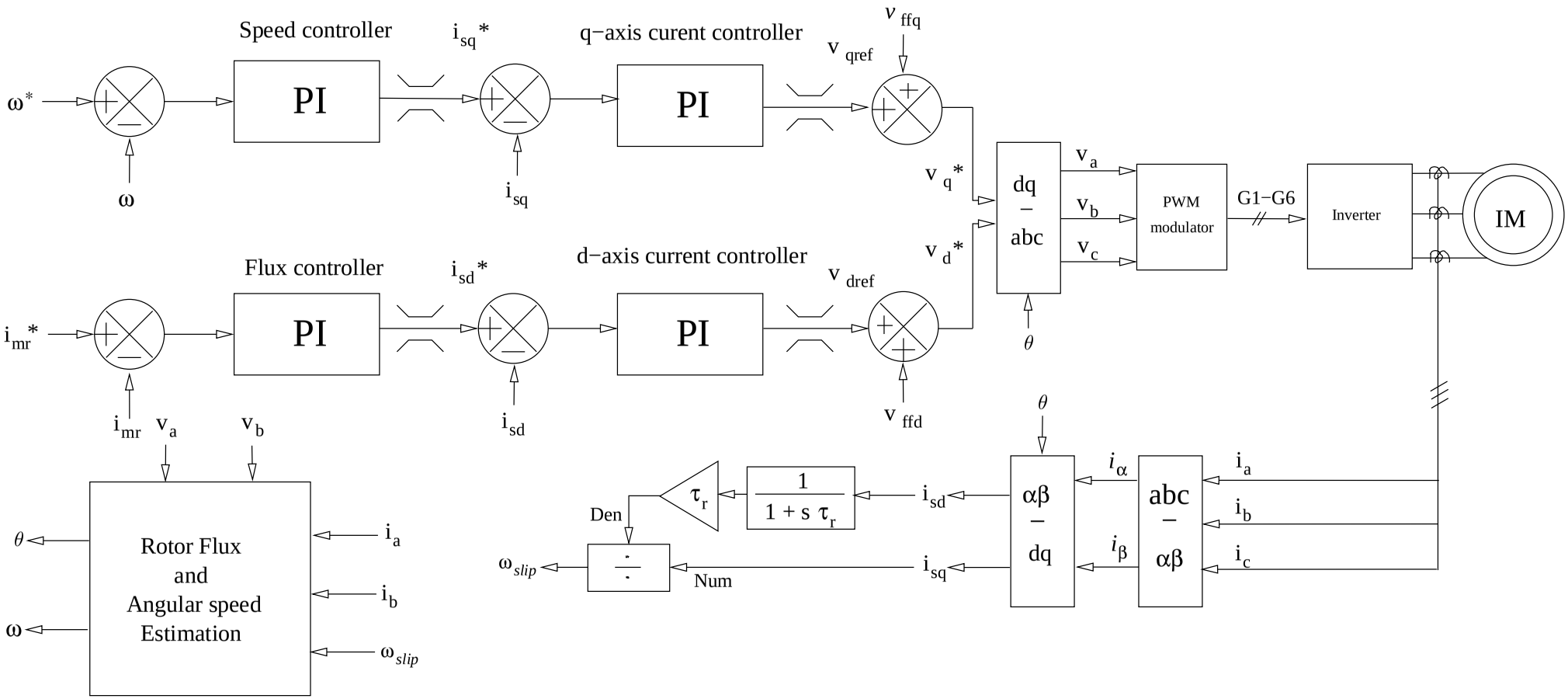

Figure 2.1: Block diagram for FOC based induction machine drive

voltage respectively. The sensed line currents undergo *abc* to $\alpha\beta$ transformation and $\alpha\beta$ to *dq* transformation to obtain the i_{sd} and i_{sq} values. In a sensor less FOC scheme, the speed and the flux position need to be estimated. The angular speed estimation module will estimate these values using feedback line current signals.

2.3 Voltage limit and current limit constraint

The voltage and current limits are critical parameters in the above base speed of operation. The maximum possible voltage that can be applied to an induction machine depends on the class of insulation provided in the machine and the available DC-link voltage. The steady state stator voltage equations of a rotor flux oriented induction machine in d-q frame is given as

$$v_{sd} = R_s i_{sd} - \omega_e L'_s \, i_{sq} \tag{2.1}$$

$$v_{sq} = R_s i_{sq} + \omega_e L_s \, i_{sd} \tag{2.2}$$

where $L'_s = \sigma L_s$ and $\sigma = 1 - \dfrac{L_m^2}{L_s L_r}$

V_{max} is the maximum possible voltage that can be applied to the machine according to the voltage limit constraint.

The safe operation is ensured when v_{sd} and v_{sq} satisfy the following relation in Eq.(2.3)

$$v_{sd}^2 + v_{sq}^2 \leq V_{max}^2 \tag{2.3}$$

If v_{sd} and v_{sq} satisfy this condition, the applied voltage to the machine will be well within the safe limit. In high speed operation, ω_e will be quite high and hence the motional emf terms will be much higher compared to resistive drop.

Then the Eq.(2.1) and Eq.(2.2) can be approximated as

$$v_{sd} = -\omega_e L'_s \, i_{sq} \tag{2.4}$$

$$v_{sq} = \omega_e L_s \, i_{sd} \tag{2.5}$$

Substituting the expression for v_{sd} and v_{sq} from Eq.(2.4) and Eq.(2.5) in the voltage constraint equation, Eq.(2.3)

$$(\omega_e L_s i_{sd})^2 + (\omega_e L'_s i_{sq})^2 \leq V_{max}^2 \tag{2.6}$$

$$\frac{i_{sd}^2}{(\frac{V_{max}}{\omega_e L_s})^2} + \frac{i_{sq}^2}{(\frac{V_{max}}{\omega_e L'_s})^2} \leq 1 \tag{2.7}$$

Where $\sigma < 1$

Fig. 2.2 shows the locus of equation Eq(2.7). Eq.(2.7) is an equation of an ellipse, which is a function of the operating frequency. The major axis of the ellipse is along q-axis since L'_s is less than L_s. The radius of the ellipse becomes smaller and smaller as the operating frequency (ω_e) increases. In order to satisfy the voltage limit constraint, the d-axis current, i_{sd} and q-axis current, i_{sq} should remain inside the voltage limit ellipse. Any point within the voltage limiting ellipse will there be a feasible point of operation considering the voltage limit constraint alone. Since the radius of the ellipse reduces as the frequency increases, the boundary of i_{sd} and i_{sq} reduces with increase in speed. This variation is shown in Fig. 2.2.

The thermal rating of the machine and the inverter current rating determine the maximum stator current I_{max}. Under this limitation, the i_{sd} and i_{sq} are related as

$$i_{sd}^2 + i_{sq}^2 \leq I_{max}^2 \tag{2.8}$$

From Eq.(2.8) the current limiting boundary will be a circle with centre at the origin. Also the current limit is independent of the speed of operation. For satisfying the current constraint i_{sq} and i_{sd} must lie within the current limit circle. All the values of i_{sd} and i_{sq} which are inside the current limit circle are feasible points considering the current limit constraint alone.

While determining the operating point of the machine, both voltage limit boundary and current limit boundary must be considered. Then the feasible operating points will be the overlapping region between the current limit circle and voltage limit ellipse. Since voltage limit ellipse is a function of operating speed, as speed increases the size

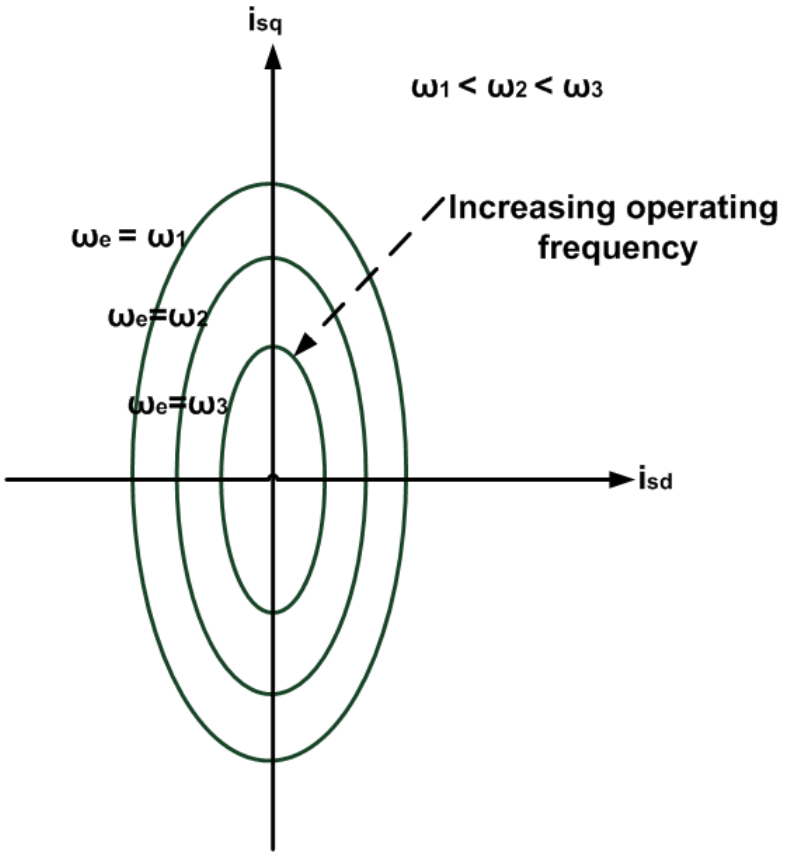

Figure 2.2: Voltage limit boundary at different operating speeds

of the ellipse gradually shrinks as observed from Fig. 2.2. For example the ellipse size at $\omega_e = \omega_3$ is smaller compared to that of $\omega_e = \omega_2$ ($\omega_2 < \omega_3$). Hence the feasible operating points also change according to the speed of operation. The feasible points of i_{sd} and i_{sq} are the dashed portion of Fig. 2.3.

2.4 The control scheme for maximum torque capability

In order to satisfy both the voltage and current limit constraints, the currents i_{sd} and i_{sq} must remain inside the overlapping area of current limit circle and voltage limit ellipse at each operating speed. Numerous combinations of i_{sd} and i_{sq} can be feasible operating points. However, among all the feasible points, the one which gives the maximum generated torque will be the optimum choice of i_{sd} and i_{sq}. Calculation of this optimum values of i_{sd} and i_{sq} will differ in different speed range of operation. The whole operating region is divided into following sections based on the choice of optimal values of i_{sd} and i_{sq}.

- *Below base speed region*

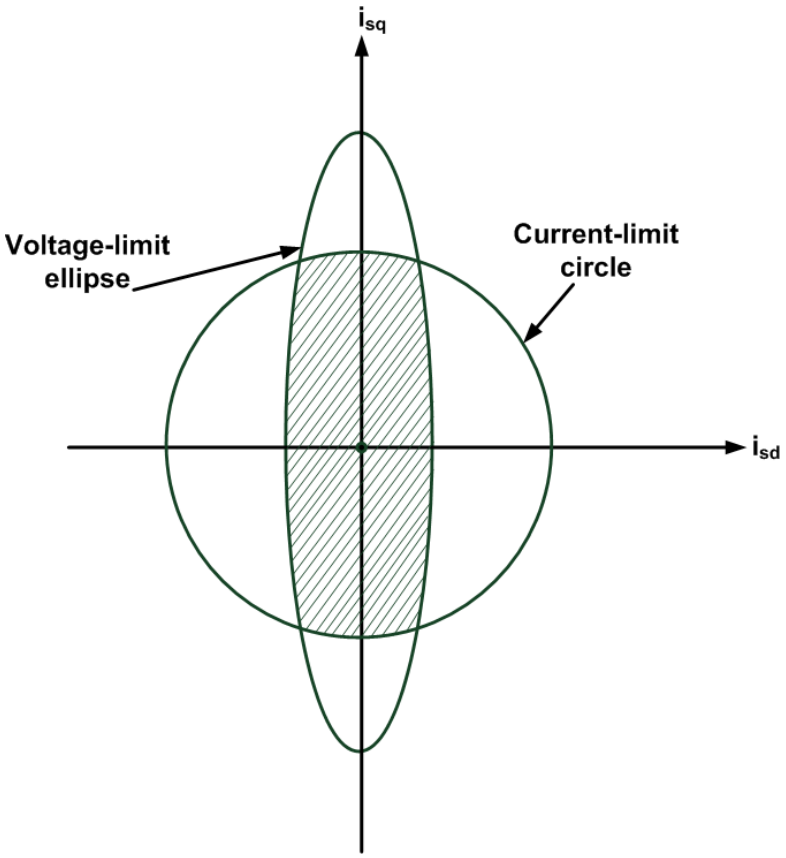

Figure 2.3: Overlapping region of voltage and current limit

- *Field weakening region I*
- *Field weakening region II*

2.4.1 Below base speed region

In this operating region, the speed of the machine varies from 0 to ω_{base}, where ω_{base} is the base speed of the machine. The flux of the machine will be at the rated maximum value in this operating region, the rotor flux component of current, i_{mr} of the machine is held constant at its rated value.

The value of i_{sq} is determined by the load on the machine. the expression for generated torque in the machine is given as

$$T_g = K_t i_{mr} i_{sq} \tag{2.9}$$

where K_t is torque constant of the machine.

Since the i_{mr} value is held at maximum, the machine will generate maximum pos-

sible torque, T_{max} when i_{sq} is maximum. At full load condition, the maximum current flow through the stator winding and the corresponding i_{sq} value will be maximum. The i_{sq} can vary from 0 to i_{sqmax} according to the load in the machine such that the current limit is not violated. Then the value of i_{sqmax} is given as

$$i_{sqmax} = \sqrt{I_{max}^2 - i_{sd}^2} \tag{2.10}$$

At steady state, value of i_{mr} and i_{sd} are same. Since i_{mr} is constant, from the Eq.(2.10), i_{sqmax} is also constant in this operating zone. So the machine can generate the maximum possible torque at any speed in this operating region. The Fig. 2.4 shows the trajectory of i_{sq} from no load to full load in this operating region.

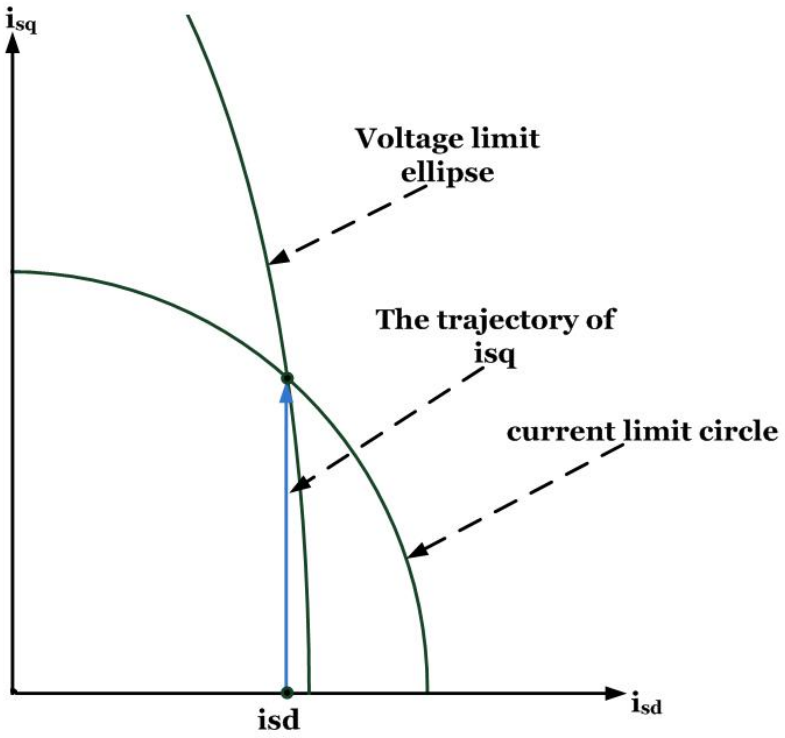

Figure 2.4: The trajectory of i_{sq} from no load to full load condition in *below base speed region*

At the base speed (ω_{base}) and at the rated load condition, the voltage applied to the machine and the current flowing through the stator winding of the machine are at its boundary values. This operating point is the intersection between the current limit circle and voltage limit ellipse at the base speed. The base speed is the boundary between the

below base speed operation and the field weakening operation. If the traction drive demands speed higher than the base speed, it is mandatory to drive the machine in field weakening region.

2.4.2 Field weakening region I

Similar to a DC machine, the operation above the base speed is achieved by reducing the flux of the machine in FOC based induction machine drive. In field weakening region, it should be ensured that the voltage applied to the machine and the current through the stator winding of the machine is within the safe limit. From the equation of voltage limiting ellipse, Eq.(2.7), it is clear that the voltage limit boundary dynamically changes with the speed of operation. Hence the overlapping area between the current limit circle and the voltage limit ellipse reduces as the speed of operation increases. Since the flux in the machine reduces in field weakening region, i_{mr} also reduces. So according to Eq.(2.9), the maximum torque capability will be reduced in this region. The developed torque capability of induction machine mainly depends on the control strategy in the field weakening region. So the control strategy should ensure that the maximum torque generation is possible over the entire speed range, without violating the voltage and current limit constraint.

Fig. 2.5 shows the variation of voltage limiting ellipse according to the speed of operation in *field weakening region I*. From Fig. 2.5, it is obvious that the optimum current vector (i_{sd} and i_{sq}) which ensures maximum developed torque will be the intersection of current limit circle and voltage limit ellipse at that speed of operation. So the optimum operating point will move along the circumference of the current limiting circle as the speed of operation increases. The trajectory of optimal current vector is shown in Fig. 2.5.

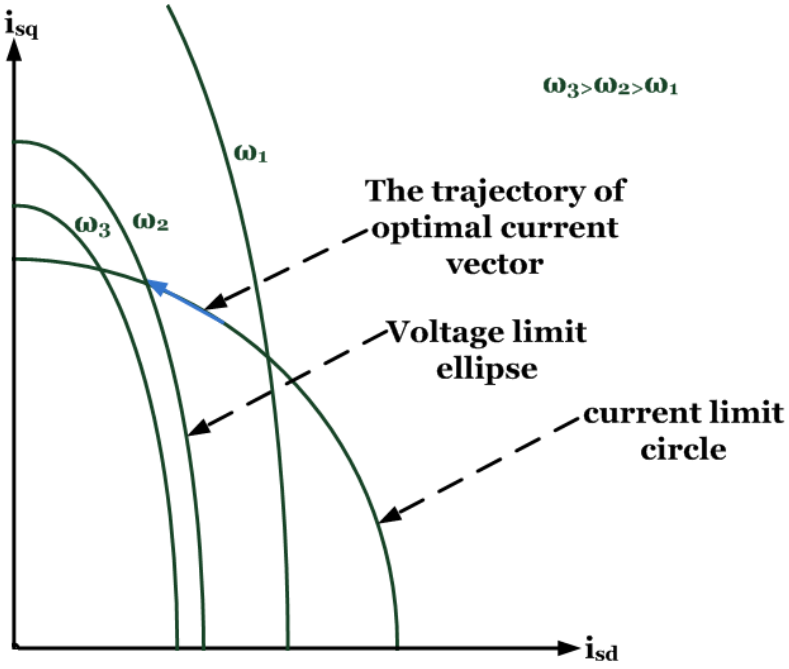

Figure 2.5: The trajectory of optimal current vector in *field weakening region I*

The i_{sd} and i_{sq} for maximum torque capability at various speed of operation are calculated by finding the intersection of current limiting circle and voltage limiting ellipse.

The voltage limiting equation is given as

$$v_{sd}^2 + v_{sq}^2 = V_{max}^2 \tag{2.11}$$

and the current limit equation is given as

$$i_{sd}^2 + i_{sq}^2 = I_{max}^2 \tag{2.12}$$

From Eq.(2.12)

$$i_{sd}^2 = I_{max}^2 - i_{sq}^2 \tag{2.13}$$

Substituting the value of i_{sd} from Eq.(2.13) in Eq.(2.11) and solving for i_{sd},

$$i_{sd} = \sqrt{\frac{V_{max}^2 - \omega_e^2 L_s^2 I_{max}^2}{L_s^2 - L_s'^2}} \tag{2.14}$$

Substituting the value of i_{sd} in Eq.(2.12)

$$I_{sq} = \sqrt{I_{max}^2 - I_{sd}^2} \tag{2.15}$$

Since the value of i_{sd} is decreased with increasing in speed in field weakening region, according to Eq.(2.15) the maximum possible value of i_{sq} slightly increases. However the drop in i_{mr} is more significant compared with slight rise in i_{sq}. So in effect the the maximum torque capability will reduce as the speed increases.

The expression for slip speed in the machine is

$$\omega_{slip} = \frac{i_{sq}}{\tau_r i_{mr}} \tag{2.16}$$

As i_{sq} increases and i_{mr} decreases in *field weakening region I*, from the Eq.(2.16), slip speed of the machine will increase in this operating region. So the losses of the machine increase and efficiency of the system reduce in *field weakening region I*.

As the speed of the machine increases further, a major portion of the ellipse become included in the circle. At a particular speed, the optimum current vector for maximum torque development considering the voltage limit constraint alone lie on the circumference of the current limit circle. The slip speed of the machine will be maximum at this operating speed. If the speed increases further, this point moves in to the region inside the circle and then the current limit will not be an active constraint. From this point onwards *field weakening region II* will start.

2.4.3 Field weakening region II

In the *field weakening region II*, the optimum current vector for maximum torque development considering the voltage limit constraint alone always lie inside the current limit circle. So this current vector, i_{sd} and i_{sq} will always satisfy Eq.(2.8). The current limit will not be a constraint for calculating the optimum values of i_{sd} and i_{sq} . So in the *field weakening region II*, the optimum current vector for the maximum torque generation is

calculated just considering the voltage limit constraint alone.

The maximizing function F is defined as

$$F = \frac{T_e}{K_t} = i_{sd} i_{sq} \tag{2.17}$$

Where K_t is the torque constant of the machine.

From Eq.(2.17)

$$i_{sq} = \frac{F}{i_{sd}} \tag{2.18}$$

The voltage limit boundary is

$$(\omega_e L_s i_{sd})^2 + (\omega_e L'_s i_{sq})^2 = V_{max}^2 \tag{2.19}$$

Substituting the value of i_{sq} from Eq.(2.18) in Eq.(2.19)

$$(\omega_e L_s i_{sd})^2 + (\omega_e L'_s)^2 \frac{F^2}{i_{sd}^2} = V_{max}^2 \tag{2.20}$$

Then

$$F^2 = \frac{V_{max}^2 i_{sd}^2 - \omega_e^2 L_s^2 i_{sd}^4}{\omega_e^2 L_s'^2} \tag{2.21}$$

for maximizing the function F, the first derivative of the function with respect to i_{sd} must be zero and second derivative of the function with respect to i_{sd} must be less than zero.

$$\frac{dF}{di_{sd}} = 0 \tag{2.22}$$

$$\frac{d^2F}{di_{sd}^2} < 0 \tag{2.23}$$

Finding the $\frac{dF}{di_{ds}}$ from Eq.(2.21) and equating to zero and solve for i_{sd} and i_{sq},

$$\frac{dF}{di_{sd}} = \frac{1}{2\sqrt{\frac{V_{max}^2 i_{sd}^2 - \omega_e^2 L_s^2 i_{sd}^4}{\omega_e^2 L_s'^2}}} \frac{2 i_{sd} V_{max}^2 - 4\omega_e^2 L_s'^2 i_{sd}^3}{\omega_e^2 L_s'^2} = 0 \tag{2.24}$$

$$V_{max}^2 - 2\omega_e^2 L_s^2 i_{sd}^2 = 0 \tag{2.25}$$

$$i_{sd} = \frac{V_{max}}{\sqrt{2}\omega_e L_s} \tag{2.26}$$

$$i_{sq} = \frac{V_{max}}{\sqrt{2}\omega_e L_s'} \tag{2.27}$$

The Eq.(2.26) and Eq.(2.27) represents the optimal current vector, i_{sd} and i_{sq} in *field weakening region II*. The optimum current vector will satisfy the Eq.(2.23). From these equations, it is clear that i_{sd} and i_{sq} inversely proportional to the speed of operation in this region. Since both the currents are reducing, the reduction rate in torque with respect to speed will be higher compared to the *field weakening region I*. The optimal current vector considering voltage limit constraint is a straight line passing through the origin. Fig. 2.6 shows the trajectory of the optimal current vector in Field weakening region II.

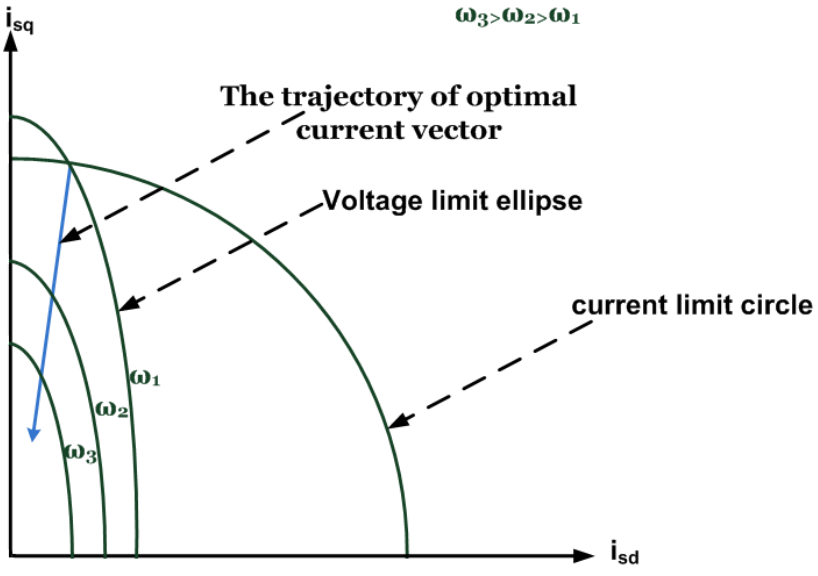

Figure 2.6: The trajectory of optimal current vector in *field weakening region II*

Since both i_{sd} and i_{sq} are decreasing in the same proportion, the slip speed of the machine is constant at its maximum value during the operation in this region, so this region is also known as constant slip region. As the speed increases further, the maximum torque capability reduces to a very small value and after some speed, maximum pos-

sible torque become less than the no load torque of the machine. At that point further increase in speed becomes impossible.

2.4.4 Base speed estimation

The base speed is the transition speed between normal and field weakening operation. Since the field weakening operation starts from ω_{base} onwards, any miscalculation in calculation of base speed will result in an unwanted reduction in torque. Calculation of base speed (ω_{base}) is very critical in field weakening operation.

The applied voltage to the machine will hit the voltage limit boundary at base speed. At base speed and rated load condition, the current vector (i_{sd} and i_{sq}) will be at the intersection of both voltage limit ellipse and current limit circle. Let I_d and I_q be the value of i_{sd} and i_{sq} at this rated condition, where

$$I_q = \sqrt{I_{max}^2 - I_d^2}$$

Since the base speed is the intersection between current limit circle and voltage limit ellipse, the current vector (I_d, I_q) will satisfy the voltage limit equation, Eq.(2.19) at ω equals ω_{base}.

$$[L_s^2 I_q^2 + L_s'^2 I_d^2]\omega_{base}^2 + 2R_s I_d I_q (L_s' - L_s)\omega_{base} + (R_s I_q)^2 + (R_s I_d)^2 - V_{max}^2 = 0 \qquad (2.28)$$

Eq.(2.28) is a quadratic equation in ω_{base}, Solving this quadratic equation, ω_{base} is obtained as

$$\omega_{base} = \frac{\sqrt{V_{max}^2[L_s^2 I_d^2 + L_s'^2 I_q^2] + [R_s I_d I_q (L_s - L_s')]^2} - R_s I_d I_q [L_s - L_s']}{L_s^2 I_d^2 + L_s'^2 I_q^2} \qquad (2.29)$$

This is the speed from which the proposed method in [1] should start the field weakening operation.

2.4.5 Transition speed between field weakening region I and region II

The speed at which transition from *field weakening region I* and *field weakening region II* occur is an important factor to be determined because the control strategy in the region I and region II are different. Therefore the exact calculation of this transition point is very critical for smooth operation of the drive in the field weakening region. The transition from *field weakening region I* to *field weakening region II* occurs when the optimum current vector considering the voltage limit constraint alone is on the current limit circle. So at transition speed (ω_1), equation in region I and region II are valid. The optimal current vector equation in region II is

$$i_{sd} = \frac{V_{max}}{\sqrt{2}\omega_e L_s} \tag{2.30}$$

$$i_{sq} = \frac{V_{max}}{\sqrt{2}\omega_e L'_s} \tag{2.31}$$

Substituting this expression of i_{sd} and i_{sq} in current limit circle equation, Eq.(2.8) at ω_e equals ω_1 will give

$$\frac{V_{max}^2}{2\omega_1^2 L_s^2} + \frac{V_{max}^2}{2\omega_1^2 L_s'^2} = I_{max}^2 \tag{2.32}$$

Simplifying the Eq.(2.32), the expression for transition speed ω_1 is obtained as

$$\omega_1 = K\frac{V_{max}}{I_{max}} \tag{2.33}$$

where

$$K = \sqrt{\frac{L_s^2 + L_s'^2}{2L_s^2 L_s'^2}} \tag{2.34}$$

The span of *field weakening region I* is depends on ω_1, which depends on machine parameters. The *field weakening region I* will be extended in the machine with a lower value of σ. The machines with higher value of σ, the *field weakening region II* will be dominant. If ω_1 value is high, the speed at which the maximum slip occur will be higher.

2.4.6 Analysis of conventional field weakening scheme

In conventional field weakening method, the rotor flux reference of the machine varies inversely with respect to the speed of the machine . The voltage limit and the current limit constraints are not considered in a conventional field weakening. So it is impossible to obtain the maximum possible developed torque by this method. Fig. 2.7 shows the comparison of conventional field weakening method and the proposed field weakening method [1] based on the maximum torque capability over a wide speed range.

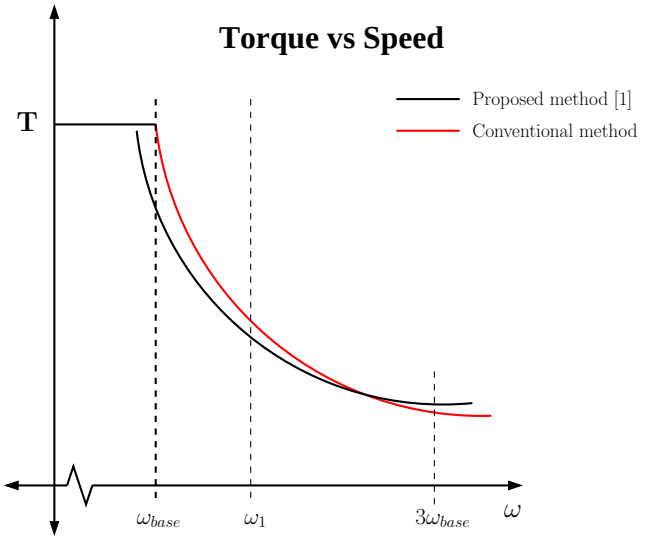

Figure 2.7: Maximum torque capability vs speed in conventional field weakening scheme and proposed field weakening scheme [1]

From Fig. 2.7 it is obvious that the proposed method [1] has higher maximum torque capability. Even though the conventional method has more developed torque after a certain higher speed, the corresponding values of i_{sd} and i_{sq} will not be feasible while considering the voltage and current limits. Then the proposed method [1] will ensure the maximum possible torque capability in entire speed range.

2.4.7 Field weakening control strategy in Field Oriented Control based induction machine drive

From the previous discussions, it is clear that the d-axis component of the current, i_{sd} and the q-axis component of the current, i_{sq} are dynamically varied with the speed in field weakening regions. Since i_{sd} and i_{sq} changes dynamically, the component of voltage in d-q axis (v_{sd} and v_{sq}) will also change in the field weakening region. So PI

controller limits of FOC based induction machine drive must be dynamically changed according to the speed of operation in field weakening region. Fig. 2.8 shows the block diagram of FOC based induction machine drive with field weakening scheme.

From 0 to ω_{base} operation, all the limits of PI controllers held at rated maximum value. As the drive moves to *field weakening region I*, the flux reference i^*_{mr} is updated based on Eq.(2.14), where the steady state value of i_{mr} and i_{sd} are same. The output limits of flux controller and speed controller are updated based on Eq.(2.14) and Eq.(2.15) respectively. The voltage limits of d-axis and q-axis current controllers are updated with respect to Eq.(2.1) and Eq.(2.2).

In *field weakening region II*, the flux component of the current, i^*_{mr} is changes based on Eq.(2.26). Steady state value of i_{mr} and i_{sd} are same in this operating condition. The flux and speed controller limits are calculated using Eq.(2.26) and Eq.(2.27) respectively. The current controller limits are calculated using Eq.(2.1) and Eq.(2.2). The calculation of base speed, ω_{base} and transition speed, ω_1 must be accurate since the equations for calculation of i^*_{mr} and PI controller limits are different in these two speed range. Hence by dynamically varying the flux reference and PI controller limits, field weakening operation with maximum torque capability can be achieved in FOC based induction machine drive.

2.5 Linear and overmodulation zone of operation of SVPWM scheme

The pulse width modulated (PWM) inverter is usually operated in linear modulation zone, where the line side fundamental voltage is proportional to the reference voltage. The operation of the PWM inverter can be extended to overmodulation region till the six step mode to obtain the highest possible line side voltage from a given DC bus voltage (V_{dc}).

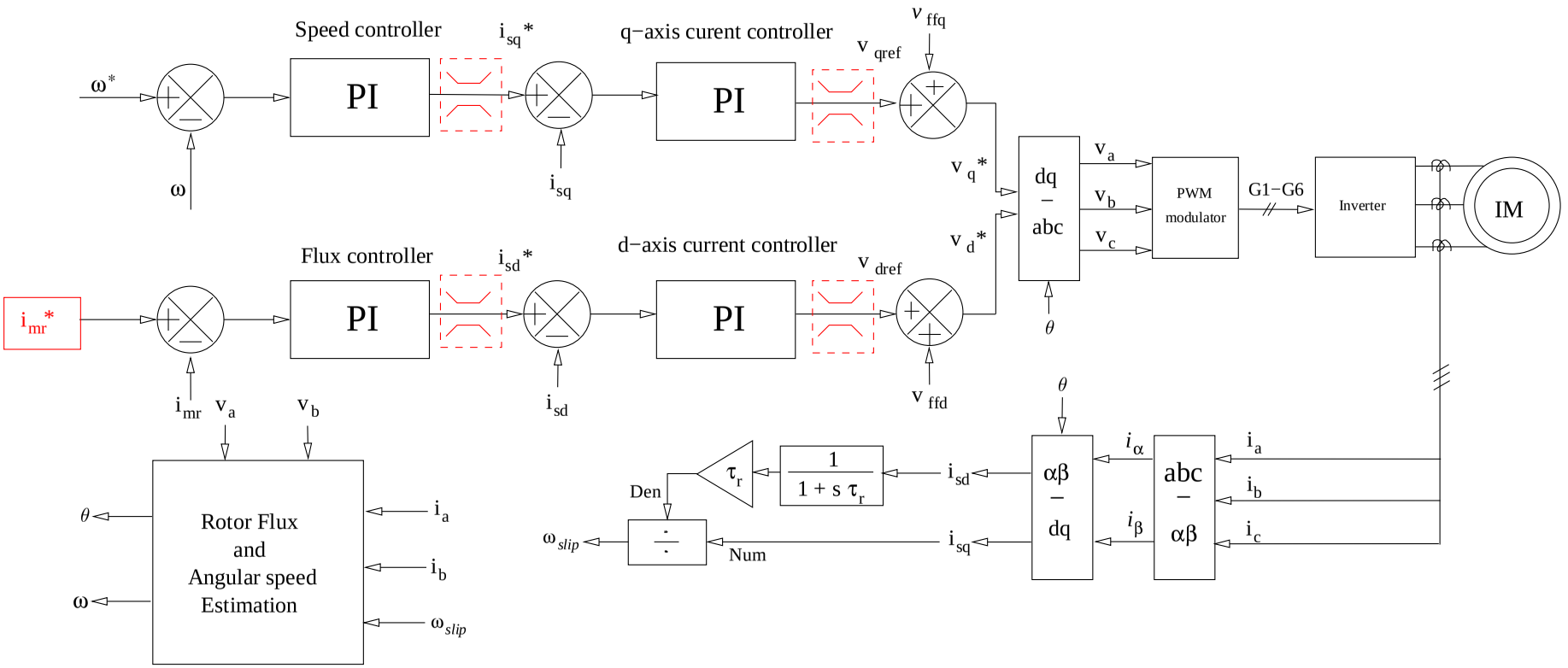

Figure 2.8: Block diagram of FOC based induction machine drive for field weakening operation

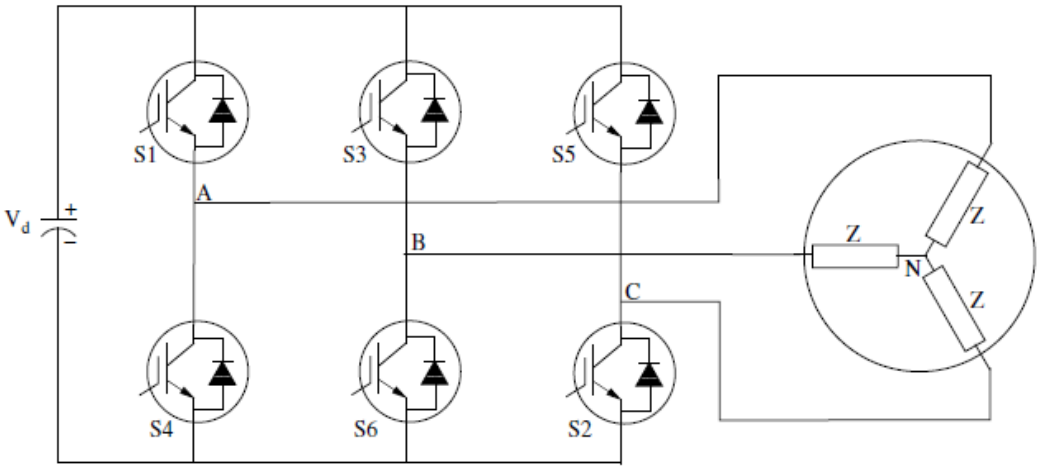

Figure 2.9: 2-level VSI

2.5.1 The linear operation scheme in SVPWM

The power circuit topology for a 2-level VSI is shown in Fig. 2.9. For this inverter, there are 8 switching combinations possible. Each of the switching combinations corresponds to particular space vector locations. These are called basic vectors. Two of the basic vectors are inactive vectors (zero vectors) corresponding to all top switches or all bottom switches ON. The other six active vectors are directed along the vertices of a regular hexagon giving six sectors $S_1 - S_6$ as shown in Fig. 2.10.

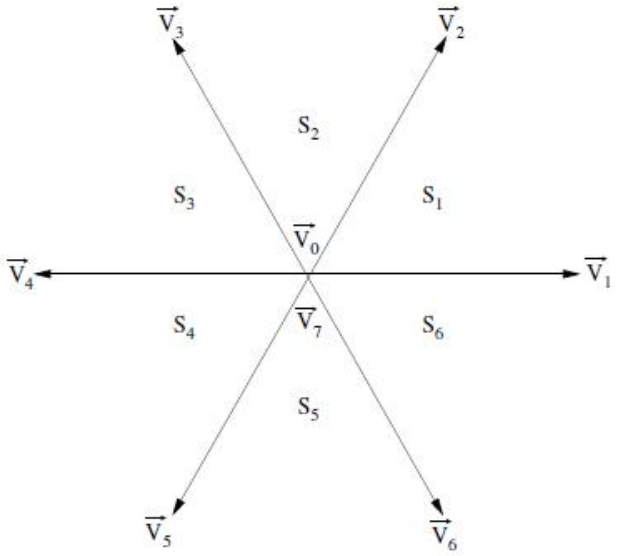

Figure 2.10: Space vector orientation for the 2-level VSI

The ideal trajectory for the voltage space vector is a circle described with uniform angular velocity, which results only when the motor is fed from a balanced three phase sinusoidal voltage source. The objective of SVPWM is to approximate this ideal trajectory of the voltage space vector by switching the eight standard positions. The reference voltage vector is obtained by mapping the desired 3-ph output voltage to the $\alpha - \beta$ frame. It is realised by using the vectors that form the boundary of the sector in which the reference lies. Fig. 2.11 illustrates this technique for a vector that lies in sector 1. The angle α represents the position of reference space vector, V_{ref} with respect to the beginning of the sector. The reference vector is realised by switching the inverter to create the vectors V_1, V_2, V_0, V_7 in some sequence. Selecting any of the other vectors would result in a greater deviation of the actual vector from the desired reference and would thus contribute to harmonics.

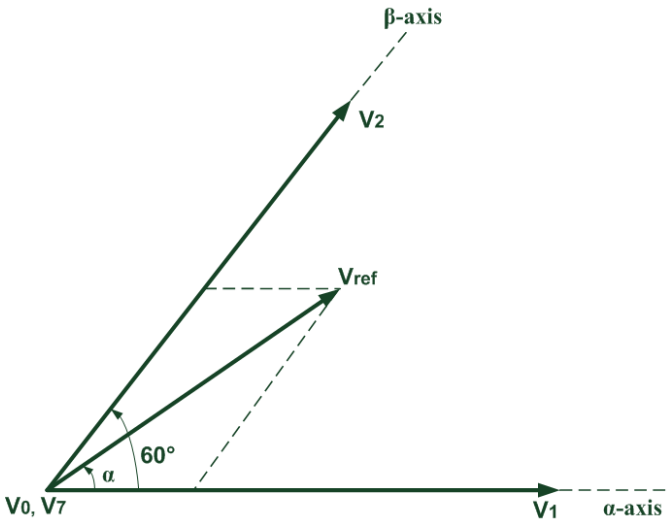

Figure 2.11: Reference vector in sector 1

The sampling time, T_s is divided into three subintervals namely T_1, T_2 and T_0. The reference space vector is realised by switching the vector $\vec{V_1}$ for T_1 seconds, $\vec{V_2}$ for T_2 seconds and $\vec{V_0}$ or $\vec{V_7}$ for T_0 seconds. In order to realise the reference space vector $\vec{V_{ref}}$ using basic vectors, the volt seconds produced by these basic vectors along α and β axis must be same as volt second produced by the reference vector. Therefore,

equating volt seconds along α axis

$$|\vec{V_{ref}}|T_s cos\alpha \; = \; T_1|\vec{V_1}| \; + \; T_2|\vec{V_2}|cos60^o \tag{2.35}$$

Equating volt seconds along β axis

$$|\vec{V_{ref}}|T_s sin\alpha = T_2|\vec{V_2}|sin60^o \tag{2.36}$$

Defining modulation index as a $= \frac{|\vec{V_{ref}}|}{V_{dc}}$ and solving the Eq.(2.35) and Eq.(2.36) for T_1 and T_2 gives

$$T_1 = aT_s\frac{\sin(60^\circ - \alpha)}{\sin(60^\circ)} \tag{2.37}$$

$$T_2 = aT_s\frac{\sin\alpha}{\sin(60^\circ)} \tag{2.38}$$

$$T_0 = T_s - T_1 - T_2 \tag{2.39}$$

Since these equations are identical in all sectors, a 60° sine lookup table is enough for calculating T_0, T_1 and T_2. Both the zero vectors are applied for equal time in a sampling period in order to obtain symmetrical switching signals. The switching signals used for realising a reference vector lying in sector 1 is shown in Fig. 2.12.

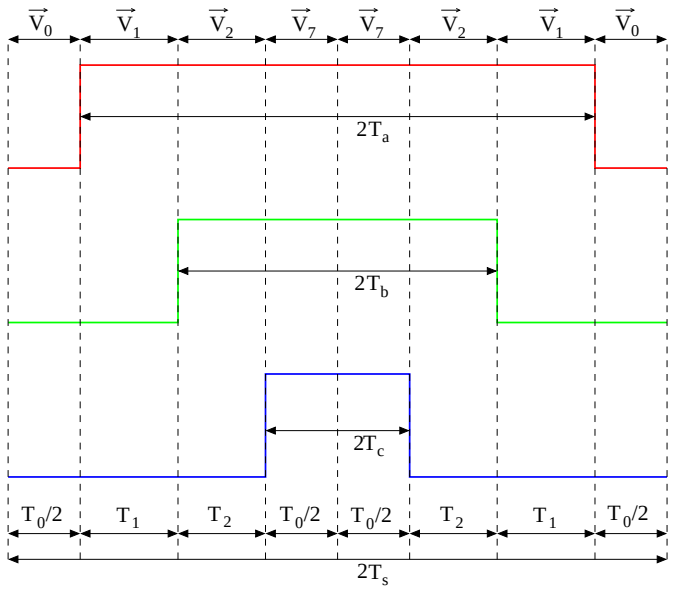

Figure 2.12: Switching pattern when reference vector is in sector 1

From the Fig. 2.12 it can be seen that

$$T_a = T_0/2$$

$$T_b = T_1 + T_0/2$$

$$T_c = T_s - T_0/2$$

Similarly, the relation between the time duration of each basic vector and the duty ratio of the switches in each leg can be obtained. The relationship between the vector duration and the duty ratios of the switches in different sectors are given in Table. 2.1

Table 2.1: Switching signal relationship in linear modulation zone

Sector	S1	S2	S3	S4	S5	S6
T_a	$T_s - T_0/2$	$T_1 + T_0/2$	$T_0/2$	$T_0/2$	$T_2 + T_0/2$	$T_s - T_0/2$
T_b	$T_2 + T_0/2$	$T_s - T_0/2$	$T_s - T_0/2$	$T_1 + T_0/2$	$T_0/2$	$T_0/2$
T_c	$T_0/2$	$T_0/2$	$T_2 + T_0/2$	$T_s - T_0/2$	$T_s - T_0/2$	$T_1 + T_0/2$

The magnitude of the reference vector, $|\vec{V_{ref}}|$ will increase with speed of operation. As the $\vec{V_{ref}}$ magnitude increases, The time duration of zero vector, T_0 will reduce. When the reference vector become the inscribed circle of the hexagon, the value of T_0 become zero. This is the boundary of linear modulation. Further increase in the magnitude of $\vec{V_{ref}}$ will result in, the locus of reference vector lying partially inside and partially outside the hexagon. The portion outside the hexagon cannot be realised by time averaging of basic vectors, so linearity is not achieved when inverter moves to overmodulation. The magnitude of $\vec{V_{ref}}$ become $0.866V_{dc}$ at the boundary of linear modulation. This situation is shown in Fig. 2.13.

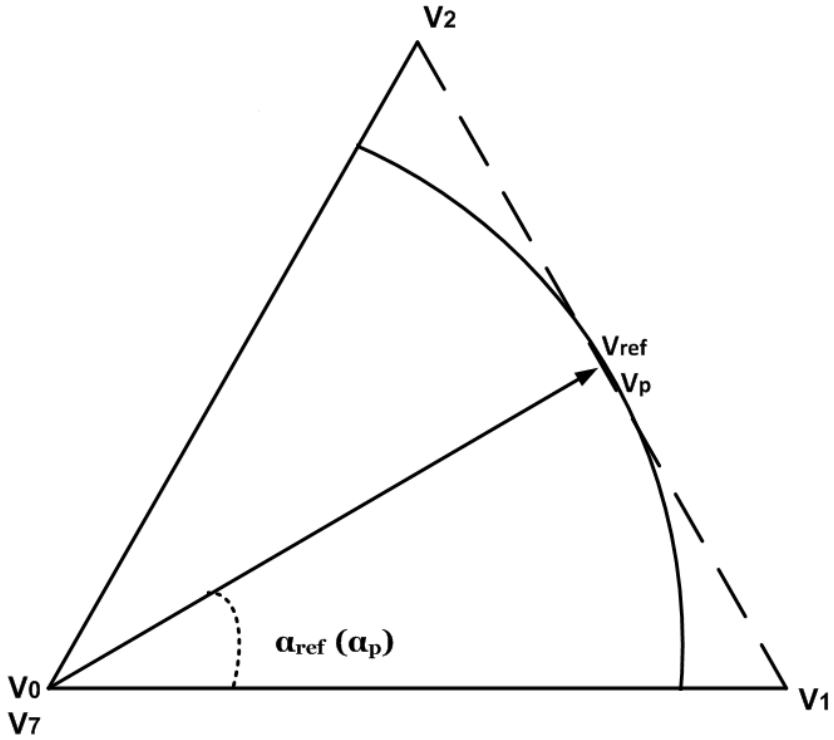

Figure 2.13: The reference vector at boundary between linear and overmodulation

2.5.2 The overmodulation scheme in SVPWM

The reference space vector $\vec{V_{ref}}$ can be realised with the basic vectors, only when it lies inside the hexagon. At lower speed of operation, the voltage required for the induction machine is low and hence the reference space vector magnitude will be less. As speed demanded by the machine increases the length of the reference vector, $\vec{V_{ref}}$ increases and moves outside the hexagon, then the portion of space vector trajectory outside the hexagon cannot be realised and hence considerable volt seconds unbalance will occur. So a proper compensation algorithm must be used to maintain the linearity between the reference and applied vectors. Based on the compensation algorithm used, the whole overmodulation region is further divided into 3 operating zones.

- *Overmodulation zone I*
- *Overmodulation zone II*
- *Six step mode*

2.5.2.1 Overmodulation zone I

When the magnitude of the reference vector, $\vec{V_{ref}}$ increases beyond $0.866V_{dc}$, it is not possible to maintain the linearity between the reference and the applied vector since some portion of the reference space vector trajectory lies outside the hexagon. Proper compensation method should be adopted such that average values of reference vector and the applied vector are the same to obtain the linearity. In the linear modulating region, the reference vector, $\vec{V_{ref}}$ and the applied vector, $\vec{V_p}$ coincide in all the switching time intervals. But in the overmodulating zones, these two vectors cannot always coincide since we modify the path of applied vector in order to achieve the linearity between the reference and applied vectors.

In order to develop the compensation algorithm, the applied vector $\vec{V_p}$ is resolved along the synchronously revolving reference frame (d-q frame). The q-axis is aligned along the direction of reference vector, $\vec{V_{ref}}$ and the d-axis is 90° lagging the q-axis. Fig. 2.14 shows the reference vector, $\vec{V_{ref}}$ and applied vector, $\vec{V_p}$ in d-q reference frame, where α_p represents the position of the applied vector $\vec{V_p}$ with respect to the beginning of the sector.

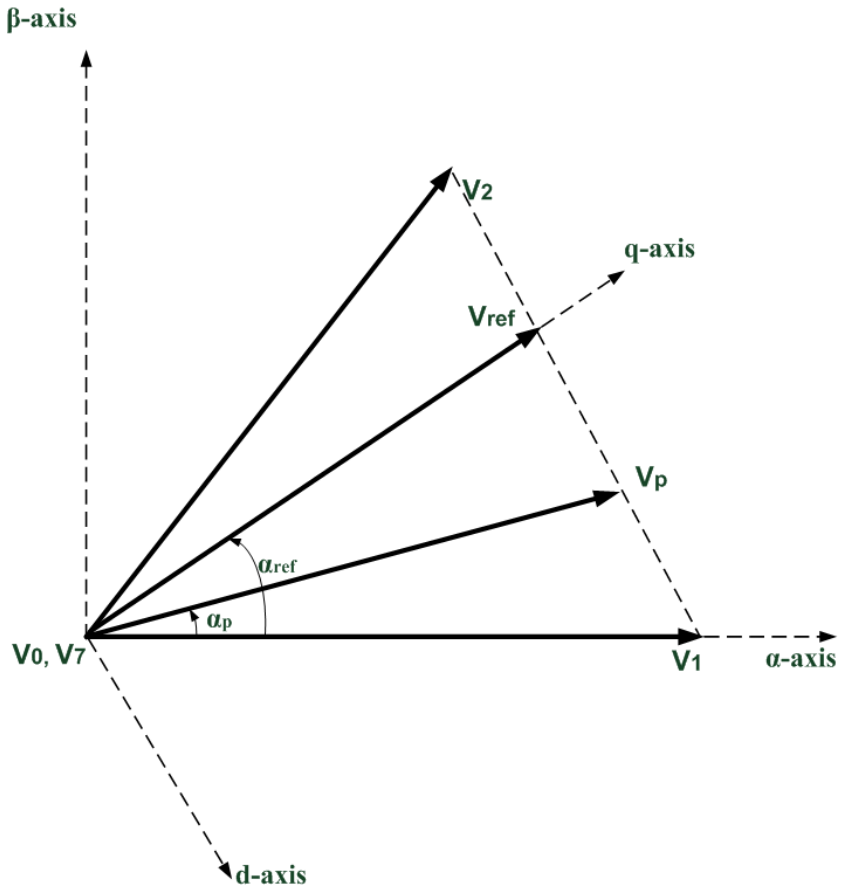

Figure 2.14: Reference vector and applied vector in d-q frame

Resolving the applied vector, $\vec{V}_p$ along the d-axis and q-axis,

$$V_{pqs} = |\vec{V}_p| cos(\alpha_{ref} - \alpha_p) \tag{2.40}$$

$$V_{pds} = |\vec{V}_p| sin(\alpha_{ref} - \alpha_p) \tag{2.41}$$

where V_{pqs} and V_{pds} are the components of $\vec{V}_p$ along q-axis and d-axis respectively.

Since the reference vector lies along q-axis, the component of reference vector along the d-axis will be zero. The compensation algorithm must ensure that the average value

of reference vector $\vec{V_{ref}}$ and the applied vector $\vec{V_p}$ along the d-axis and q-axis are equal.

$$V_{pqs(AV)} = \frac{3}{\pi}\int_0^{\frac{\pi}{3}} (V_{pqs})\, d\alpha_{ref} = |V_{ref}| \tag{2.42}$$

$$V_{pds(AV)} = \frac{3}{\pi}\int_0^{\frac{\pi}{3}} (V_{pds})\, d\alpha_{ref} = 0 \tag{2.43}$$

Now to maintain linearity, the average q-axis voltage, $V_{pqs(AV)}$ should be equal to the magnitude of reference voltage vector as given by Eq.(2.42). In *overmodulation zone I*, and sector 1 operation, the applied vector will move in a circular trajectory till it hits the edge of the hexagon, after that it moves along the edge of the hexagon. When the applied vector moves in the circular trajectory, the magnitude of $\vec{V_p}$ is kept higher than the magnitude of $\vec{V_{ref}}$ to compensate for the volt seconds losses which would occur in the portion outside the hexagon. The Fig. 2.15 shows the trajectory of $\vec{V_p}$ and $\vec{V_{ref}}$ in *overmodulation zone I*. The V_{cir} and α_{cir} are the magnitude and angle of $\vec{V_p}$ when the circular trajectory touches the edge of the hexagon.

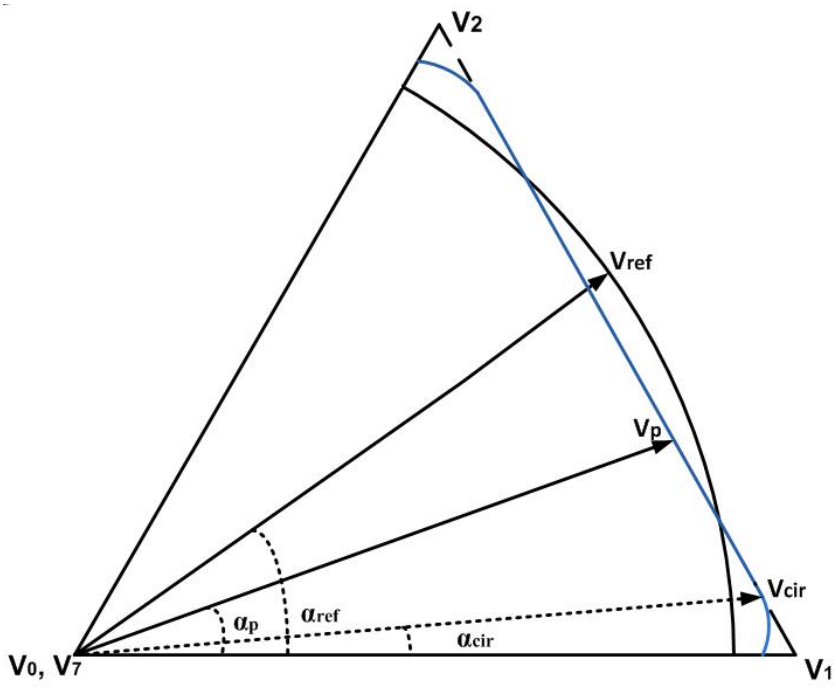

Figure 2.15: Reference vector and applied vector in *Overmodulation zone I*

The magnitude of $\vec{V_p}$ in this zone is given as

$$|\vec{V_p}| = \begin{cases} \frac{0.866V_{dc}}{sin(\frac{\pi}{3}+\alpha_p)} & \text{if } \alpha_{cir} < \alpha_{ref} < (\frac{\pi}{3} - \alpha_{cir}) \\ V_{cir} & \text{otherwise} \end{cases} \quad (2.44)$$

The angle α_{ref} and α_p are equal in the entire *overmodulation zone I*.

substituting $|\vec{V_p}|$ from Eq.(2.44) in Eq.(2.42) and Eq.(2.43)

$$|\vec{V_{ref}}| = \frac{V_{cir}\ \alpha_{cir}}{\frac{\pi}{6}} + \frac{3\sqrt{3}}{\pi} \ln|cot(\frac{\pi}{6} + \frac{\alpha_{cir}}{2})| \quad (2.45)$$

$$V_{cir} = \frac{\sqrt{3}}{2}\, cosec(\frac{\pi}{3} + \alpha_{cir}) \quad (2.46)$$

The Eq.(2.45) and Eq.(2.46) are used to develop a lookup table between V_{cir} and $|\vec{V_{ref}}|$. This lookup table provides the value of $|V_{cir}|$ for the corresponding value of $|V_{ref}|$ so that the proper compensation is made.

The circular trajectory of the vector $\vec{V_p}$ is realised by volt seconds balance method similar to linear modulation region. All the equations of the linear zone used to calculate T_0, T_1, T_2, T_a, T_b and T_c are also valid in this overmodulation zone. When the space vector moves along the edge of the hexagon, the value of T_0 become zero and the switching time of vector $\vec{V}_1$, T_1' and switching time of vector $\vec{V}_2$, T_2' are calculated based on volt seconds equal criterion.

$$T_1' = \frac{T_1}{T_1 + T_2} \quad (2.47)$$

$$T_2' = T_s - T_1' \quad (2.48)$$

Table. 2.2 elaborates the expression for the switching signal when the space vector is moving along the edge of the hexagon in different sectors.

Table 2.2: Switching signal relationship in overmodulation zone I

Sector	S1	S2	S3	S4	S5	S6
T_a	T_s	T_1'	0	0	T_2'	T_s
T_b	T_2'	T_s	T_s	T_1'	0	0
T_c	0	0	T_2'	T_s	T_s	T_1'

When the magnitude of reference space vector is more than $0.9085V_{dc}$, the value of V_{cir} become V_{dc} and α_{cir} become and 30°. This is the boundary between *overmodulation zone I* and *overmodulation zone II*. Further increase in the magnitude of the reference vector will lead the inverter to operate in *overmodulation zone II*.

2.5.2.2 Overmodulation zone II

The *overmodulation zone I* cannot keep the linearity between the reference and applied vectors when the reference space vector magnitude is more than $0.9085V_{dc}$. Keeping the magnitude of $\vec{V_p}$ higher than $\vec{V_{ref}}$ in the circular region will not give enough compensation in this condition. In *overmodulation zone II* the applied vector $\vec{V_p}$ is held at the vertices of the hexagon for a calculated time duration so that the linearity in the average voltage is achieved. The calculation of hold angle, α_h is based on equating the average voltage of reference and applied vectors along d-axis and q-axis. The applied vector is held at each vertex of the hexagon for a calculated time, then moves along the edge of the hexagon to the next vertex and so on. The angle α_p and $|\vec{V_p}|$ of applied vector is given as.

$$\alpha_p = \begin{cases} 0 & \text{if } 0 \leqslant \alpha_{ref} \leqslant \alpha_h \\ \alpha_{ref} & \text{if } \alpha_h < \alpha_{ref} \leqslant (\frac{\pi}{3} - \alpha_h) \\ \frac{\pi}{3} & \text{if } (\frac{\pi}{3} - \alpha_h) < \alpha_{ref} \leqslant \frac{\pi}{3} \end{cases} \tag{2.49}$$

$$|\vec{V_p}| = \begin{cases} V_{dc} & \text{if } 0 \leqslant \alpha_{ref} \leqslant \alpha_h \\ \frac{0.866V_{dc}}{sin(\frac{\pi}{3}+\alpha_p)} & \text{if } \alpha_h < \alpha_{ref} \leqslant (\frac{\pi}{3} - \alpha_h) \\ V_{dc} & \text{if } (\frac{\pi}{3} - \alpha_h) < \alpha_{ref} \leqslant \frac{\pi}{3} \end{cases} \tag{2.50}$$

By equating the average value of the of reference and applied vector along d-axis and q-axis, the relationship between the magnitude of reference vector, $|\vec{V_{ref}}|$ and hold angle α_h can be obtained as

$$|V_{ref}| = \frac{sin(\alpha_h)}{\frac{\pi}{6}} + \frac{3\sqrt{3}}{\pi} \ln|cot(\frac{\pi}{6} + \frac{\alpha_h}{2})| \tag{2.51}$$

using Eq.(2.51), it is possible to create a lookup table which gives the value of hold angle, α_h according to the reference space vector magnitude, $|V_{ref}|$ such that the linearity is maintained. The trajectory of reference vector and applied vector in *overmodulation zone II* is shown in Fig. 2.16

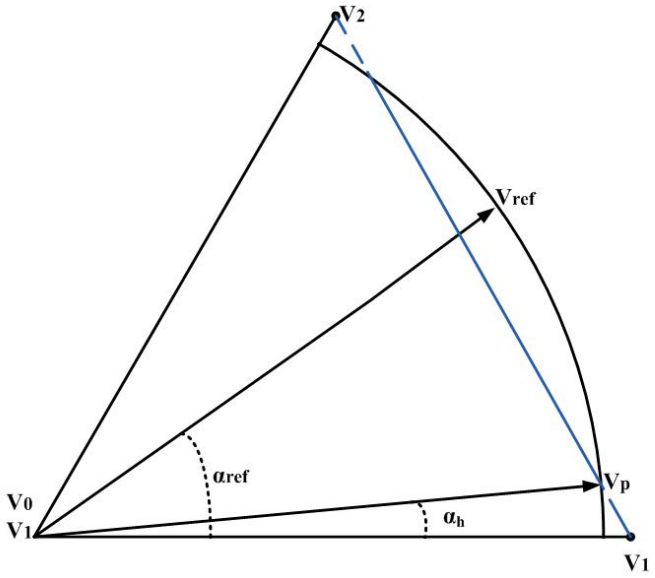

Figure 2.16: Reference vector and applied vector in *overmodulation zone II*

As the reference space vector magnitude increases further, the hold angle, α_h will increase and the portion of space vector trajectory which moves along the edge of the hexagon will reduce. When $|\vec{V_{ref}}|$ become $0.9549V_{dc}$, the hold angle becomes 30° and the applied space vector hold at each vertex of hexagon for 60°. This is the time inverter entered into the *six step mode*. At *six step mode* of operation maximum DC-bus utilization is possible. The switching signal for sixstep mode of operation is given in Table. 2.3

Table 2.3: Switching signal relationship in six step mode

α_{ref}	330°-30°	30°-90°	90°-150°	150°-210°	210°-270°	270°-330°
T_a	T_s	T_s	0	0	0	T_s
T_b	0	T_s	T_s	T_s	0	0
T_c	0	0	0	T_s	T_s	T_s

The highest possible line side voltage can be generated from a given DC bus voltage (V_{dc}) in *six step mode* of operation. The inverter switches only 6 times per fundamental time period, so the switching loss will be very less in this operating mode. So at high speed operating regions, the induction machine drive prefers to operate in near to *six step mode*.

2.5.3 The fundamental current estimation in overmodulation regions

When the inverter operates in the linear modulating region and the switching frequency is considerably high, the output voltage will be a pure sine wave. In overmodulation regions, as the switching frequency reduces and the relationship between the reference voltage vector and the applied voltage vector is nonlinear, the output voltage will have considerable amount of lower order harmonics. Then the stator current will also consist of lower order harmonics in addition to the fundamental and high frequency components. The current harmonics of orders 5,7,11,13 etc, will be dominant in this condition. The frequency of the lower order current harmonics are close to the controller bandwidth of the FOC based induction machine drive. So these components also get amplified by the controller. Hence the voltage reference produced by the current controller will have a considerable amount of low frequency component which degrades the performance of the drive. The lower order harmonics also affect the proper sensorless operation of the drive. So it is important to estimate the fundamental component current from the distorted phase currents. This is achieved by estimating the current ripple and subtracting this quantity from the actual current.

In overmodulation zone, the applied voltage vector, realised by switching the inverter switches is not same in magnitude as well as in phase at all the instant of time with respect to the reference vector.

The average error in the voltage vector, $\vec{V'}$ in a subinterval is given as

$$\vec{V'} = \vec{V_p} - \vec{V_{ref}}$$

The error voltage resolved along q-axis is given as

$$V'_{qs} = V_{pqs} - |\vec{V_{ref}}| \tag{2.52}$$

$$V'_{ds} = V_{pds} \tag{2.53}$$

Resolving the average error in to $\alpha - \beta$ axis is given as

$$V'_{\alpha} = V'_{ds}\, sin(\omega t) + V'_{qs}\, cos(\omega t) \tag{2.54}$$

$$V'_{\beta} = -V'_{ds}\, cos(\omega t) + V'_{qs}\, sin(\omega t) \tag{2.55}$$

The relationship between harmonic voltage and harmonic current is given as

$$(\sigma_s + \sigma_r)L_0 \frac{di'_{\alpha}}{dt} + (R_s + R_r)i'_{\alpha} = V'_{\alpha} \tag{2.56}$$

$$(\sigma_s + \sigma_r)L_0 \frac{di'_{\beta}}{dt} + (R_s + R_r)i'_{\beta} = V'_{\beta} \tag{2.57}$$

The solution of these differential equation will give the harmonic current. This current is subtrated from sensed current to extract the fundamental component of current.

2.6 Conclusion

This chapter presented the design of control strategy for field weakening region operation of an FOC based induction machine drive. The basic idea of field oriented control is explained with the help of control block diagram. The equations required for updating the limits of the controller in field weakening region is derived and variation of slip speed in different operating regions is discussed in this chapter. The derivation of the base speed and the transition speed between region I and region II is included. The detailed theory of SVPWM in linear and overmodulation zones are discussed and the relevant equation used for generating the switching signals are derived. The fundamental current extraction principle explained with relevant equations.

CHAPTER 3

HARDWARE ORGANISATION FOR FIELD WEAKENING STRATEGY FOR FOC BASED INDUCTION MACHINE DRIVE

3.1 Introduction

This chapter features about the hardware organisation for the field weakening strategy of FOC based induction machine drive. In this project the field weakening control strategy has been implemented on TMS320F28335, 32-bit digital signal controller from Texas instruments. In this chapter we will have a brief overview about Digital Signal Control board and the hardware organization that helps in implementing field weakening strategy of FOC based induction machine drive.

3.2 Brief overview of the TMS320F28335

TMS320F28335 has a 32-bit DSP core with modified Harvard architecture, and also includes a single precision IEEE754 floating point unit. The floating point unit enables floating point computations to be performed in hardware. The C/C++ engine of device supports the user to implement the control algorithm in high level languages. The memory bus architecture has Program read bus, Data read and write bus. Real-time JTAG of the device supports the user for real time debugging alone with Code Composer Studio(CCS) from Texas instruments. The memory space contains individual sections of flash memory, Single access RAM(SRAM), One Time Programmable(OTP) memory and Boot ROM. The Boot ROM is factory programmed memory space with boot loading software. It also has 88 GPIO pins multiplexed with other peripherals like PWM, capture unit, ADC etc. The standard communications interface like I2C and CAN are supported by the controller.

3.3 Current and voltage sensing

The feedbacks of line currents and the DC bus voltage are required for the proper operation of sensor less FOC based induction machine drive. The hall effect based voltage sensor and current sensors are used for obtaining the feedback signals. Hall Effect sensors LA100P are used for obtaining the current feedback where Hall Effect sensor LV25P is used for obtaining the DC-bus voltage. The burden resistors for current sensor is chosen such that it produces an output voltage of 5V for a 100A current flow in power circuit. The burden resistors for voltage sensor is chosen such that it produces an output voltage of 5V for a voltage of 1000V in primary of hall effect sensor. The outputs of these sensors are also used for providing protection for the inverter against over voltage and over current.

3.4 Three phase inverter module

A three phase 2-level Voltage Source Inverter(VSI) from Semikron is used in this project for feeding the 3- phase induction machine. The power switches of each leg of the inverter is made of 1200V, 100A, IGBT modules. The front end diode bridge rectifier of the inverter is used for energising the DC bus from an input three phase supply. A pre-charging circuit consisting of resistors in parallel with relays, is connected in series with each line to control the flow of inrush currents into the capacitor during energisation. When the capacitor is charged to an appreciable voltage level, the relay will bypass the resistors from the charging circuit. The rectifier and the modules are mounted on the heat sink and connected to the DC bus capacitor by conducting sheets. Three Gate driver cards are mounted on the module for giving gate drive and proper isolation for the IGBT gate terminals.

3.5 Protection and Delay card

The main functions of Protection and Delay(PD) card are given below

- Protecting the inverter against under voltage, over voltage and over current faults.
- Generate complementary PWM signals with proper rising edge delay.

- Shifting the 5V level PWM signals from DSC board to 15V level PWM that is required to drive the inverter.
- Controlling the pre charging circuit relay.

The PD card has provision to provide protection for six sensed currents and two DC bus voltages. The current limit and voltage limit for sensing the fault can be changed using potentiometer provided in PD card. The LEDs provided on board are used for fault indication.

3.6 Hardware setup

The vector control algorithms discussed are implemented on a 30 kW laboratory prototype. Some photographs of the drive setup and the various additional circuitry built for interfacing will be presented in this section.

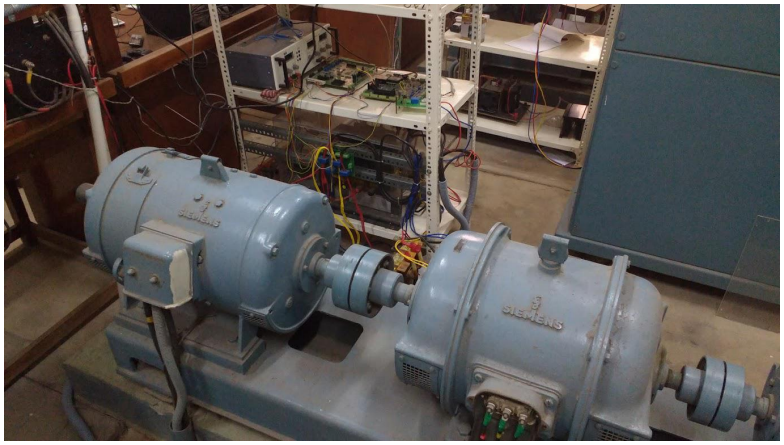

Figure 3.1: Machine setup for implementing the field weakening strategy

Figure.3.1 shows the machine setup for implementing the field weakening of FOC based induction machine drive.

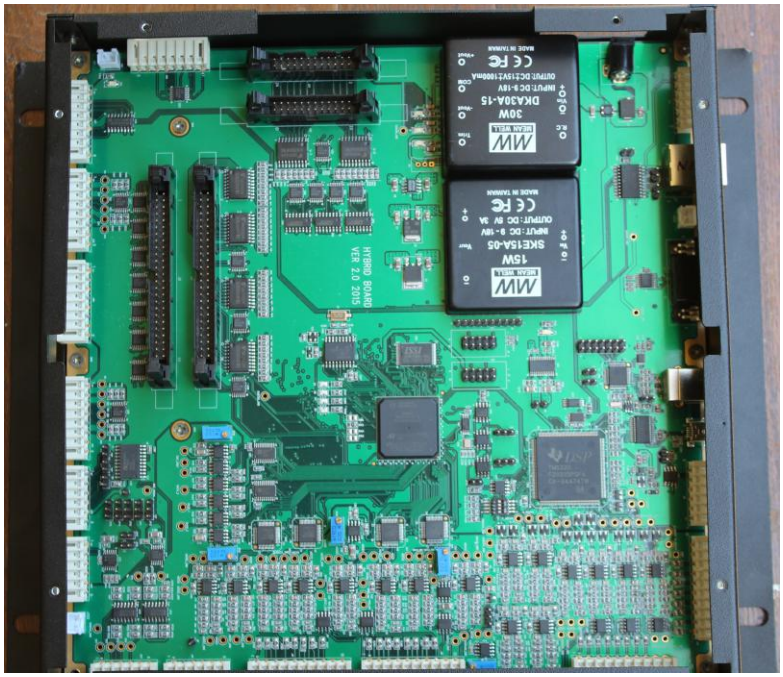

Figure 3.2: The DSP board which is developed in the lab

Figure.3.2 shows the DSP board, which is used for the digital controller implementation of FOC based field weakening of induction machine.

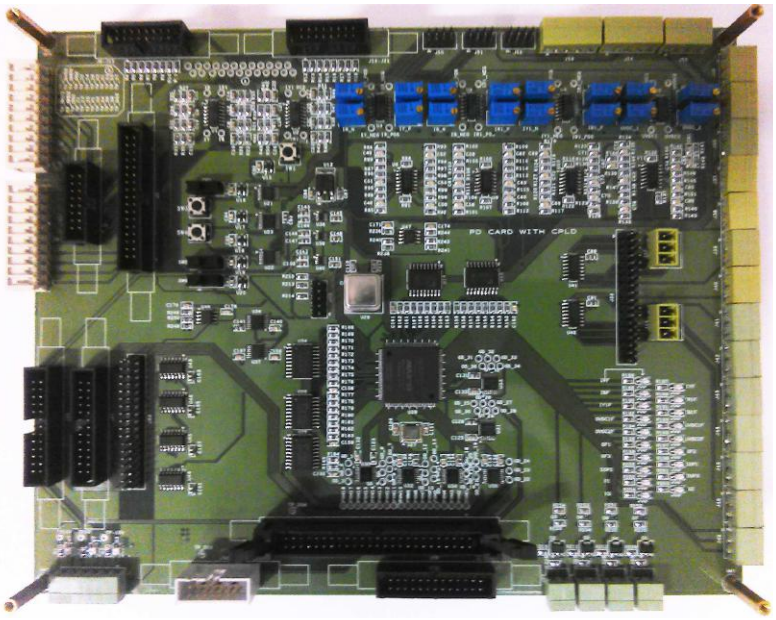

Figure 3.3: Protection and delay card

Figure.3.3 shows the Protection and delay card used in this project.

Figure 3.4: Voltage sensor

Figure.3.4 shows Hall effect based LV25P voltage sensor used in this project.

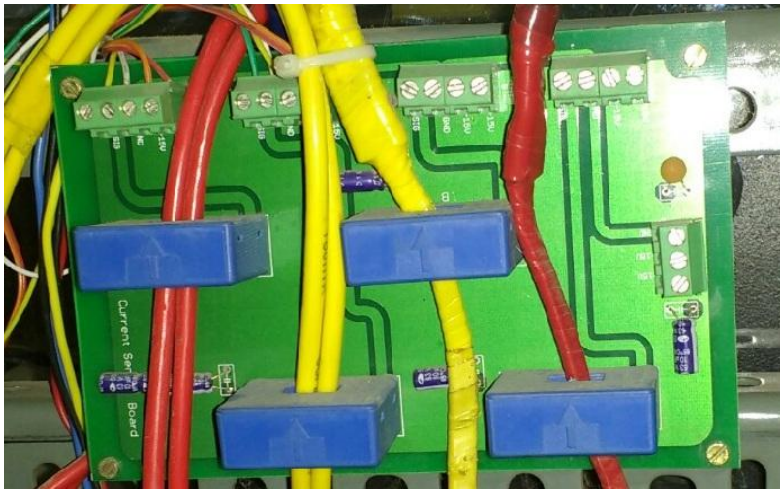

Figure 3.5: Current sensor

Figure.3.5 shows the hall effect based LA100P current sensors used in this project.

3.7 Conclusion

This chapter outlined the features of the TMS320F28335 that are used in implementing the field weakening algorithms. The additional hardware used for sensing the voltages and currents and interfacing between the various circuits are also discussed.

CHAPTER 4

RESULTS AND INFERENCES

4.1 Simulation Results

The simulation of the FOC based field weakening method is done in SIMULINK using the model of 630 kW induction machine. The same simulation is done in 30 kW induction machine used for hardware implementation. The results obtained are presented in the following sections. The machine rating and parameters of 630 kW machine are given in Table. 4.1 and Table. 4.2. The base speed value of 129.46 rad/sec(elect) and transition speed value of 842.12 rad/sec (elect) are calculated using the parameters of the 630 kW machine.

Table 4.1: Ratings for the 630 kW motor

Parameter	**Value**
Power	630 kW
Voltage	2028 V
Current	330 A
No of poles	4
Connection	Star
Speed	600 rpm
Rotor type	Squirrel Cage

Table 4.2: Model parameters of 630 kW machine

R_s	$R_r^{'}$	L_{ls}	L_{lr}	L_m	J
0.114 Ω	0.130 Ω	2.711 mH	2.033 mH	73.51 mH	250 $kg-m^2$

4.1.1 630 kW induction machine

The simulation results of 630 kW induction machine for a speed reference of 3000 rpm are given below.

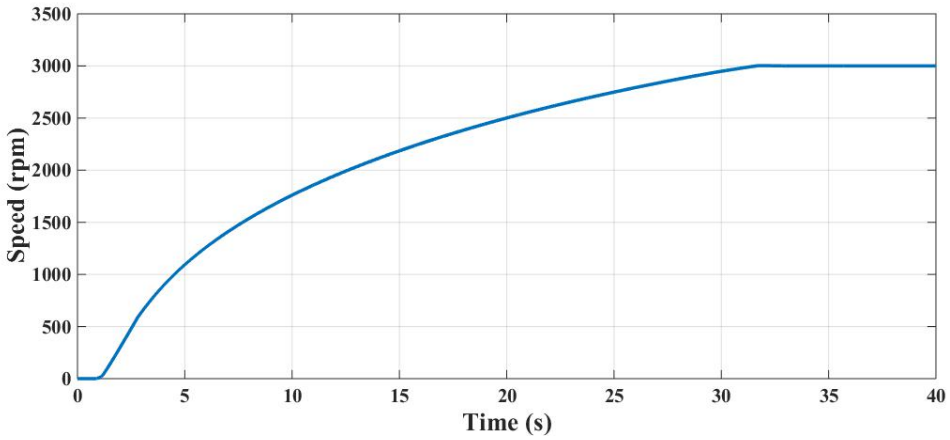

Figure 4.1: *Simulation result*: Speed response for a speed reference of 3000 rpm (*Scale: X-axis: 5.0 s/div, Y-axis: 500 rpm/div)*

Fig. 4.1 shows the simulated speed response for a speed reference of 3000 rpm. The motor accelerates after the initial flux build up and settles to the reference speed after 32 seconds.

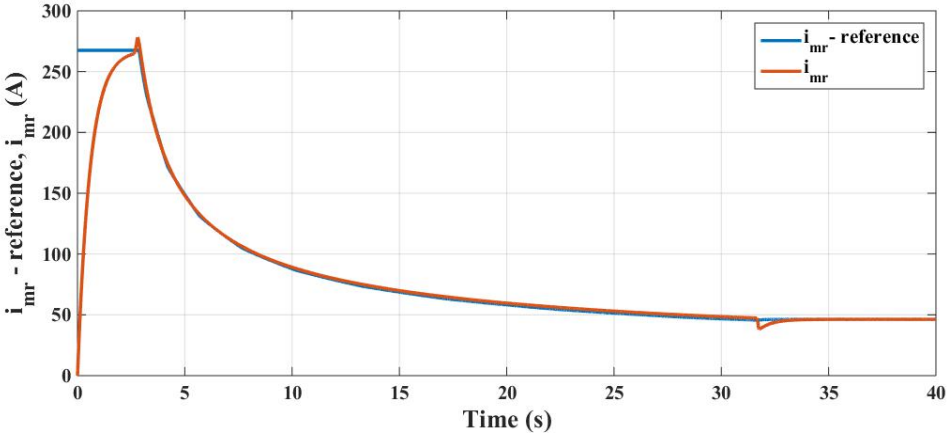

Figure 4.2: *Simulation result*: i^*_{mr} and i_{mr} waveforms for a speed reference of 3000 rpm (*Scale: X-axis: 5.0 s/div, Y-axis: 50 A/div)*

Fig. 4.2 shows the reference and actual magnetising component of current ($i_{mr} - reference$ and i_{mr}) for a speed reference of 3000 rpm. The i_{mr} takes initial flux building

time to reach $i_{mr} - reference$. It can be seen that the $i_{mr} - reference$ and i_{mr} are constant below the base speed and are reducing in the *field weakening region I*.

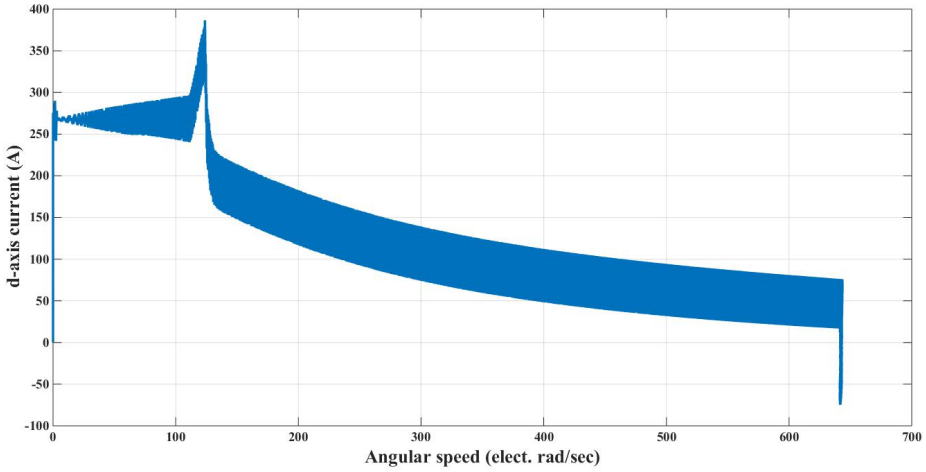

Figure 4.3: *Simulation result*: Response of i_{sd} with respect to ω for a speed reference of 3000 rpm (*Scale: X-axis: 100 elect. rad/sec/div, Y-axis: 50 A/div)*

Fig. 4.3 shows the response of i_{sd} with respect to ω for a speed reference of 3000 rpm. The i_{sd} is constant below the base speed and is decreasing in *field weakening region I*. A kink is seen in the simulated i_{sd} waveform at the base speed of the machine which can be smoothened by fine tuning the PI controllers.

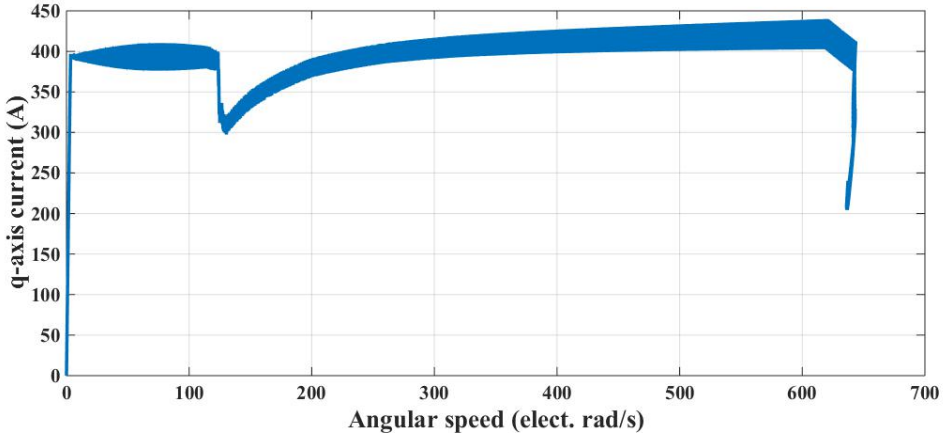

Figure 4.4: *Simulation result*: Response of i_{sq} with respect to ω for a speed reference of 3000 rpm (*Scale: X-axis: 100 elect. rad/sec/div, Y-axis: 50 A/div)*

Fig. 4.4 shows the response of i_{sq} with respect to ω for a speed reference of 3000 rpm. The i_{sq} value is constant below the base speed and slightly increasing in *field*

weakening region I since i_{sq}-limit is increasing. Here also the dip in the i_{sq} waveform can be smoothened by fine tuning of the PI controllers.

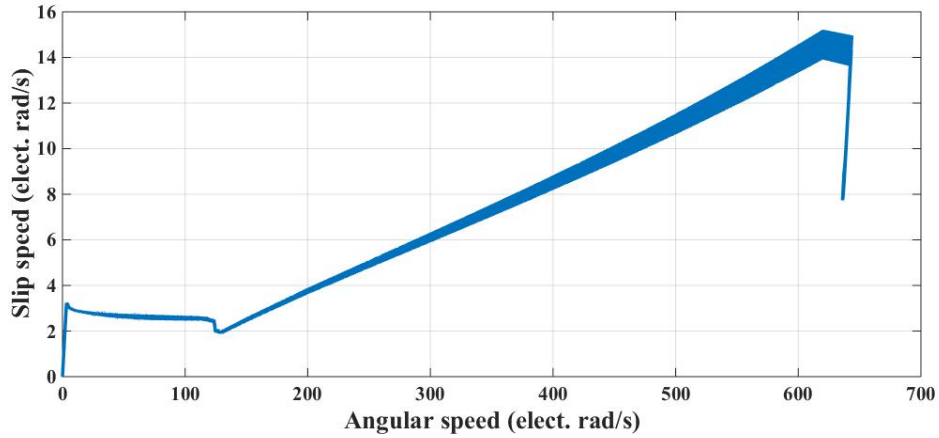

Figure 4.5: *Simulation result*: Variation of Slip speed with respect to ω for a speed reference of 3000 rpm (*Scale: X-axis: 100 elect. rad/sec/div, Y-axis: 2 elect. rad/sec/div)*

Fig. 4.5 shows the variation of slip speed of the machine with respect to ω for a speed reference of 3000 rpm. The slip speed of the machine is constant below the base speed since controller limits are constant. The slip speed is increasing in *field weakening region I* due to dynamic nature of controller limits and flux reference in this region.

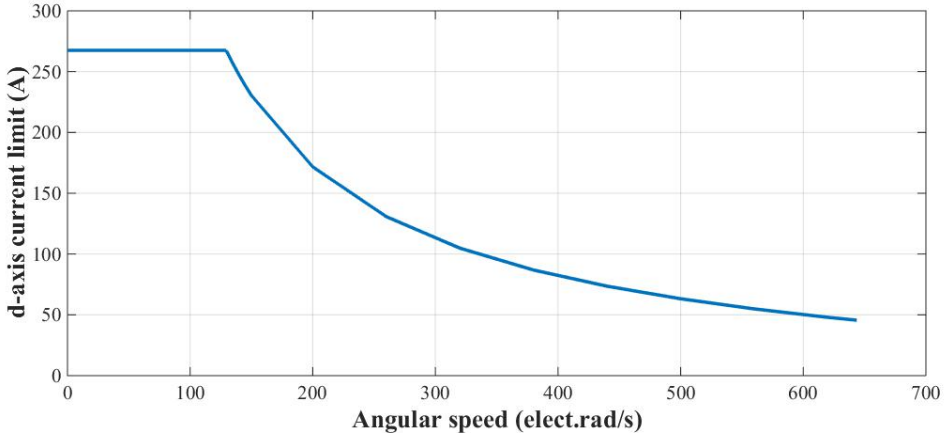

Figure 4.6: *Simulation result*: Variation of $i_{sd} - limit$ with respect to ω for a speed reference of 3000 rpm (*Scale: X-axis: 100 elect. rad/sec/div, Y-axis: 50 A/div)*

Fig. 4.6 shows the variation of $i_{sd} - limit$ with respect to ω for a speed reference

of 3000 rpm . The $i_{sd} - limit$ is constant below the base speed and decreasing in *field weakening region I.*

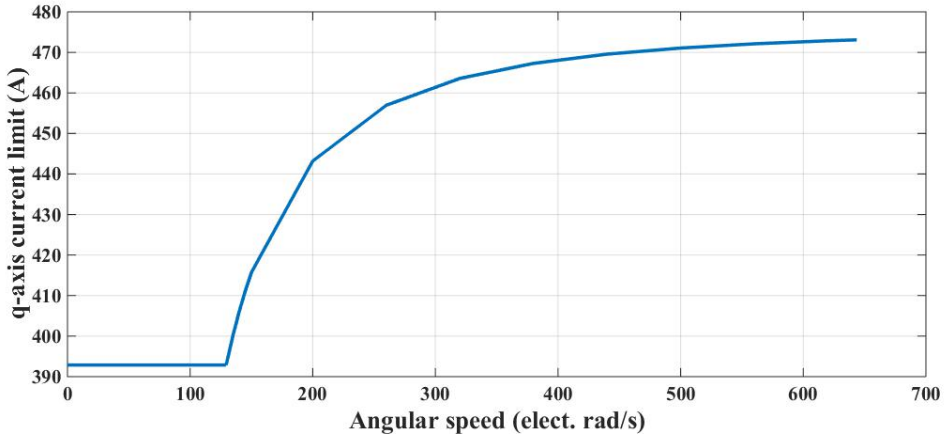

Figure 4.7: *Simulation result*: Variation of $i_{sq} - limit$ with respect to ω for speed reference of 3000 rpm (*Scale: X-axis: 100 elect. rad/sec/div, Y-axis: 10 A/div)*

Fig. 4.7 shows the variation of $i_{sq} - limit$ with respect to ω for a speed reference of 3000 rpm. The $i_{sq} - limit$ is constant below the base speed and increasing in *field weakening region I.* However, it can be noted that the increase in $i_{sq} - limit$ is much smaller when compared to the decrease in $i_{sd} - limit$ in *field weakening region I.*

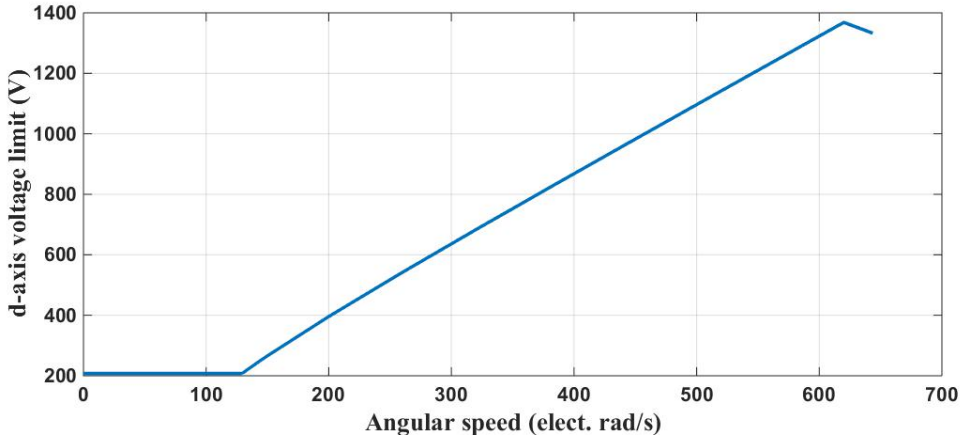

Figure 4.8: *Simulation result*: Variation of $v_{sd} - limit$ with respect to ω for speed reference of 3000 rpm (*Scale: X-axis: 100 elect. rad/sec/div, Y-axis: 200 V/div)*

Fig. 4.8 shows the variation of $v_{sd} - limit$ with respect to ω for a speed reference of 3000 rpm. The $v_{sd} - limit$ is constant below the base speed and dynamically changes with respect to speed in *field weakening region I.*

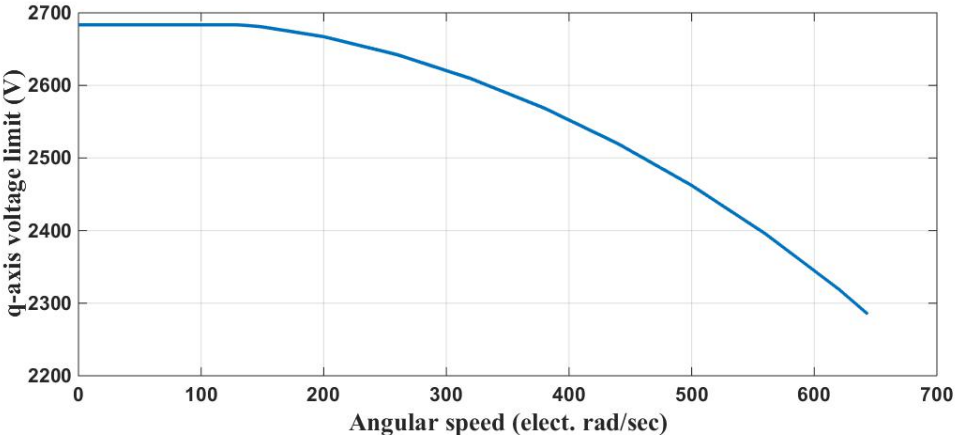

Figure 4.9: *Simulation result*: Variation of $v_{sq} - limit$ with respect to ω for speed reference of 3000 rpm (*Scale: X-axis: 100 elect. rad/sec/div, Y-axis: 100 V/div)*

Fig. 4.9 shows the variation of $v_{sq} - limit$ with respect to ω for a speed reference of 3000 rpm. The $v_{sq} - limit$ is constant below the base speed and dynamically changes with speed in *field weakening region I*.

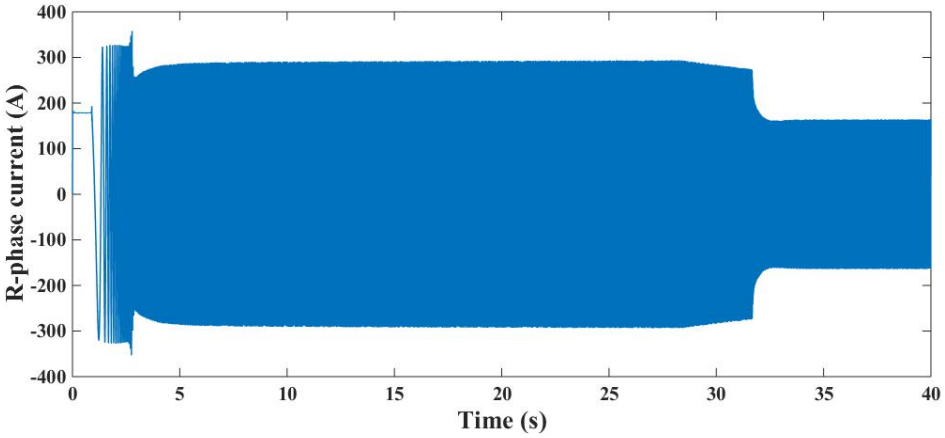

Figure 4.10: *Simulation result*: R-phase current profile for speed reference of 3000 rpm (*Scale: X-axis: 5s/div, Y-axis: 100 A/div)*

Fig. 4.10 shows the simulated response of phase current for a speed reference of 3000 rpm. The phase current drawn is very high during the accelaration region and once the motor reaches the steady state, the current drawn will reduce to a value decided by the load that is applied.

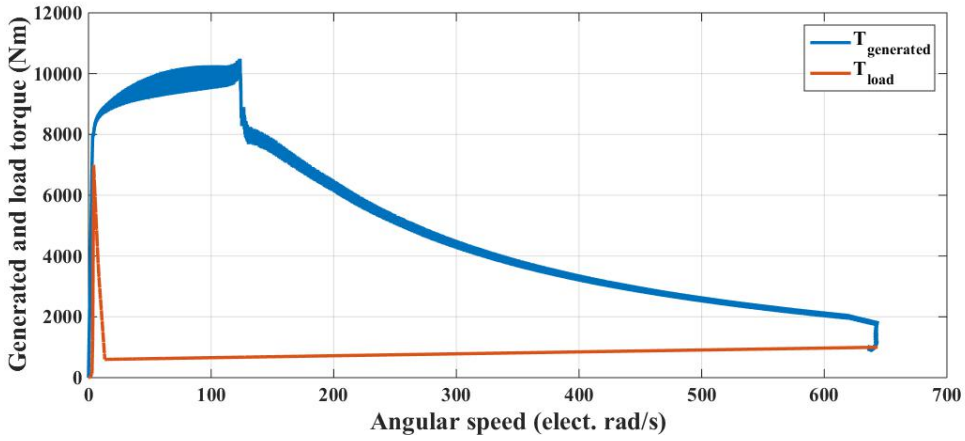

Figure 4.11: *Simulation result*: Response of generated and load torque with respect to ω for speed reference of 3000 rpm (*Scale: X-axis: 100 elect. rad/sec/div, Y-axis: 2000 Nm/div)*

Fig. 4.11 shows the simulated response of the generated torque and load torque of the machine with respect to the angular speed for a speed reference is 3000 rpm. The generated torque of the machine is reducing in the *field weakening region I*. The load on the machine is very high during starting of the machine since it is a traction load.

4.1.2 30 kW induction machine

The machine rating and parameters of 30 kW machine is given in Table. 4.3 and Table. 4.4

Table 4.3: Ratings for the 30 kW motor

Parameter	**Value**
Power	30 kW
Voltage	380 V
Current	59 A
Power factor	0.88
Connection	Δ
Speed	1450 rpm
Rotor type	Squirrel Cage

Table 4.4: Model parameters of 30 kW machine

R_s	$R_r^{'}$	L_{ls}	L_{lr}	L_m	J
0.127 Ω	0.127 Ω	1.341 mH	1.341 mH	45.219 mH	1.631 $kg-m^2$

For studying the performance of the 30 kW induction machine in field weakening region, the base speed, ω_{base} of the machine is kept as $62.83 rad/s(elect)$ by reducing the DC-bus voltage. The transition speed between *field weakening region I* and *field weakening region II*, ω_1 is $230.57 rad/s(elect)$ at this condition.

4.1.2.1 The step change of speed reference from below base speed region to field weakening region I

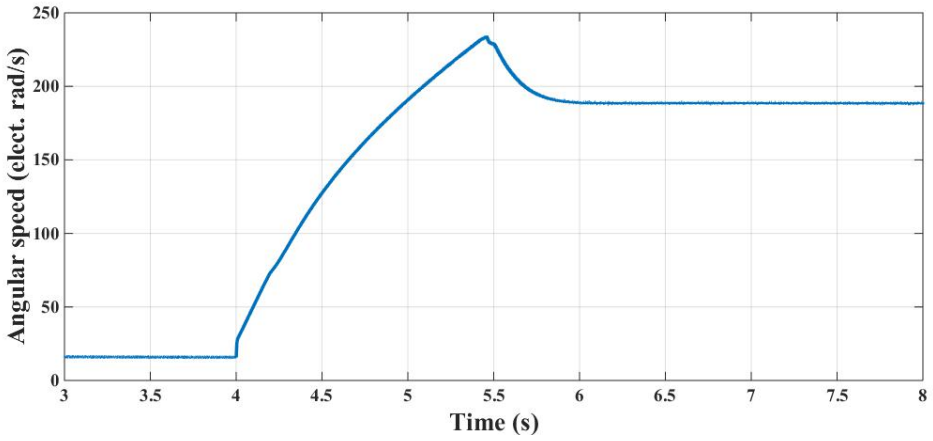

Figure 4.12: *Simulation result*: Angular speed waveform for a step change of speed reference (*Scale: X-axis: 0.5 s/div, Y-axis: 50 elect. rad/s/div)*

Fig. 4.12 shows the angular speed of the machine for a step change of speed reference. The motor accelerates from 4 seconds and settles to the reference speed after 6 seconds. The overshoot in the speed response can be reduced by tuning the parameters of speed controller.

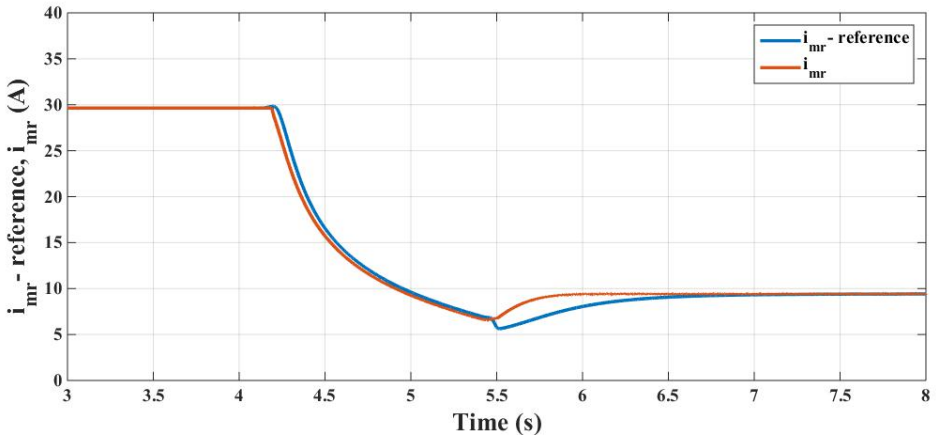

Figure 4.13: *Simulation result*: i^*_{mr} and i_{mr} waveforms for a step change of speed reference (*Scale: X-axis: 0.5 s/div, Y-axis: 5 A/div)*

Fig. 4.13 shows the reference and actual magnetising component of current ($i_{mr} - reference$ and i_{mr}) for a step change of speed reference. Both the currents are constant below the base speed and decreases in the *field weakening region I*. At 5.5 sec, a mismatch is seen between actual and reference values of i_{mr}. This is the region where the motor speed overshoots and settle to the steady state value. Finer tuning of speed controller will minimize this mismatch.

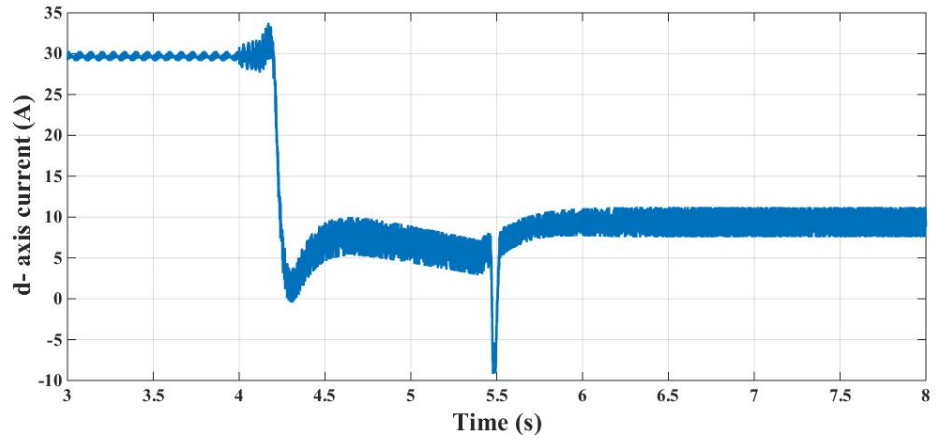

Figure 4.14: *Simulation result*: Response of i_{sd} for a step change of speed reference (*Scale: X-axis: 0.5 s/div, Y-axis: 5 A/div)*

Fig. 4.14 shows the response of i_{sd} for a step change of speed reference. The i_{sd} remains constant below the base speed and decreases in *field weakening region I*. An abrupt dip in i_{sd} is seen at 5.5 sec which can be attributed to the speed overshoot mentioned above.

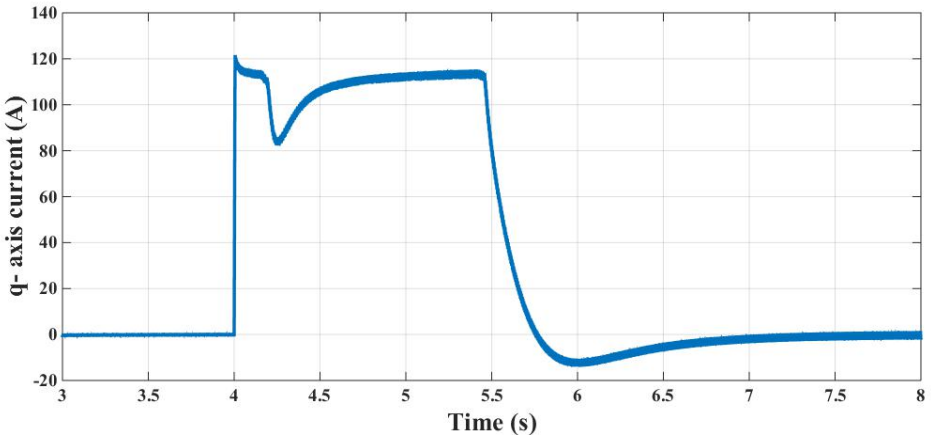

Figure 4.15: *Simulation result*: Response of i_{sq} for a step change of speed reference (*Scale: X-axis: 0.5 s/div, Y-axis: 20 A/div)*

Fig. 4.15 shows the response of i_{sq} for a step change of speed reference. Here also the dip in the i_{sq} waveform can be smoothened by fine tuning of the PI controller. The i_{sq} become very small at steady state since load applied to the machine is low.

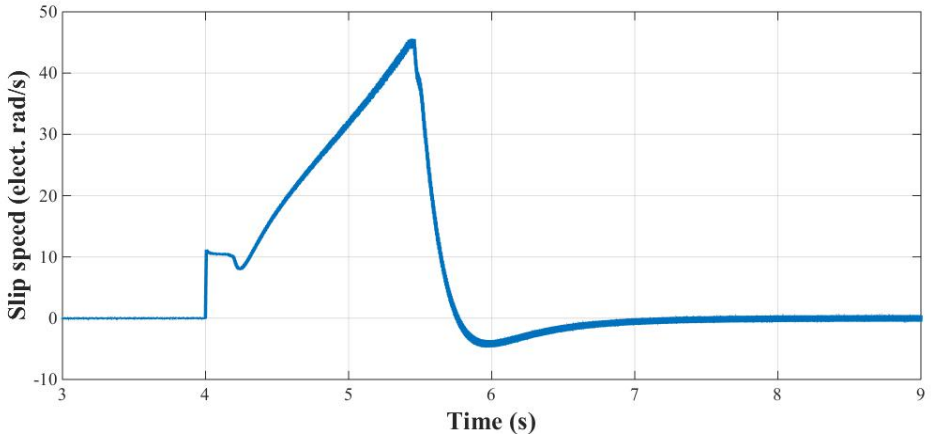

Figure 4.16: *Simulation result*: Variation in Slip speed of the machine for a step change of speed reference (*Scale: X-axis: 1 s/div, Y-axis: 10 elect. rad/s/div)*

Fig. 4.16 shows the variation in slip speed of the machine for a step change of speed reference. The slip speed of the machine is constant below the base speed since controller limits are constant. The slip speed is increasing in *field weakening region I* due to dynamic nature of controller limits and $i_{mr} - reference$ in this region.

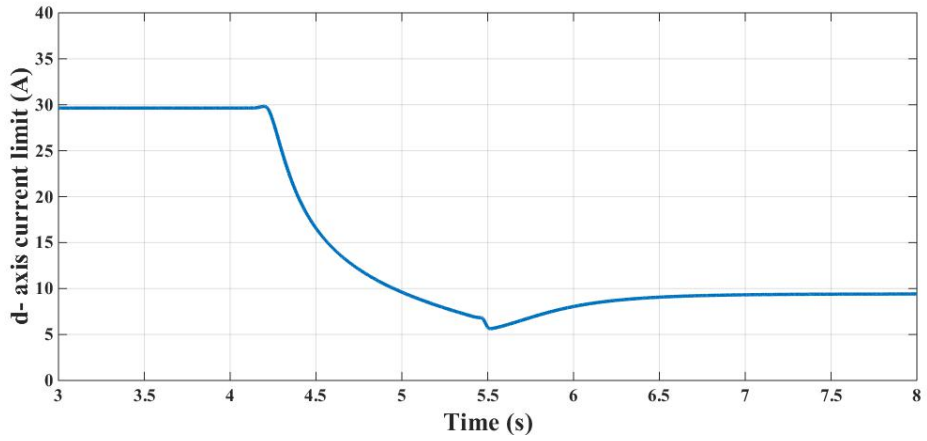

Figure 4.17: *Simulation result*: Variation in $i_{sd} - limit$ for a step change of speed reference (*Scale: X-axis: 0.5 s/div, Y-axis: 5 A/div)*

Fig. 4.17 shows the variation in $i_{sd} - limit$ for a step change of speed reference. The $i_{sd} - limit$ remains constant below base the speed and decreases in *field weakening region I*. The steady state value of $i_{sd} - limit$ is determined by the steady state angular speed of the drive.

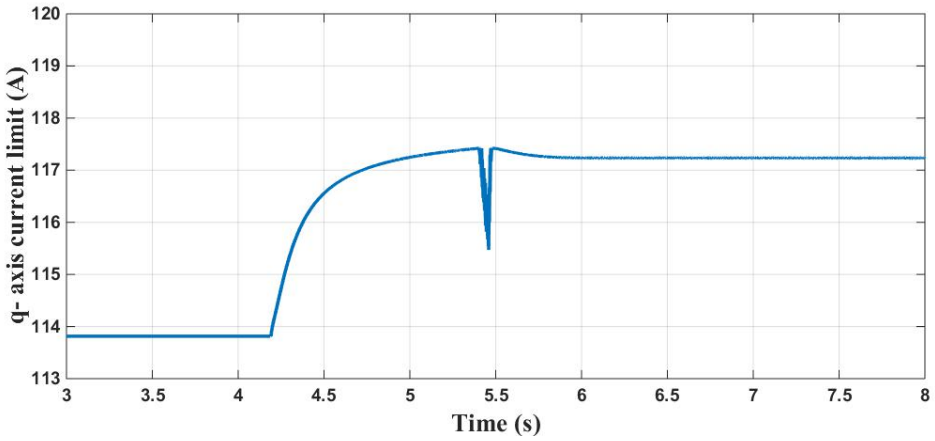

Figure 4.18: *Simulation result*: Variation in $i_{sq} - limit$ for a step change of speed reference (*Scale: X-axis: 0.5 s/div, Y-axis: 1 A/div)*

Fig. 4.18 shows the variation in $i_{sq} - limit$ for a step change of speed reference. The $i_{sq} - limit$ is remains constant below the base speed and slightly increases in *field weakening region I*. However it can be noted that the increase in i_{sq} is much smaller when compared to decrease in i_{sd} in *field weakening region I*. Here also a kink is observed in the waveform at 5.5 sec where the speed overshoot happens. Finer tuning of PI controller will smoothen this kink.

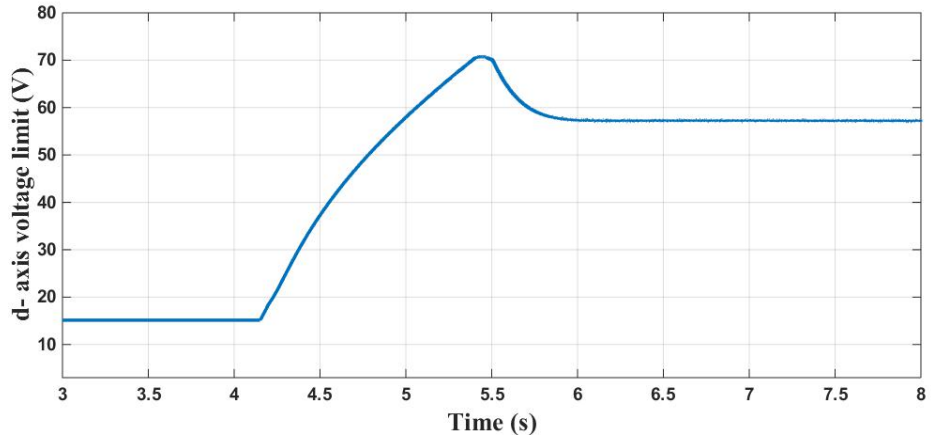

Figure 4.19: *Simulation result*: Variation in $v_{sd} - limit$ for a step change of speed reference (*Scale: X-axis: 0.5 s/div, Y-axis: 10 V/div)*

Fig. 4.19 shows the variation in $v_{sd} - limit$ for a step change of speed reference. The $v_{sd} - limit$ remains constant below the base speed and dynamically varies in *field weakening region I*. The steady state value of $v_{sd} - limit$ determined by the steady state angular speed of the drive.

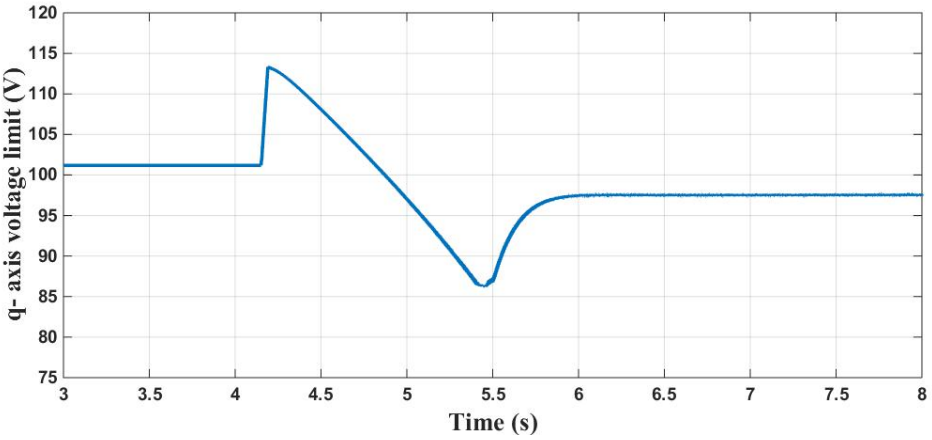

Figure 4.20: *Simulation result*: Variation in $v_{sq} - limit$ for a step change of speed reference (*Scale: X-axis: 0.5 s/div, Y-axis: 5 V/div)*

Fig. 4.20 shows the variation in $v_{sq} - limit$ for a step change of speed reference. The $v_{sq} - limit$ remains constant in below base speed region and dynamically varies in *field weakening region I*. The steady state value of $v_{sq} - limit$ determined my steady state angular speed of the drive.

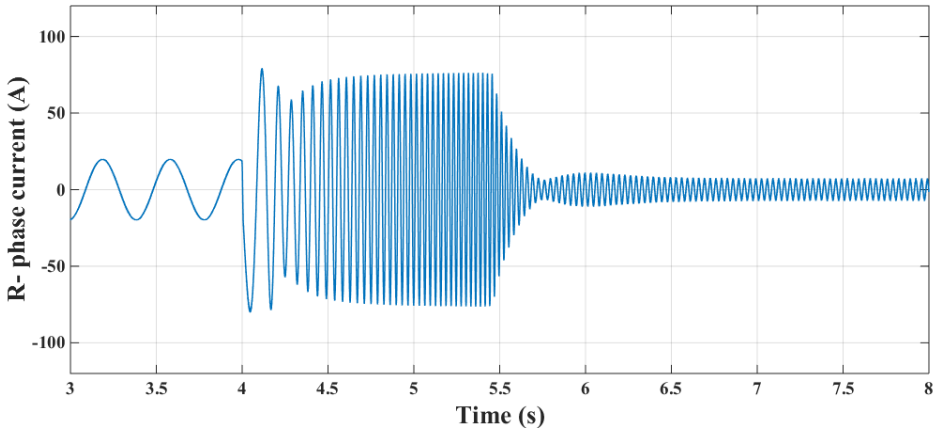

Figure 4.21: *Simulation result*: R- phase current waveform for a step change of speed reference (*Scale: X-axis: 0.5 s/div, Y-axis: 50 A/div)*

Fig. 4.21 shows the R- phase current waveform for a step change of speed reference. The phase current drawn is very high during the acceleration region and once the motor reaches the steady state, the current drawn will reduced to small value since the machine operates at no load.

4.1.2.2 The step change of speed reference from field weakening region I to field weakening region II

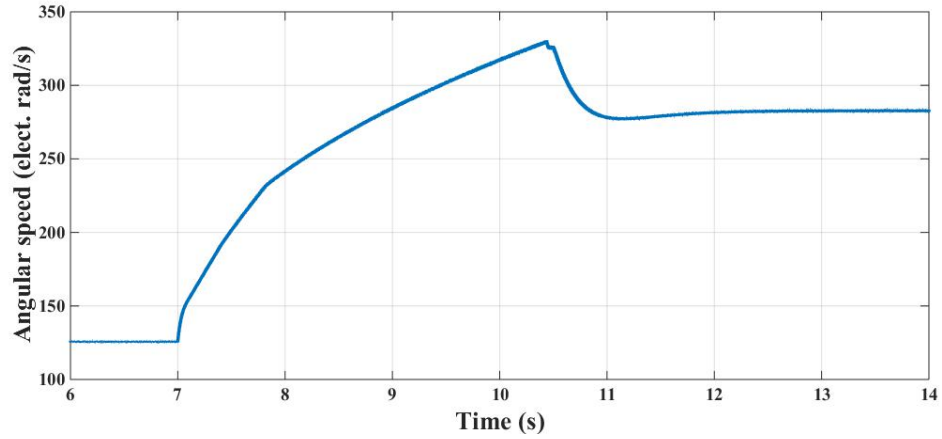

Figure 4.22: *Simulation result*: Angular speed waveform for a step change of speed reference (*Scale: X-axis: 1 s/div, Y-axis: 50 elect. rad/s/div)*

Fig. 4.22 shows the angular speed response of the machine for a step change of speed reference. Transition of speed from 0.4 pu to 0.9 pu will result in switching of the drive

from *field weakening region I* to *field weakening region II*. The overshoot in the speed response can be reduced by tuning the speed controller.

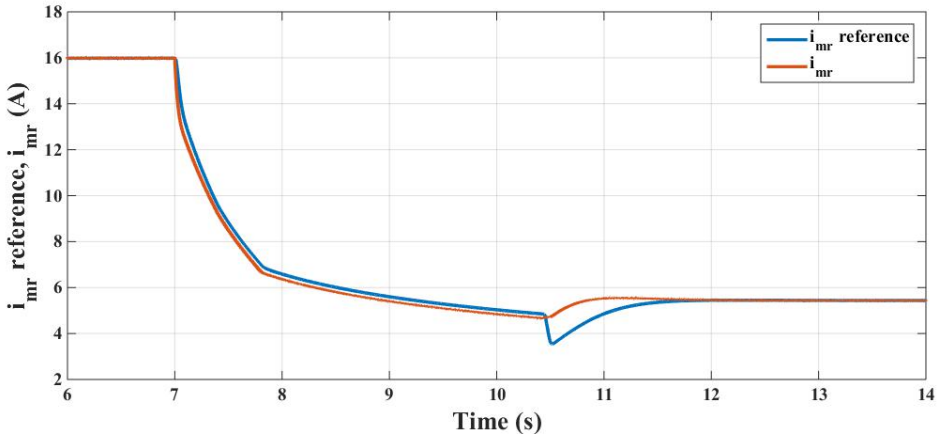

Figure 4.23: *Simulation result*: i^*_{mr} and i_{mr} for a step change of speed reference (*Scale: X-axis: 1 s/div, Y-axis: 2 A/div)*

Fig. 4.23 show the reference and actual magnetising component of current ($i_{mr} - reference$ and i_{mr}) for a step change of speed reference. The $i_{mr} - reference$ and i_{mr} are reduce in the *field weakening region I* and *field weakening region II*. At 10.5 sec, a mismatch is seen between the actual and reference values of i_{mr}. This is the region where the motor speed overshoots and settles to the steady state value. Finer tuning of speed controller will minimize this mismatch.

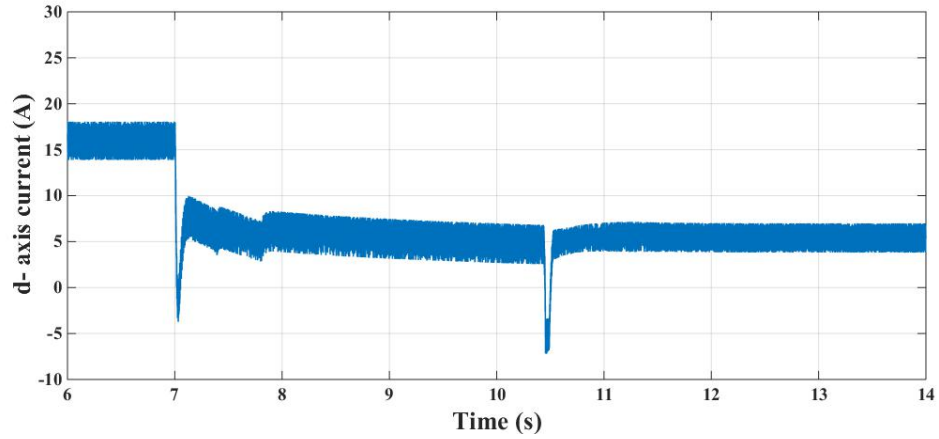

Figure 4.24: *Simulation result*: Response of i_{sd} for a step change of speed reference (*Scale: X-axis: 1 s/div, Y-axis: 5 A/div)*

Fig. 4.24 shows the response of i_{sd} for a step change of speed reference. The i_{sd} is

decreasing in *field weakening region I* and *field weakening region II*. An abrupt dip in i_{sd} is seen at 10.5 sec which can be attributed to the speed overshoot mentioned above.

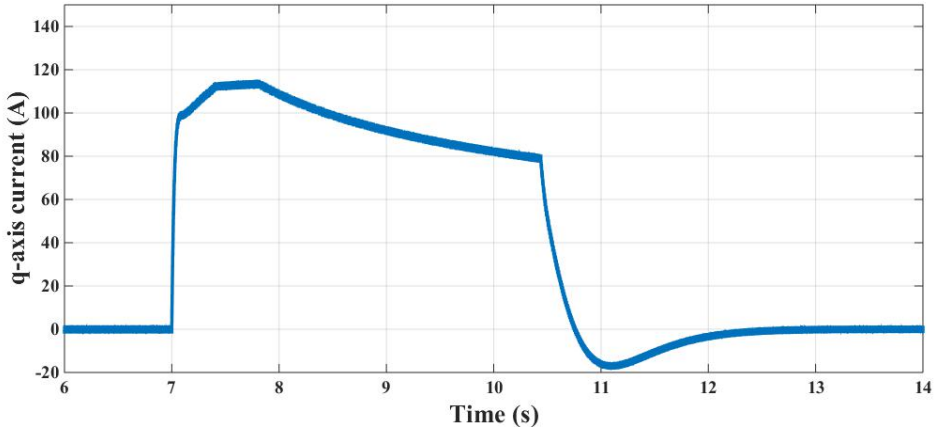

Figure 4.25: *Simulation result*: Response of i_{sq} for a step change of speed reference (*Scale: X-axis: 1 s/div, Y-axis: 20 A/div)*

Fig. 4.25 shows the response of i_{sq} for a step change of speed reference The i_{sq} becomes very small at steady state since load applied to the machine is low.

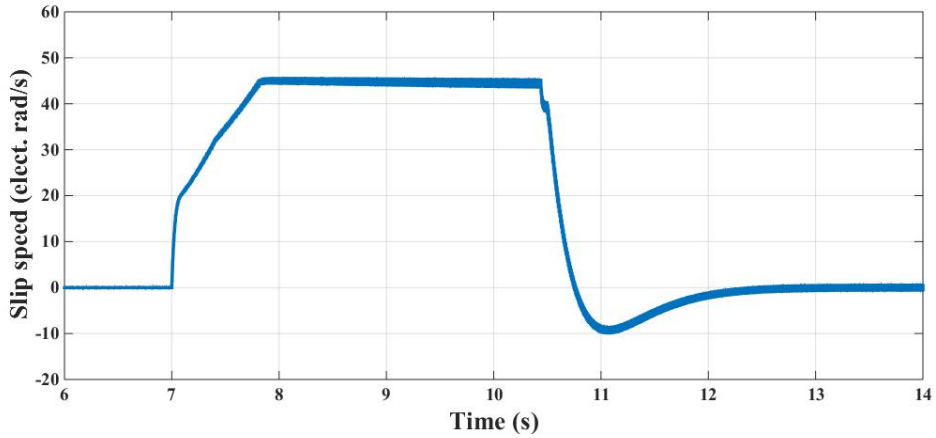

Figure 4.26: *Simulation result*: Variation of slip speed of the machine for a step change of speed reference (*Scale: X-axis: 1 s/div, Y-axis: 10/div)*

Fig. 4.26 shows the response of slip speed of the machine for a step change of speed reference. The slip speed is increasing in *field weakening region I* due to dynamic nature of controller limits and i_{mr} in this region. At the transition speed where *field weakening region I* to *field weakening region II* occur, the slip speed becomes maximum and remains there in *field weakening region II*. When the speed of the machine settles

to the reference speed, the slip speed of the machine reduces to a small value since i_{sq} is very small in no load condition.

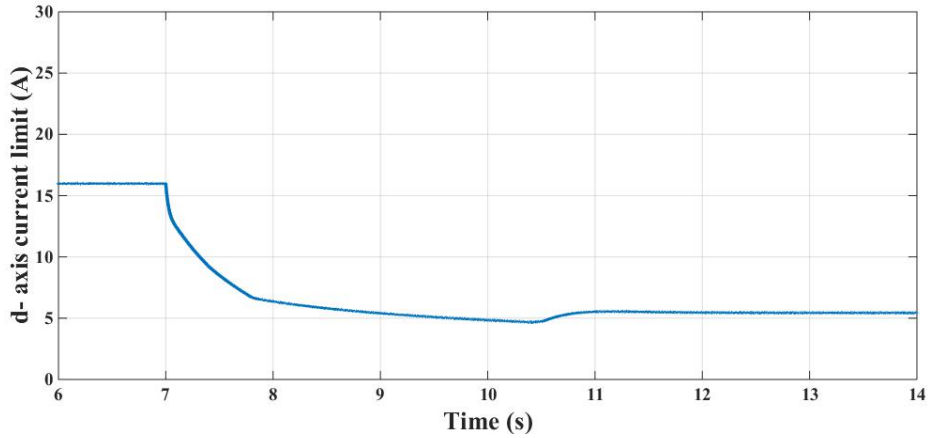

Figure 4.27: *Simulation result*: Variation in $i_{sd} - limit$ for a step change of speed reference (*Scale: X-axis: 1 s/div, Y-axis: 5 A/div)*

Fig. 4.27 shows the variation in $i_{sd} - limit$ for a step change of speed reference. The $i_{sd} - limit$ decreases in *field weakening region I* and *field weakening region II* at different rates. The steady state value of $i_{sd} - limit$ is decided by the steady state angular speed of the machine.

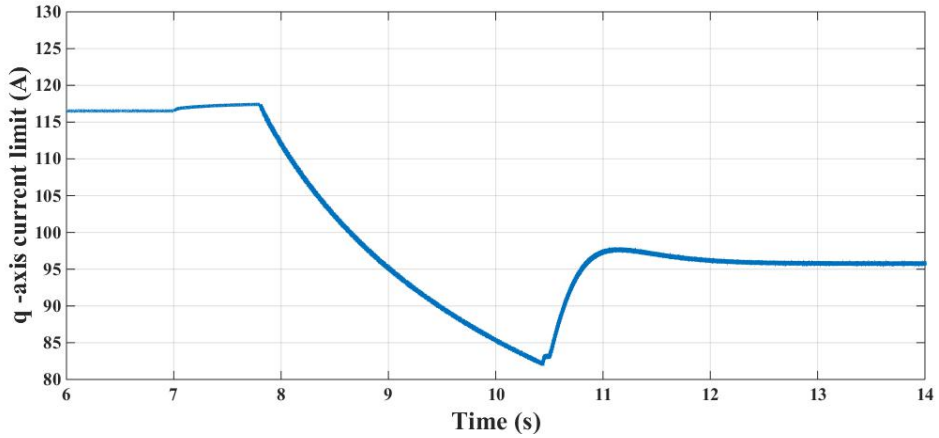

Figure 4.28: *Simulation result*: Variation in $i_{sq} - limit$ for a step change of speed reference from 0.4 pu to 0.9 pu (*Scale: X-axis: 1 s/div, Y-axis: 5 A/div)*

Fig. 4.28 shows the variation in $i_{sq} - limit$ for a step change of speed reference. The $i_{sq} - limit$ is slightly increasing in *field weakening region I* and decreasing in *field weakening region II*. The increase in $i_{sq} - limit$ in *field weakening region I* is very small

compared with decrease in $i_{sd} - limit$ in that region. The steady state value of $i_{sq} - limit$ is decided by steady state angular speed of the drive.

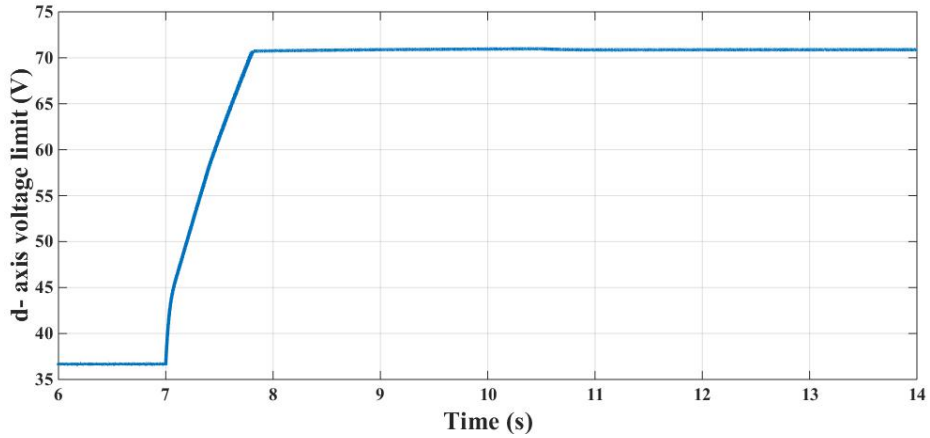

Figure 4.29: *Simulation result*: Variation in $v_{sd} - limit$ for a step change of speed reference (*Scale: X-axis: 1 s/div, Y-axis: 5 V/div)*

Fig. 4.29 shows the variation in $v_{sd} - limit$ for a step change of speed reference. The $v_{sd} - limit$ is dynamically varying in *field weakening region I* and *field weakening region II*. The steady state value of $v_{sd} - limit$ is decided by steady state angular speed of the drive.

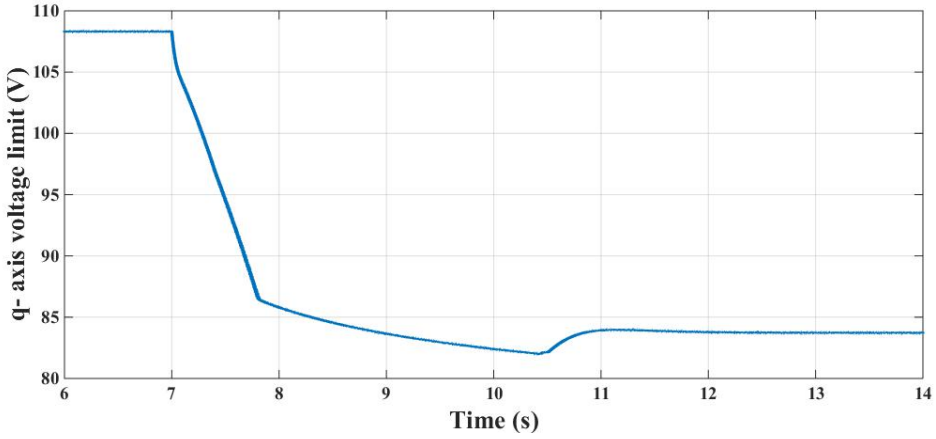

Figure 4.30: *Simulation result*: Variation in $v_{sq} - limit$ for a step change of speed reference (*Scale: X-axis: 1 s/div, Y-axis: 5 V/div)*

Fig. 4.40 shows the variation in $v_{sq} - limit$ for a step change of speed reference. The $v_{sq} - limit$ is dynamically varying in *field weakening region I* and *field weakening region region II*.The steady state value of $v_{sq} - limit$ is decided by steady state angular speed of the drive.

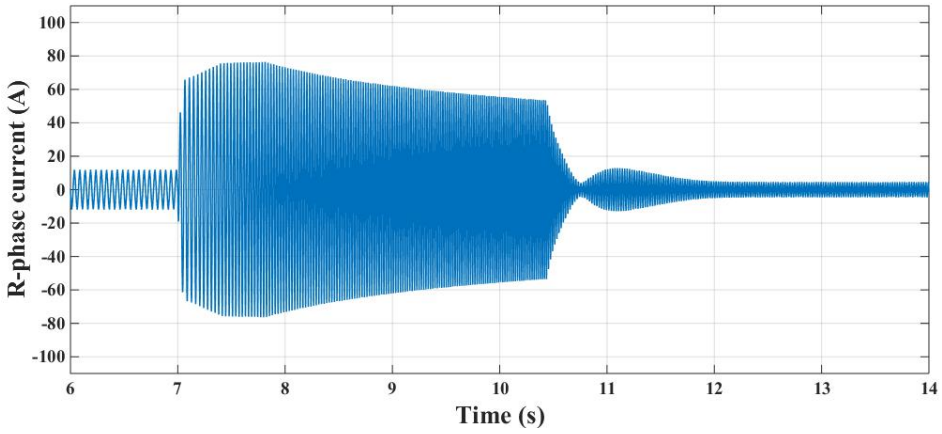

Figure 4.31: *Simulation result*: R- phase current waveform for a step change of speed reference from 0.4 pu to 0.9 pu (*Scale: X-axis: 1 s/div, Y-axis: 20 A/div)*

Fig. 4.31 shows the R- phase current waveform for a step change of speed reference. The phase current drawn is very high during the acceleration region and once the motor reaches the steady state, the current drawn will reduced to small value since the machine operates at no load.

4.1.2.3 Gradual change of speed reference from below base speed region to field weakening region II

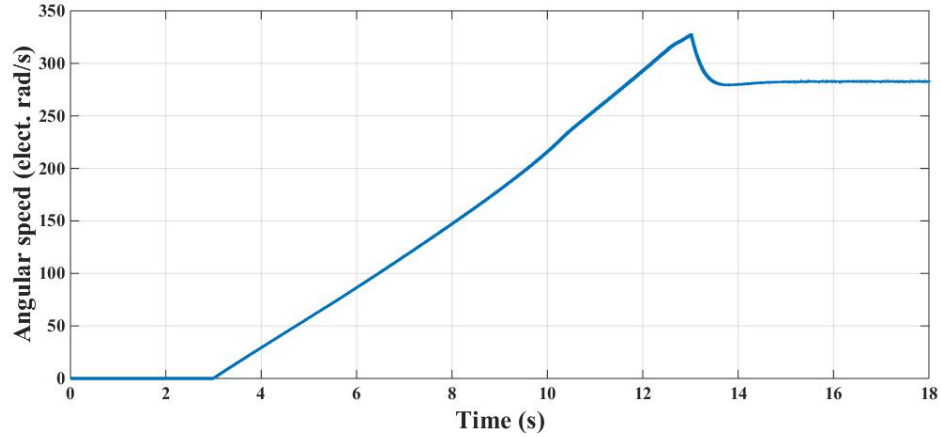

Figure 4.32: *Simulation result*: Angular speed waveform for a gradual change of speed reference (*Scale: X-axis: 2 s/div, Y-axis: 50 elect. rad/s/div)*

Fig. 4.32 shows the angular speed of the machine for a gradual change of speed reference. The motor accelerates after the initial flux build up and settles to the reference

speed after 13.5 seconds.

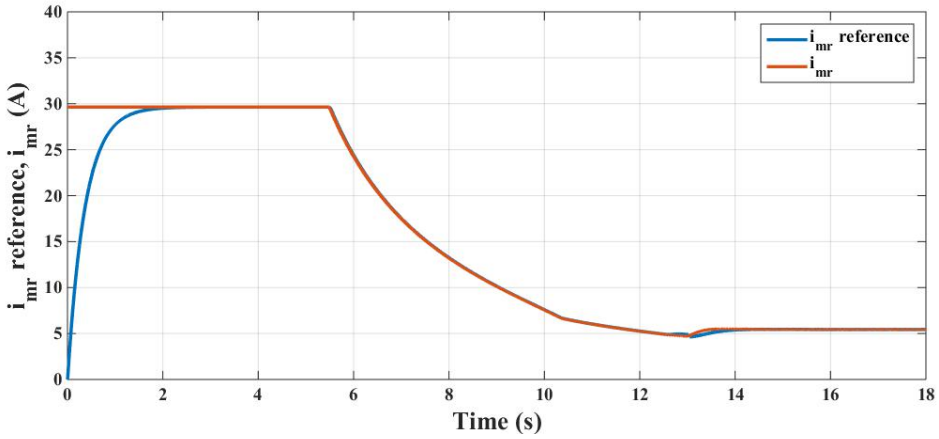

Figure 4.33: *Simulation result*: i^*_{mr} and i_{mr} for a gradual change of speed reference (*Scale: X-axis: 2 s/div, Y-axis: 5 A/div)*

Fig. 4.33 shows the reference and actual magnetising component of current ($i_{mr} - reference$ and i_{mr}) for a gradual change of speed reference. The $i_{mr} - reference$ and i_{mr} are constant below the base speed and reducing in the *field weakening region I* and*field weakening region II*. The rate of decrease is different in *field weakening region I* and *field weakening region II*.

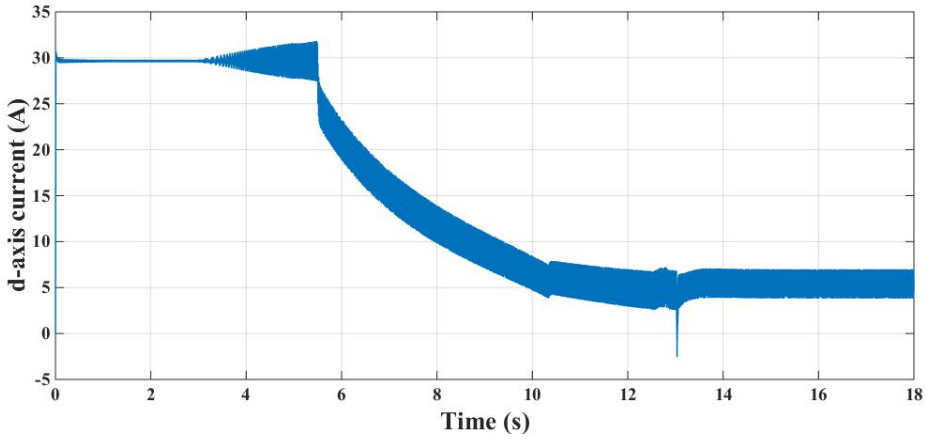

Figure 4.34: *Simulation result*: Response of i_{sd} for a gradual change of speed reference (*Scale: X-axis: 2 s/div, Y-axis: 5 A/div)*

Fig. 4.34 shows the response of i_{sd} for a gradual change of speed reference. The i_{sd} is constant below the base speed and decreasing in *field weakening region I* and *field weakening region II*. The rate of decrease is different in *field weakening region I* and *field weakening region II*. The steady state value of i_{sd} and i_{mr} are same.

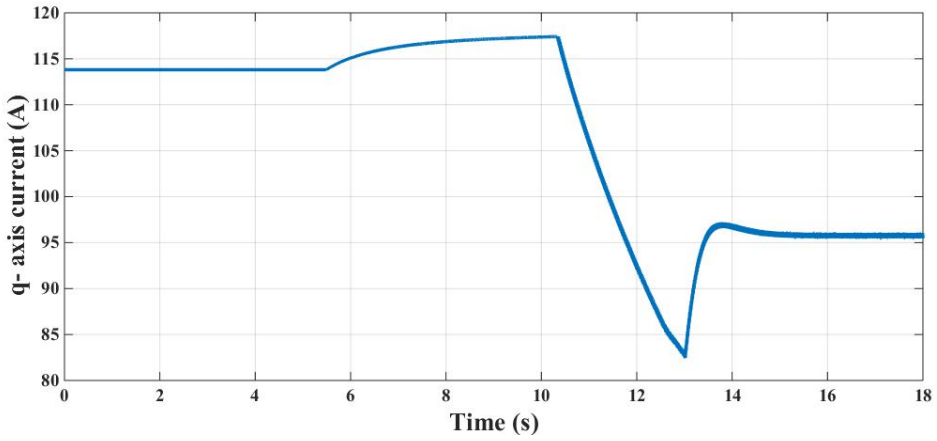

Figure 4.35: *Simulation result*: Response of i_{sq} for a gradual change of speed reference (*Scale: X-axis: 2 s/div, Y-axis: 5 A/div)*

Fig. 4.35 shows the response of i_{sq} for a gradual change of speed reference. Here also the dip in the i_{sq} waveform can be smoothened by fine tuning of the PI controller.

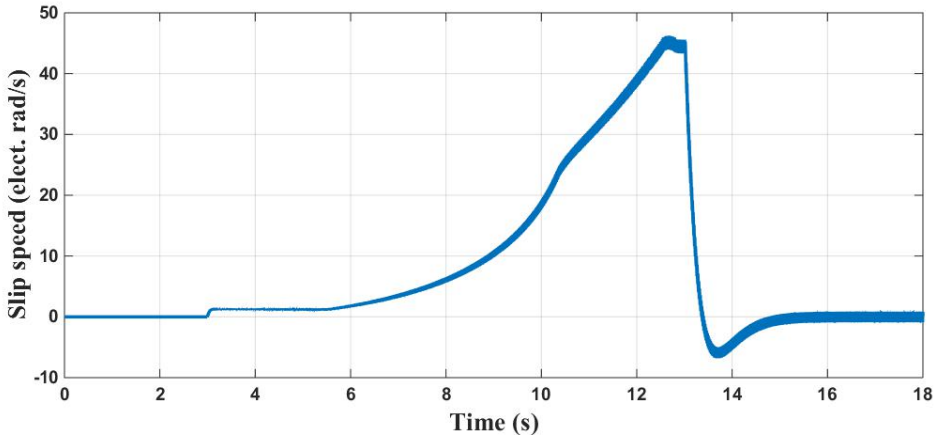

Figure 4.36: *Simulation result*: Variation in slip speed of the machine for a gradual change of speed reference (*Scale: X-axis: 2 s/div, Y-axis: 10/div)*

Fig. 4.36 shows the variation in slip speed of the machine for a gradual change of speed reference. Slip speed of the machine is constant below the base speed, since controller limits are constant. The slip speed increases in *field weakening region I* due to dynamic nature of controller limits and $i_{mr} - reference$ in this region. At the transition speed, ω_1 the slip speed become maximum and remains there in *field weakening region II*. When the speed of the machine settles to the reference speed, the slip speed of the machine reduces to a small value, since i_{sq} is very small in no load condition.

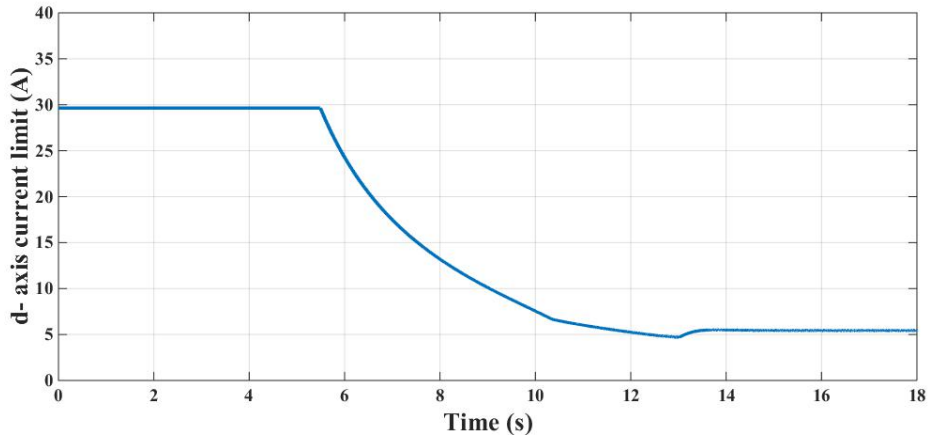

Figure 4.37: *Simulation result*: Variation in $i_{sd} - limit$ for a gradual change of speed reference (*Scale: X-axis: 2 s/div, Y-axis: 5 A/div)*

Fig. 4.37 shows the variation in $i_{sd} - limit$ for a gradual change of speed reference. The $i_{sd} - limit$ is constant below the base speed region and decreases in *field weakening region I* and *field weakening region II* at different rates. The steady state value of $i_{sd} - limit$ is decided by steady state angular speed of the drive.

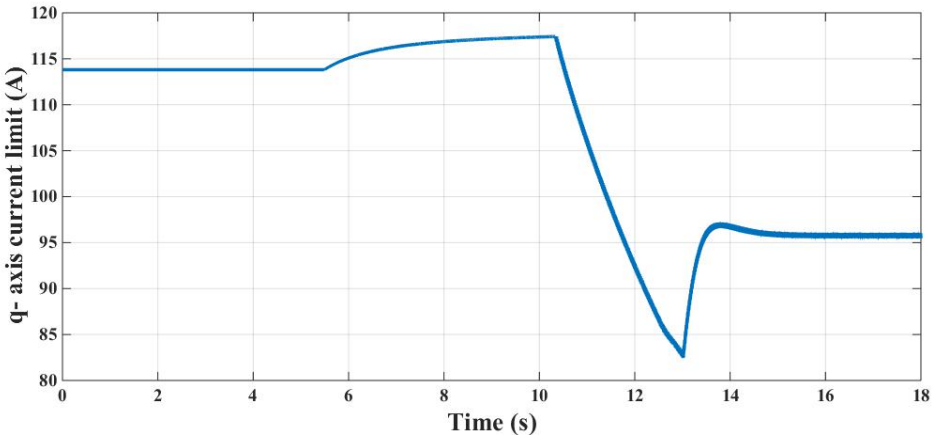

Figure 4.38: *Simulation result*: Variation in $i_{sq} - limit$ for a gradual change of speed reference (*Scale: X-axis: 2 s/div, Y-axis: 5 A/div)*

Fig. 4.38 shows the variation in $i_{sq} - limit$ for a gradual change of speed reference. The $i_{sq} - limit$ is slightly increases in *field weakening region I* and decreases in *field weakening region II*. It can be noted that the increase in $i_{sq} - limit$ is much smaller when compared to decrease in $i_{sd} - limit$ in *field weakening region I*. The steady state value of $i_{sq} - limit$ is decided by steady state angular speed of the drive.

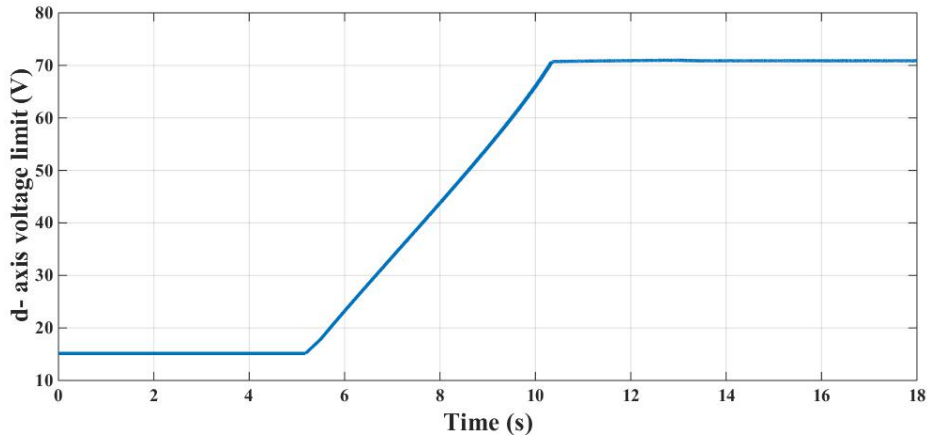

Figure 4.39: *Simulation result*: Variation in $v_{sd} - limit$ for a gradual change of speed reference (Scale: X-axis: 2 s/div, Y-axis: 10 V/div)

Fig. 4.39 shows the variation in $v_{sd} - limit$ for a gradual change of speed reference. The $v_{sd} - limit$ is constant below the base speed and dynamically varying in *field weakening region I* and *field weakening region II*. The steady state value of $v_{sd} - limit$ is decided by steady state angular speed of the drive.

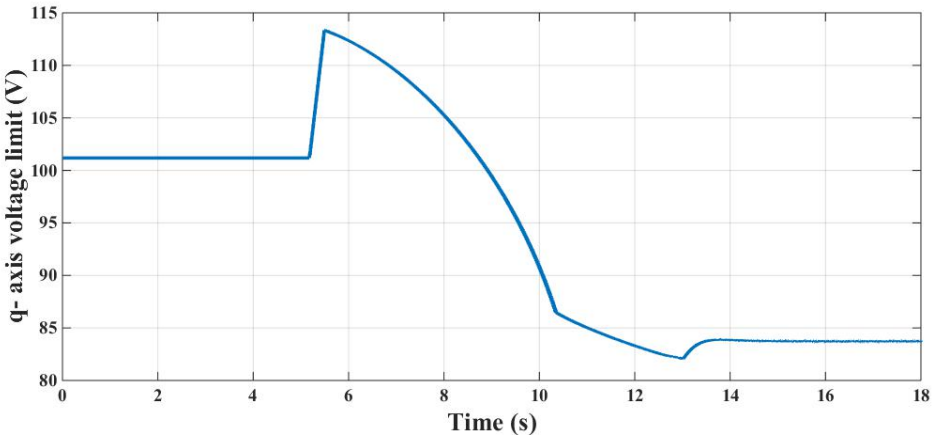

Figure 4.40: *Simulation result*: Variation $v_{sq} - limit$ for an gradual change of speed reference (Scale: X-axis: 2 s/div, Y-axis: 5 V/div)

Fig. 4.40 shows the variation in $v_{sq} - limit$ for a gradual change of speed from zero to 0.953 pu. The $v_{sq} - limit$ is constant below the base speed and dynamically varying in *field weakening region I* and *field weakening region II*. The steady state value of $v_{sq} - limit$ is decided by steady state angular speed of the drive.

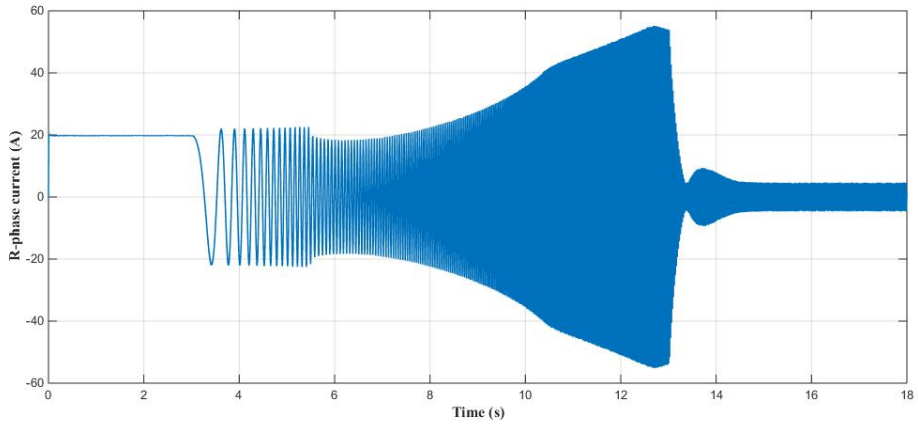

Figure 4.41: *Simulation result*: R- phase current waveform for a gradual change of speed reference (*Scale: X-axis: 2 s/div, Y-axis: 20 A/div)*

Fig. 4.41 shows the R- phase current waveform for a gradual change of speed reference. The phase current drawn is very high during the acceleration region and once the motor reaches the steady state, the current drawn will reduced to small value since the machine operates at no load.

4.1.3 Fundamental current estimation

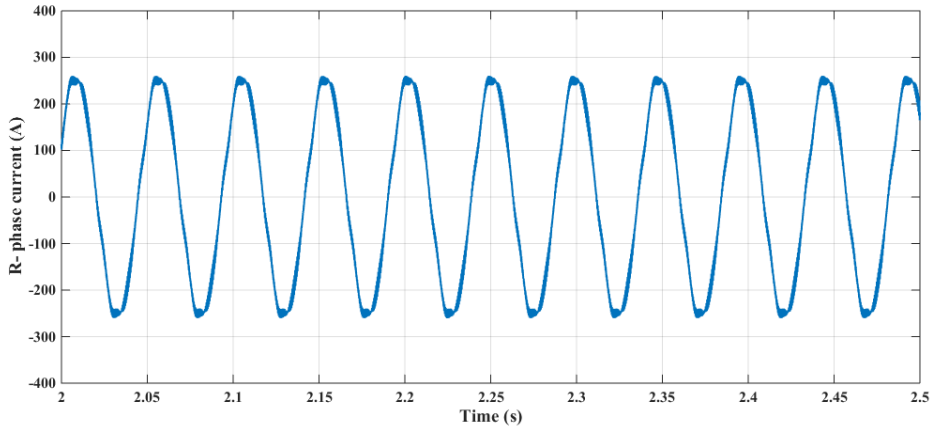

Figure 4.42: *Simulation result*: R- phase current waveform of induction machine when the inverter operates in *overmodulation zone I* (*Scale: X-axis: 0.05 s/div, Y-axis:100 A/div)*

Fig. 4.42 shows the R- phase current waveform when the inverter operates in *overmodulation zone I*. The phase current contains harmonics since the inverter operates in

overmodulation region.

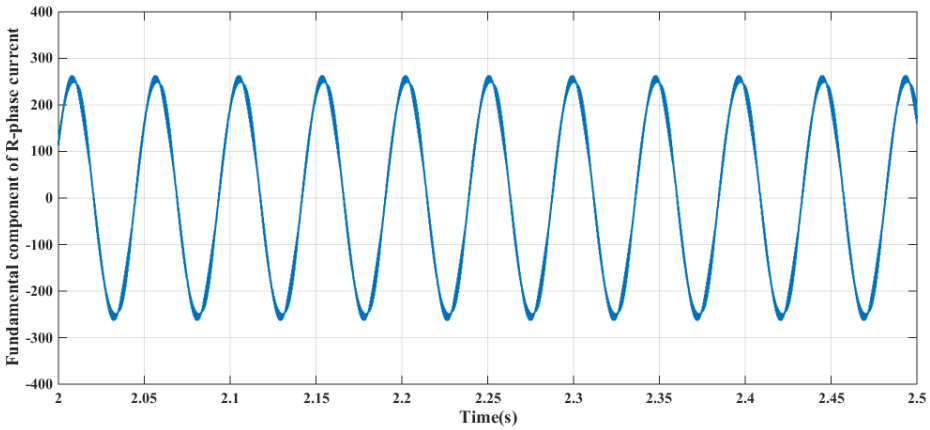

Figure 4.43: *Simulation result*: Fundamental component of R- phase current waveform when the inverter operates in *overmodulation zone I* (*Scale: X-axis: 0.05 s/div, Y-axis: 100 A/div)*

Fig. 4.43 shows the fundamental component of R- phase current when the inverter is operating in *overmodulation zone I*. The fundamental current estimation algorithm which is explained in 3^{ed} chapter is used for estimating the fundamental component of current. This current is used for obtaining the feedback values required by FOC and sensor less operation of the drive.

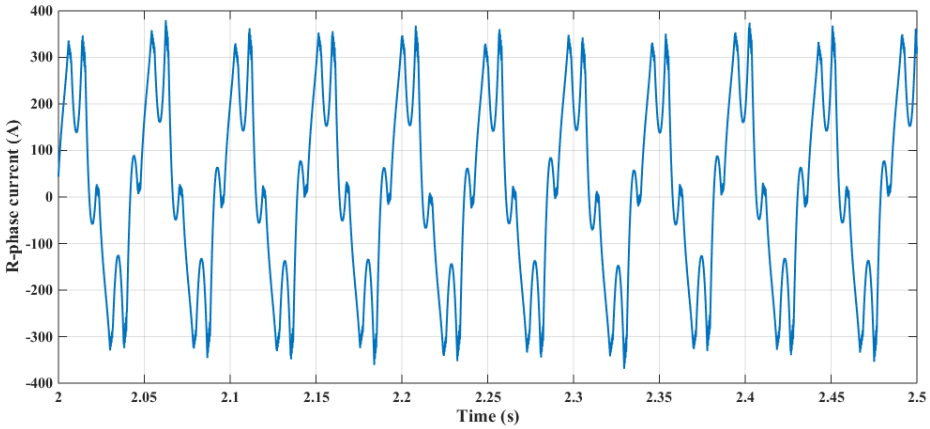

Figure 4.44: *Simulation result*: R- phase current waveform of induction machine when the inverter operates in *overmodulation zone II* (*Scale: X-axis: 0.05 s/div, Y-axis:100 A/div)*

Fig. 4.44 shows the R- phase current of induction machine when the inverter operates in *overmodulation zone II*. The harmonic content in the phase current is higher

than that of *overmodulation zone I* operation.

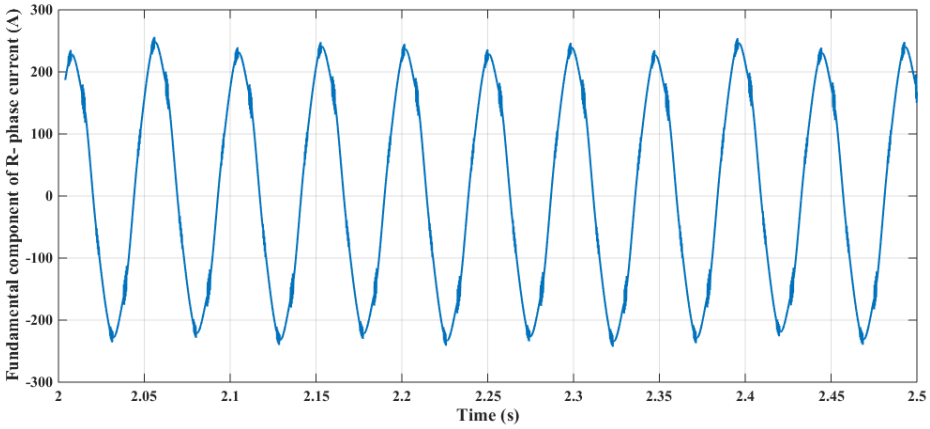

Figure 4.45: *Simulation result*: Fundamental component of R- phase current waveform of induction machine when the inverter operates in *overmodulation zone II* (*Scale: X-axis: 0.05 s/div, Y-axis: 100 A/div)*

The Fig. 4.45 shows the fundamental component of R- phase current when the inverter is operating in *overmodulation zone II*. The fundamental current estimation algorithm which is explained in 3^{ed} chapter is used for estimating the fundamental component of current. This current is used for obtaining the feedback values required by FOC and sensor less operation of the drive.

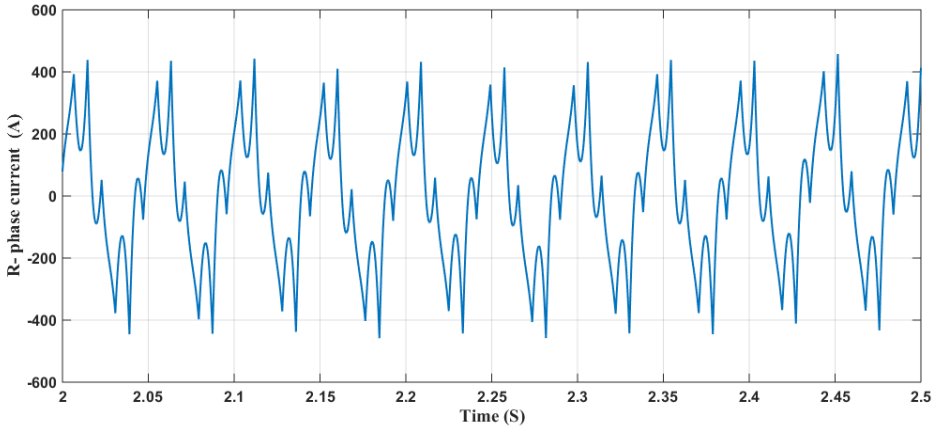

Figure 4.46: *Simulation result*: R- phase current waveform of induction machine when the inverter operates in *six step mode*.(*Scale: X-axis: 0.05 s/div, Y-axis:200 A/div)*

The Fig. 4.46 shows the R- phase current waveform of induction machine when the

inverter operates in *six step mode of operation*. The phase current contains harmonics since the inverter is operates in overmodulation region.

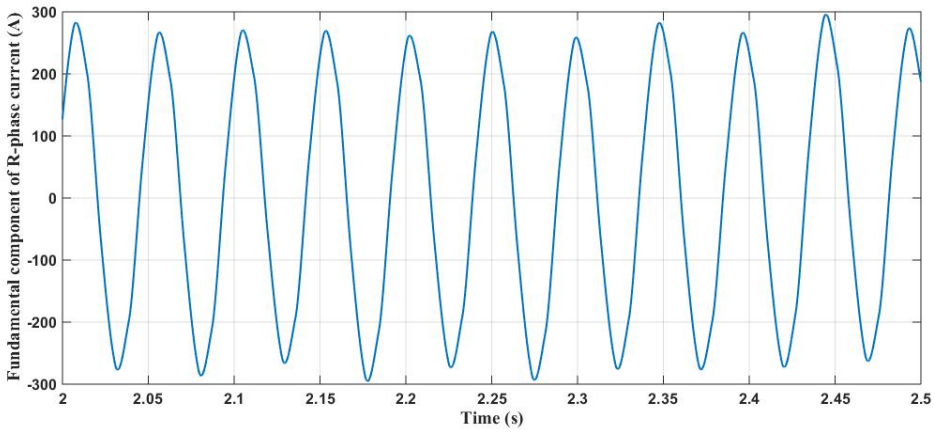

Figure 4.47: Simulation result: Fundamental component of R- phase current waveform of induction machine during *six step made* of operation.(Scale: X-axis: 0.05 s/div, Y-axis: 200 A/div)

Fig. 4.47 shows the fundamental component of R- phase current when the inverter operates in *six step mode of operation*. The fundamental current estimation algorithm which is explained in 3^{ed} chapter is used for estimating the fundamental component of current. At *six step mode* the maximum possible output fundamental voltage is obtained from a given DC-bus voltage.

4.2 Hardware Results

For studying the performance of the 30 kW laboratory model induction machine in field weakening region, the base speed ω_{base} of the machine is kept as $62.83 rad/s(elect)$ by reducing the DC-bus voltage. The transition speed between *field weakening region I* and *field weakening region II*, ω_1 is $230.57 rad/s(elect)$ at this condition.

In this project, a Per-Unit (pu) system has been followed for implementing the control algorithms experimentally. The pu system will make the digital controller implementation simple and all quantities are brought to the same range of values. The base values used for the per-unitisation of quantities are given in Table.4.5

Table 4.5: PU base quantities

Voltage(V_b)	155.13 V
Current(I_b)	50 A
Frequency(f_b)	50 Hz
Angle(θ)	2π rad

4.2.1 The step change of speed reference from below base speed region to field weakening region I (0.05 pu to 0.7 pu)

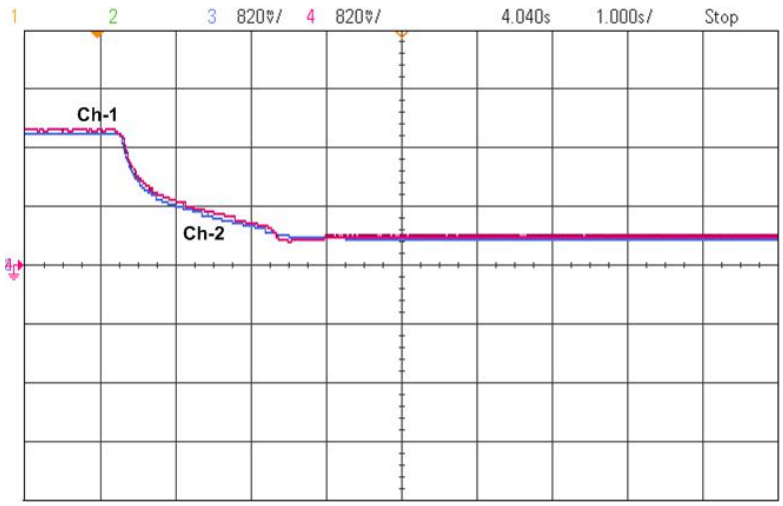

Figure 4.48: *Hardware result*: i^*_{mr} and i_{mr} waveforms for a step change of speed reference (*Ch1-* i^*_{mr}, *Ch2-* i_{mr}, *Scale: X-axis: 1 s/div, Y-axis: Ch1- 0.166 pu/div, Ch2- 0.166 pu/div)*

Fig. 4.48 shows the oscilloscope waveforms of the i_{mr}^{*} and i_{mr} for a step change of speed reference. i_{mr}^{*} and i_{mr} are at their rated values below the base speed and start reducing in *field weakening region I*. The steady state value of i_{mr} is decided by the steady state operating speed of the drive.

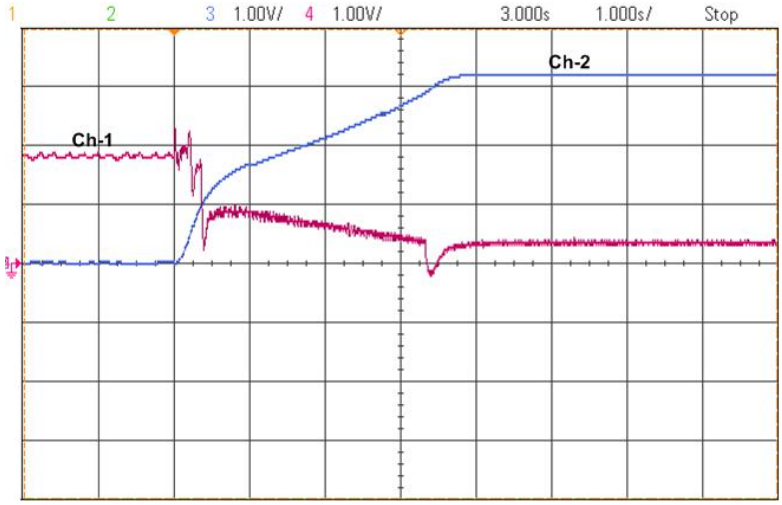

Figure 4.49: *Hardware result*: i_{sd} and ω waveforms for a step change of speed reference (*Ch1- i_{sd}, Ch2 - ω, Scale: X-axis: 1 s/div, Y-axis: Ch1- 0.2 pu/div, Ch2- 0.2 pu/div)*

Fig. 4.49 shows the oscilloscope waveforms of the i_{sd} and ω for a step change of speed reference. i_{sd} is at its rated values below the base speed and start reducing in *field weakening region I*. The steady state value of i_{sd} and i_{mr} are same.

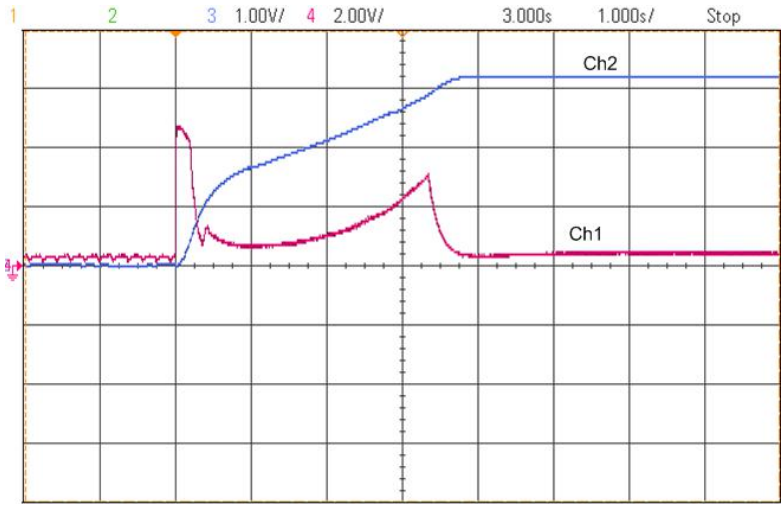

Figure 4.50: *Hardware result*: i_{sq} and ω waveforms for a step change of speed reference (*Ch1- i_{sq}, Ch2 - ω, Scale: X-axis: 1 s/div, Y-axis: Ch1- 0.4 pu/div, Ch2- 0.2 pu/div)*

Fig. 4.50 shows the oscilloscope waveforms of the i_{sq} and ω for a step change of speed reference. i_{sq} value is constant below the base speed and dynamically varying with respect to speed in *field weakening region I*. The steady state value of i_{sq} is very small since drive is operating at no load condition.

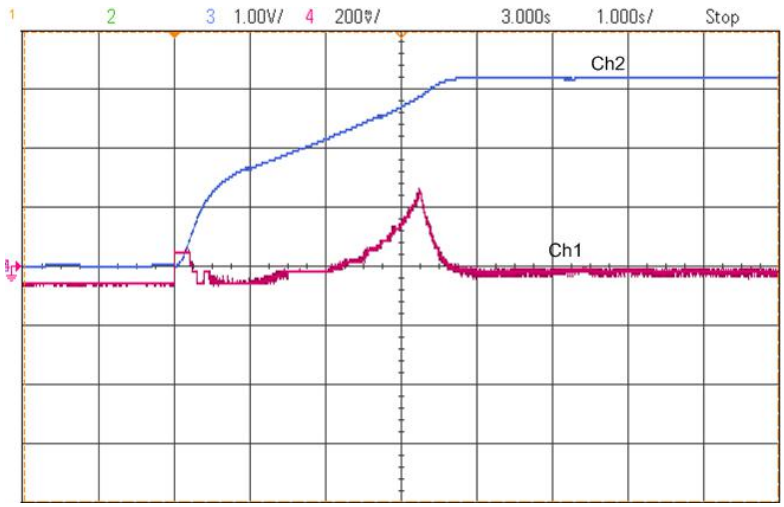

Figure 4.51: *Hardware result*: Slip speed and ω waveforms for a step change of speed reference (*Ch1*- Slip speed, *Ch2* - ω, *Scale: X-axis: 1 s/div, Y-axis: Ch1- 0.04 pu/div, Ch2- 0.2 pu/div)*

Fig. 4.51 shows the oscilloscope waveforms of the slip speed and ω for step change of speed reference. The slip speed is constant below the base speed and increases in *field weakening region I*. The steady state value of slip speed is very small since drive is working at no load condition.

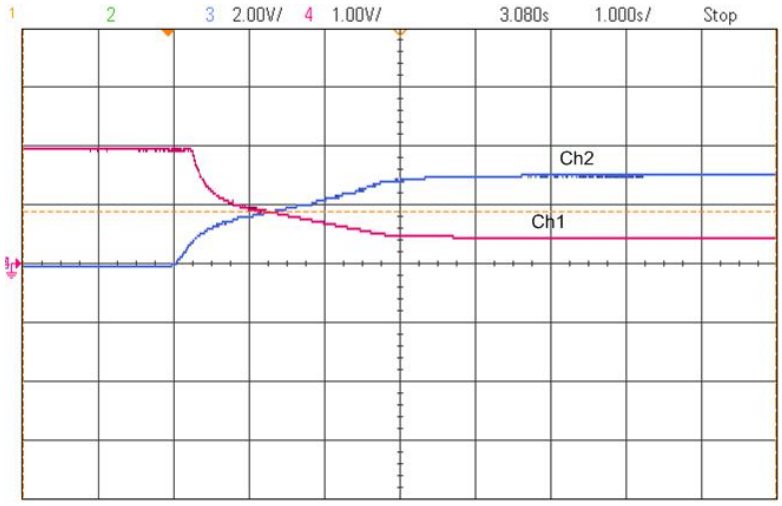

Figure 4.52: *Hardware result*: $i_{sd} - limit$ and ω waveforms for a step change of speed reference (*Ch1-* $i_{sd} - limit$, *Ch2 -* ω, *Scale: X-axis: 1 s/div, Y-axis: Ch1- 0.2 pu/div, Ch2- 0.4 pu/div)*

Fig. 4.52 shows the oscilloscope waveforms of the $i_{sd} - limit$ and ω for a step change of speed reference. The $i_{sd} - limit$ is constant below the base speed and decreases when speed increases in the *field weakening region I*. The steady state angular speed determines the steady state $i_{sd} - limit$.

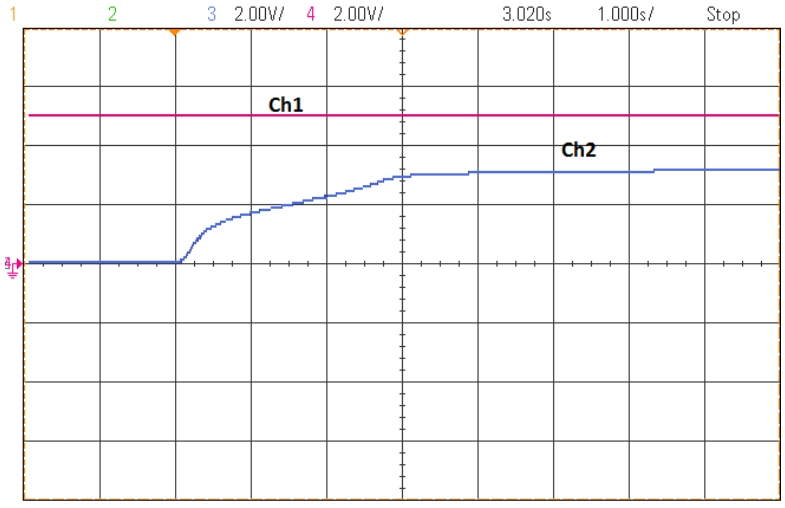

Figure 4.53: *Hardware result*: $i_{sq} - limit$ and ω waveforms for a step change of speed reference. (*Ch1-* $i_{sq} - limit$, *Ch2 -* ω, *Scale: X-axis: 1 s/div, Y-axis: Ch1- 0.4 pu/div, Ch2- 0.4 pu/div)*

Fig. 4.53 shows the oscilloscope waveforms of the $i_{sq} - limit$ and ω for a step change of speed reference. The $i_{sq} - limit$ value is almost constant below the base

speed and *field weakening region I*. The increase in $i_{sq} - limit$ is much smaller when compared to decrease in $i_{sd} - limit$ in *field weakening region I*. The steady state angular speed determines the steady state $i_{sq} - limit$.

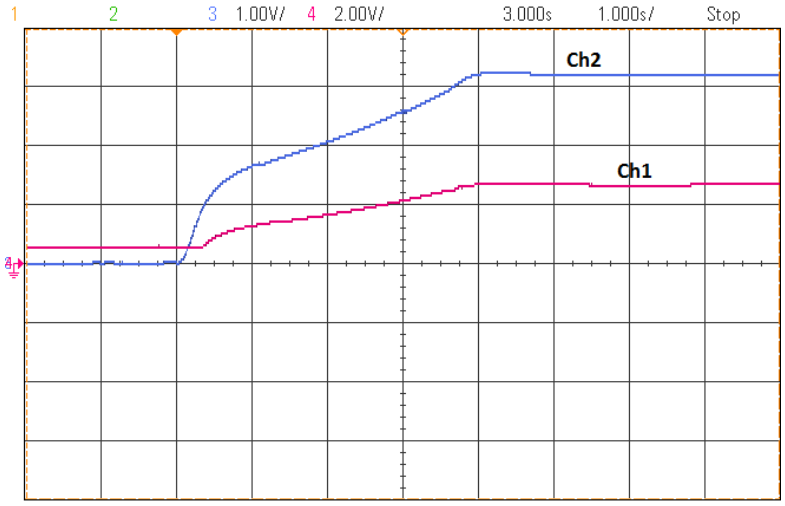

Figure 4.54: *Hardware result*: $v_{sd} - limit$ and ω waveforms for a step change of speed reference. (*Ch1-* $v_{sd} - limit$, *Ch2 -* ω, *Scale: X-axis: 1 s/div, Y-axis: Ch1- 0.4 pu/div, Ch2- 0.2 pu/div)*

Fig. 4.54 shows the oscilloscope waveforms of the $v_{sd} - limit$ and ω for a step change of speed reference. The $v_{sd} - limit$ is constant below the base speed and dynamically varies in *field weakening region I*. The steady state value of $v_{sd} - limit$ depends on steady state angular speed of the drive.

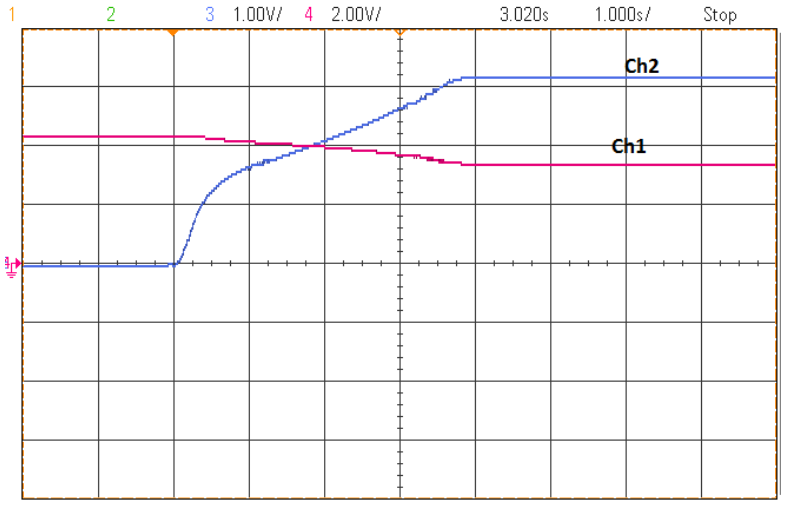

Figure 4.55: *Hardware result*: $v_{sq} - limit$ and ω waveforms for a step change of speed reference. (*Ch1-* $v_{sq} - limit$, *Ch2 -* ω, *Scale: X-axis: 1 s/div, Y-axis: Ch1- 0.4 pu/div, Ch2- 0.2 pu/div)*

Fig. 4.55 shows the oscilloscope waveforms of the $v_{sq} - limit$ and ω for a step change of speed reference. The $v_{sq} - limit$ is constant below the base speed and dynamically varies in *field weakening region I*. The steady state value of $v_{sq} - limit$ depends on steady state angular speed of the machine.

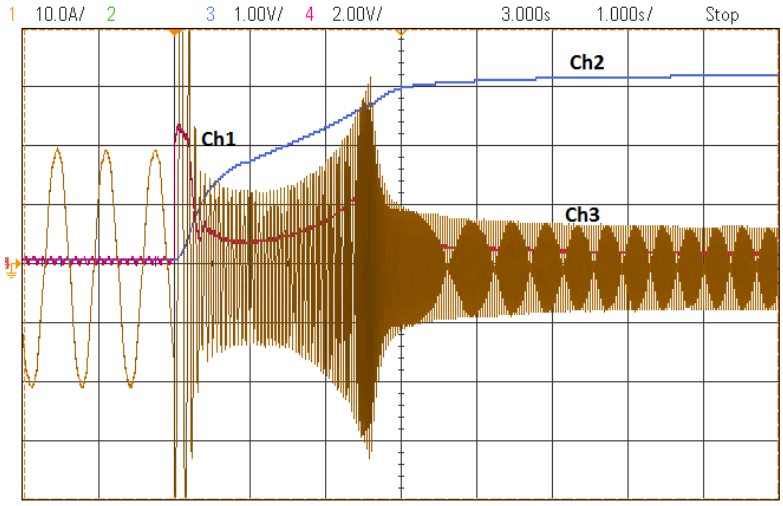

Figure 4.56: *Hardware result*: $i_{sq} - limit$, ω and phase current waveforms for a step change of speed reference. (*Ch1-* $i_{sq} - limit$, *Ch-2 -* ω, *Ch3-* phase current. *Scale: X-axis: 1 s/div, Y-axis: Ch1- 0.4 pu/div, Ch2- 0.2 pu/div, Ch3- 10A/div)*

Fig. 4.56 shows the oscilloscope waveforms of the $i_{sq} - limit$, ω and phase current for a step change of speed reference. The phase current drawn is very high during the acceleration region and once the motor reaches the steady state, the current drawn will reduced to small value since the machine operates at no load.

4.2.2 The step change of speed reference from field weakening region I to field weakening region II (0.4 pu to 0.9 pu)

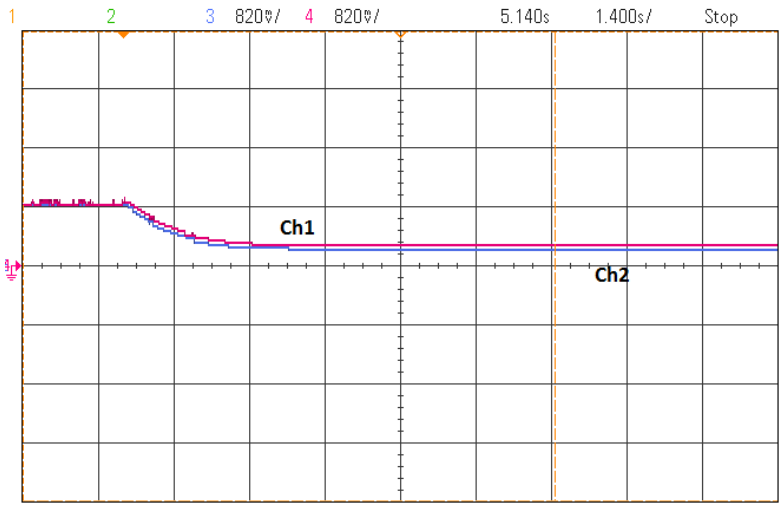

Figure 4.57: *Hardware result*: i^*_{mr} and i_{mr} waveforms for a step change of speed reference. (*Ch1-* i^*_{mr}, *Ch2-* i_{mr}, *Scale: X-axis: 1.4 s/div, Y-axis: Ch1- 0.164 pu/div, Ch2- 0.164 pu/div)*

Fig. 4.57 shows the oscilloscope waveforms of the i^*_{mr} and i_{mr} for a step change of speed reference. The i^*_{mr} and i_{mr} are decreasing in the *field weakening region I* and *field weakening region II* at different rates. The steady state value of i^*_{mr} and i_{mr} depends on steady state speed of the drive.

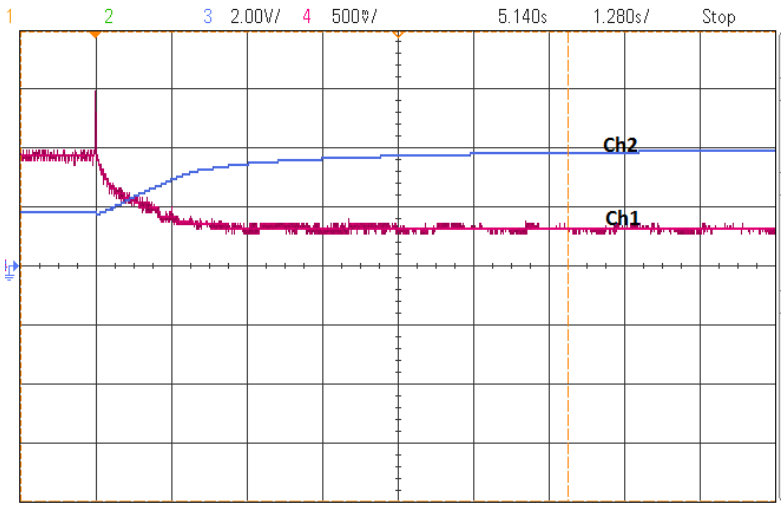

Figure 4.58: *Hardware result*: i_{sd} and ω waveforms for a step change of speed reference. (*Ch1-* i_{sd}, *Ch2 -* ω, *Scale: X-axis: 1.28 s/div, Y-axis: Ch1- 0.1 pu/div, Ch2- 0.4 pu/div)*

Fig. 4.58 shows the oscilloscope waveforms of the i_{sd} and ω for a step change of speed reference. The i_{sd} value is reducing in *field weakening region I* and *field weakening region II*. The steady state values of i_{sd} and i_{mr} are same.

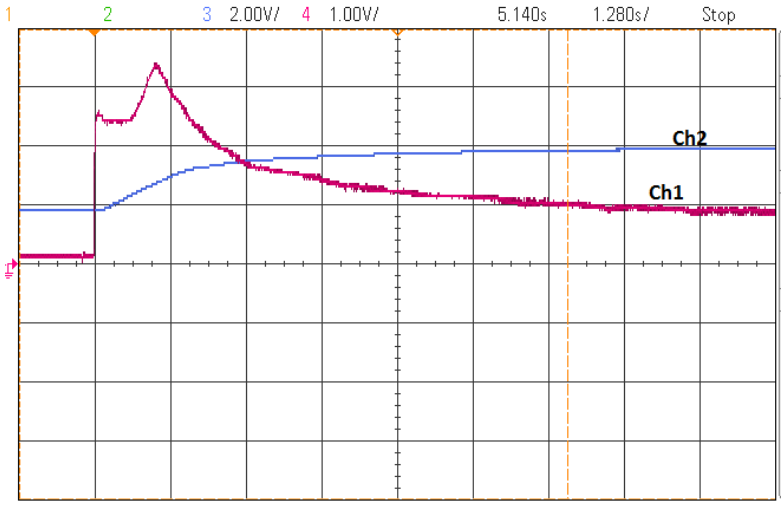

Figure 4.59: *Hardware result*: i_{sq} and ω waveforms for a step change of speed reference. (*Ch1-* i_{sq}, *Ch2 -* ω, *Scale: X-axis: 1.280 s/div, Y-axis: Ch1- 0.2 pu/div, Ch2- 0.4 pu/div)*

Fig. 4.59 shows the oscilloscope waveforms of the i_{sq} and ω for a step change of speed reference. The i_{sq} value is high during the acceleration region and once the motor reaches the steady state, it reduces to a small value since drive is operating at no load condition..

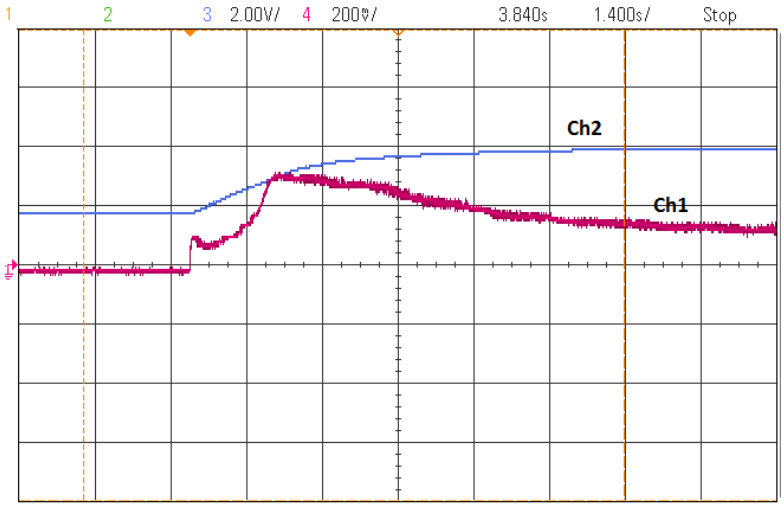

Figure 4.60: *Hardware result*: Slip speed and ω waveforms for a step change of speed reference. (*Ch1-* Slip speed, *Ch2 -* ω, *Scale: X-axis: 1.4 s/div, Y-axis: Ch1- 0.04 pu/div, Ch2- 0.4 pu/div)*

Fig. 4.60 shows the oscilloscope waveforms of the slip speed and ω for a step change of speed reference. The slip speed of the machine increases in *field weakening region I* and reaches its maximum possible value at boundary between *field weakening region I* and *field weakening region II* and remain at that value in *field weakening region II*. The steady state value of slip speed is determined by how much load is applied to the machine.

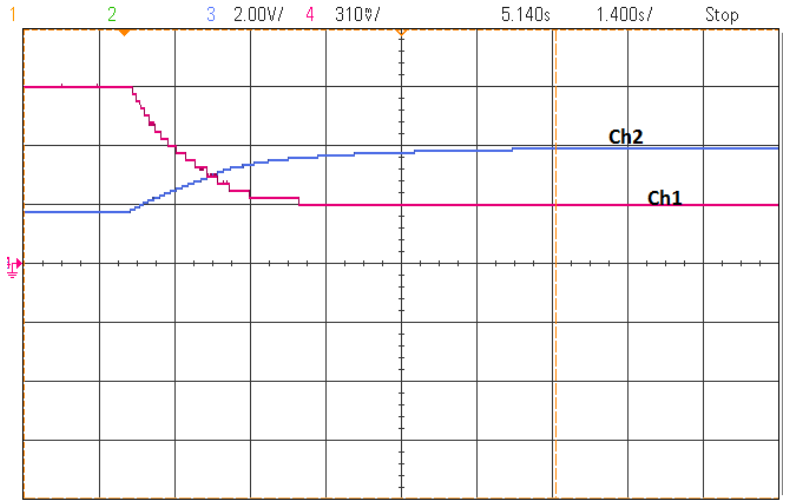

Figure 4.61: *Hardware result*: $i_{sd} - limit$ and ω waveforms for a step change of speed reference (*Ch1-* $i_{sd} - limit$, *Ch2 -* ω, *Scale: X-axis: 1.4 s/div, Y-axis: Ch1- 0.04 pu/div, Ch2- 0.4 pu/div)*

Fig. 4.61 shows the oscilloscope waveforms of the $i_{sd} - limit$ and ω for a step change of speed reference. The $i_{sd} - limit$ is reducing in both *field weakening region I* and *field weakening region II*. The steady state value of $i_{sd} - limit$ depends on angular speed of the drive.

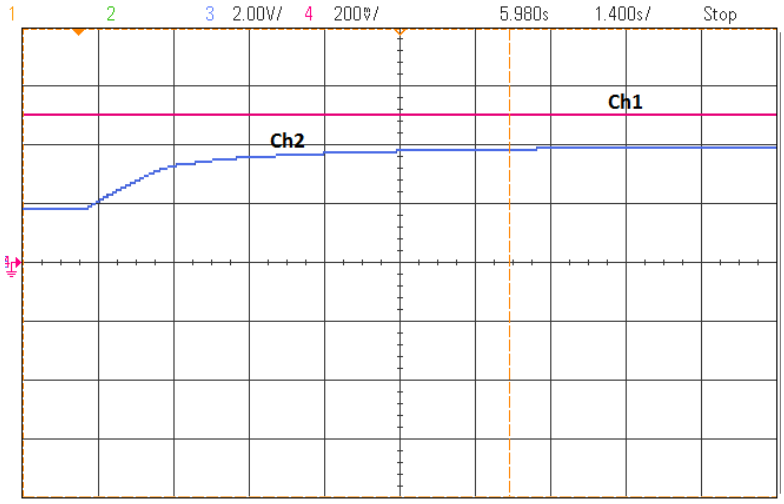

Figure 4.62: *Hardware result*: $i_{sq} - limit$ and ω waveforms for a step change of speed reference (*Ch1-* $i_{sq} - limit$, *Ch2 -* ω, *Scale: X-axis: 1.4 s/div, Y-axis: Ch1- 0.04 pu/div, Ch2- 0.4 pu/div)*

Fig. 4.62 shows the oscilloscope waveforms of the $i_{sq} - limit$ and ω for a step change of speed reference. The variation in $i_{sq} - limit$ is very small compared with the variation in $i_{sd} - limit$ with respect to speed.

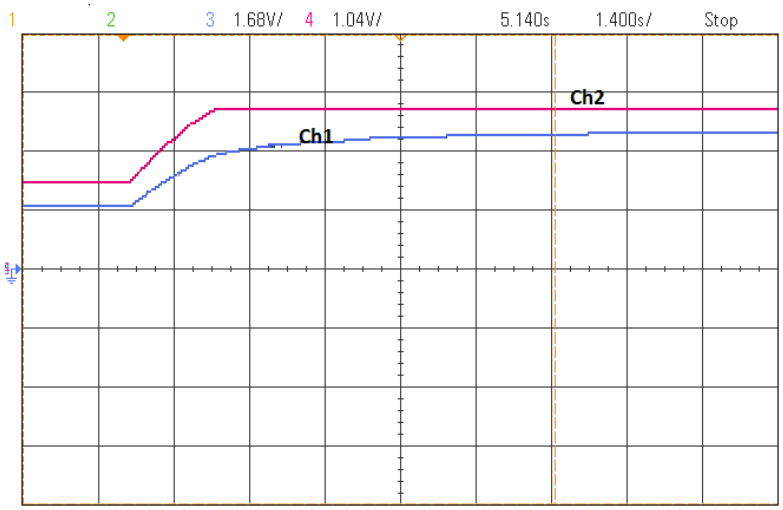

Figure 4.63: *Hardware result*: $v_{sd} - limit$ and ω waveforms for a step change of speed reference (*Ch1-* $v_{sd} - limit$, *Ch2 -* ω, *Scale: X-axis: 1.4 s/div, Y-axis: Ch1- 0.208 pu/div, Ch2- 0.336 pu/div)*

Fig. 4.63 shows the oscilloscope waveforms of the $v_{sd} - limit$ and ω for a step change of speed reference. The $v_{sd} - limit$ dynamically varies in *field weakening region I* and *field weakening region II*. The steady state value of $v_{sd} - limit$ is decided by steady

state angular speed of the drive.

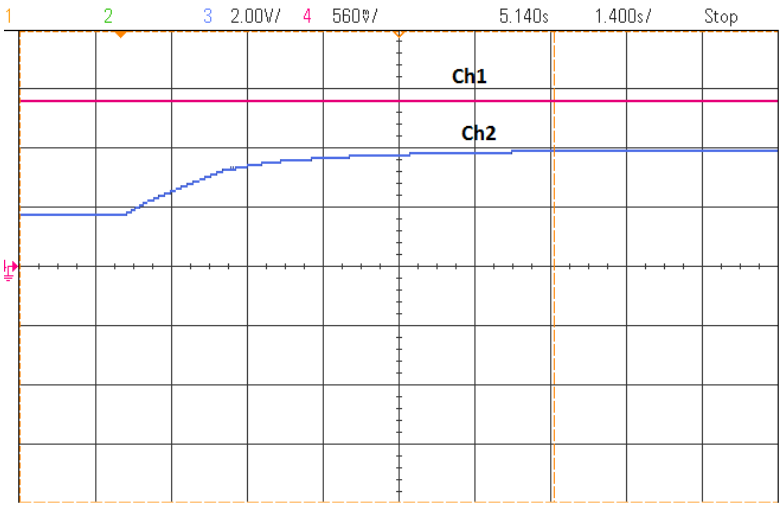

Figure 4.64: *Hardware result*: $v_{sq} - limit$ and ω waveforms for a step change of speed reference. (*Ch1-* $v_{sd} - limit$, *Ch2 -* ω, *Scale: X-axis: 1.4 s/div, Y-axis: Ch1- 0.112 pu/div, Ch2- 0.4 pu/div)*

Fig. 4.64 shows the oscilloscope waveforms of the $v_{sq} - limit$ and ω for a step change of speed reference. The Variation in $v_{sq} - limit$ is very small in *field weakening region I* and *field weakening region II*.

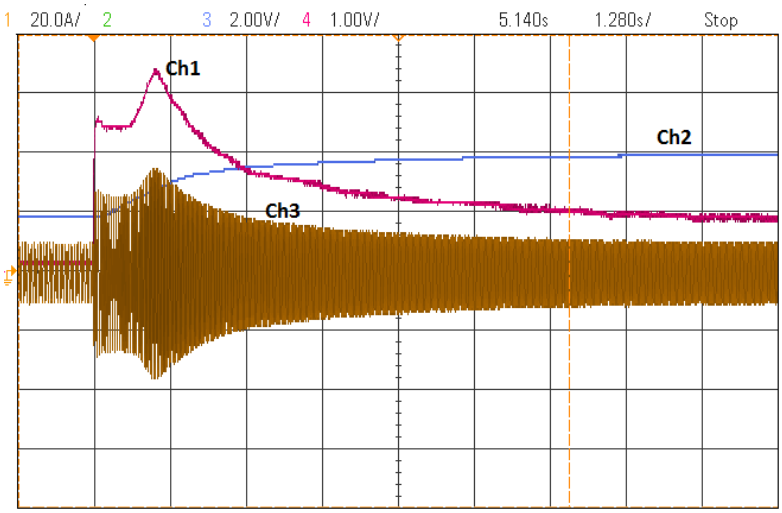

Figure 4.65: *Hardware result*: $i_{sq} - limit$, ω and phase current waveforms for a step change of speed reference. (*Ch1-* $i_{sq} - limit$, *Ch-2 -* ω, *Ch3-* phase current. *Scale: X-axis: 1.280 s/div, Y-axis: Ch1- 0.2/div, Ch2- 0.4 pu/div, Ch3- 20A/div)*

Fig. 4.65 shows the oscilloscope waveforms of the $i_{sq} - limit$, ω and phase current

for a step change of speed reference. The phase current drawn is very high during the acceleration region and once the motor reaches the steady state, the current drawn will reduced to small value since the machine operates at no load.

4.2.3 Gradual change of speed reference from zero to 0.953 pu

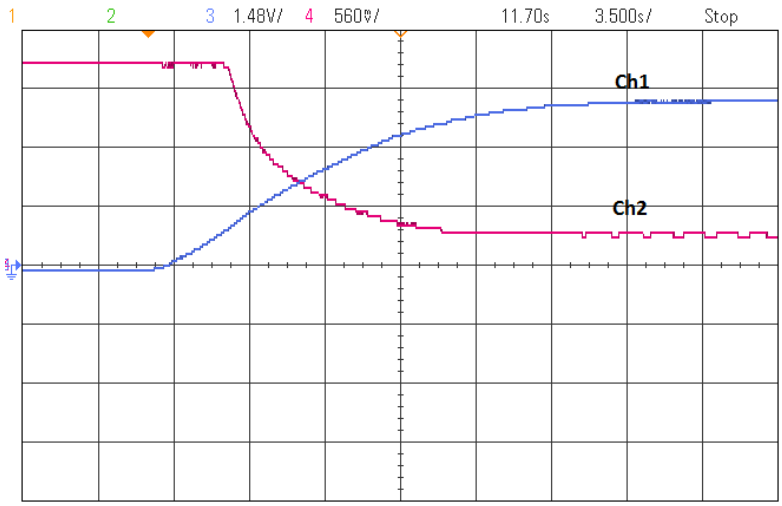

Figure 4.66: *Hardware result*: i_{mr} and ω waveforms for a gradual change of speed reference from zero to 0.953 pu . (*Ch1-* i_{mr}, *Ch2-* ω, *Scale: X-axis: 3.5 s/div, Y-axis: Ch1- .112 pu/div, Ch2- 0.296 pu/div)*

Fig. 4.66 shows the oscilloscope waveforms of the i_{mr} and ω for a gradual change of speed reference from zero to 0.953 pu. The i_{mr} is at rated value below the base speed and starts reducing in *field weakening region I* and *field weakening region II* at different rates. The steady state value of i_{mr} is decided by the steady state angular speed of the drive.

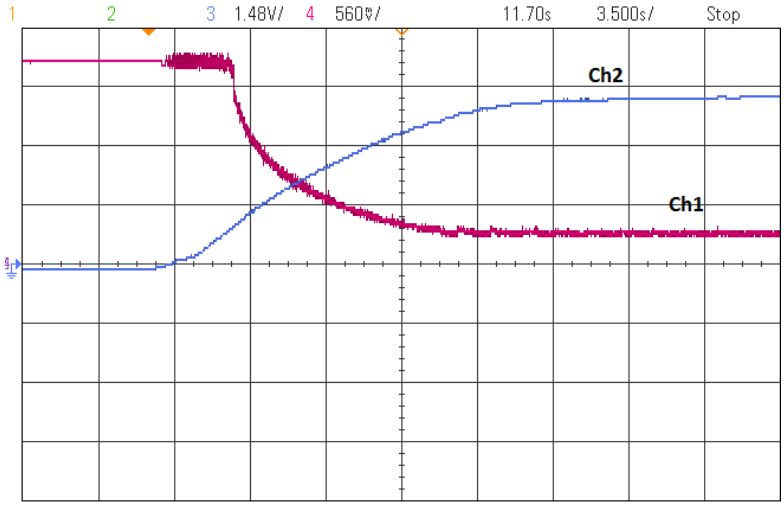

Figure 4.67: *Hardware result*: i_{sd} and ω waveforms for a gradual change of speed reference from zero to 0.953 pu. (*Ch1- i_{sd}, Ch2 - ω, Scale: X-axis: 3.5 s/div, Y-axis: Ch1- .112 pu/div, Ch2- 0.296 pu/div)*

Fig. 4.67 shows the oscilloscope waveforms of the i_{sd} and ω for a gradual change of speed reference from zero to 0.953 pu. The i_{sd} is constant below the base speed and decreases in the *field weakening region I* and *field weakening region II* at different rates. At steady state, i_{sd} and i_{mr} are equal.

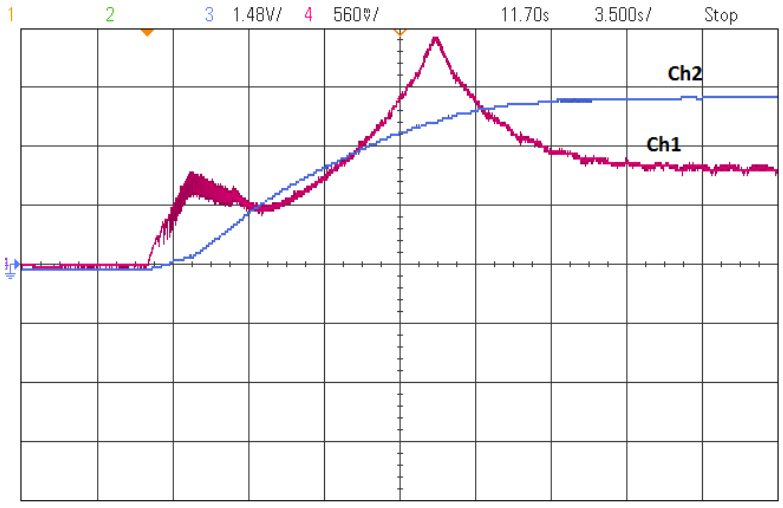

Figure 4.68: *Hardware result*: i_{sq} and ω waveforms for a gradual change of speed reference from zero to 0.953 pu. (*Ch1- i_{sq}, Ch2 - ω, Scale: X-axis: 3.5 s/div, Y-axis: Ch1- .112 pu/div, Ch2- 0.296 pu/div)*

Fig. 4.68 shows the oscilloscope waveforms of the i_{sq} and ω for a gradual change of speed reference from zero to 0.953 pu. The value of i_{sq} is high during acceleration

and it settled to a small value since the machine operates at no load.

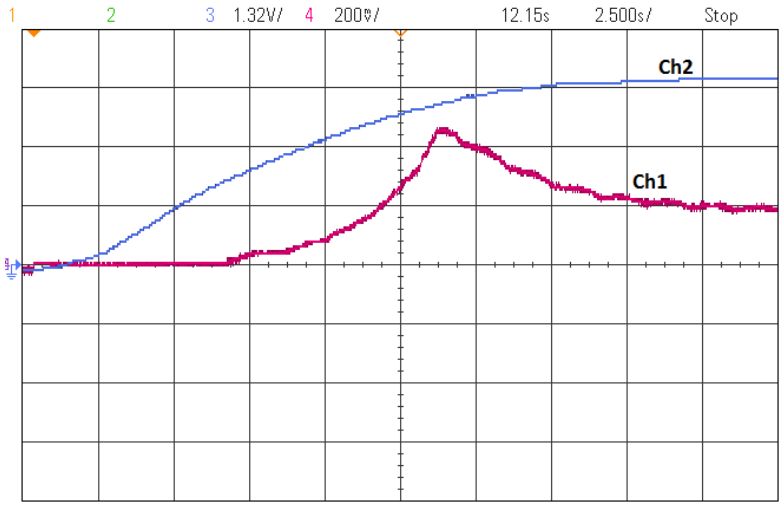

Figure 4.69: *Hardware result*: Slip speed and ω waveforms when a gradual change of speed reference from zero to 0.953 pu. (*Ch1*- Slip speed, *Ch2* - ω, *Scale: X-axis: 2.5 s/div, Y-axis: Ch1- 0.04 pu/div, Ch2- 0.264 pu/div)*

Fig. 4.69 shows the oscilloscope waveforms of the slip speed and ω for a gradual change of speed reference from zero to 0.953 pu. Slip speed of the machine is constant in below base speed region and increases in *field weakening region I* due to dynamic nature of controller limits and $i_{mr} - reference$ in this region. At the transition speed, ω_1 the slip speed become maximum and maintain that value in *field weakening region II*. When the speed of the machine is settled to the reference speed, the slip speed of the machine is reduces to a small value, since i_{sq} is very small in no load condition.

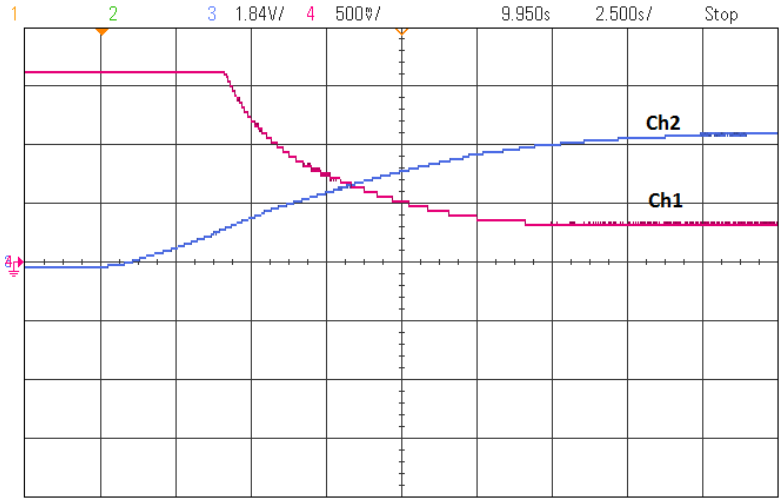

Figure 4.70: *Hardware result*: $i_{sd} - limit$ and ω waveforms for a gradual change of speed reference from zero to 0.953 pu (*Ch1-* $i_{sd} - limit$, *Ch2 -* ω, *Scale: X-axis: 2.5 s/div, Y-axis: Ch1- 0.368 pu/div, Ch2- 0.1 pu/div)*

Fig. 4.70 shows the oscilloscope waveforms of the $i_{sd} - limit$ and ω for a gradual change of speed reference from zero to 0.953 pu. The $i_{sd} - limit$ is constant below the base speed and decreases with speed in *field weakening region I* and *field weakening region II* at different rate.

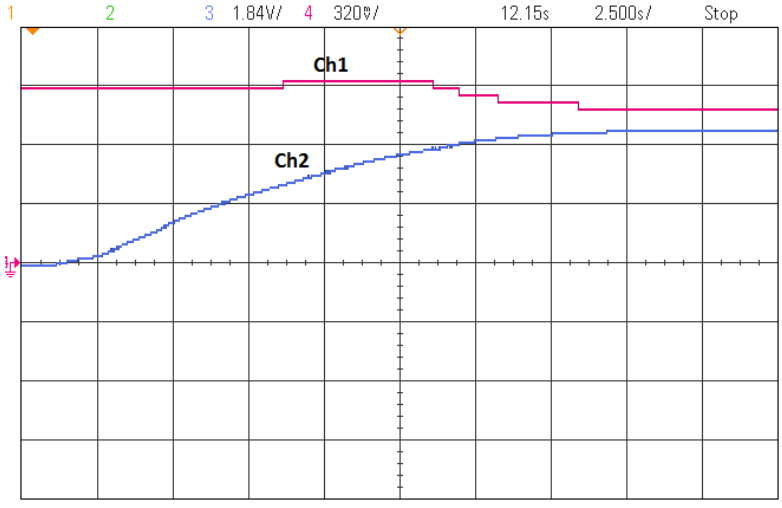

Figure 4.71: *Hardware result*: $i_{sq} - limit$ and ω waveforms for a gradual change of speed reference from zero to 0.953 pu (*Ch1-* $i_{sq} - limit$, *Ch2 -* ω, *Scale: X-axis: 2.5 s/div, Y-axis: Ch1- 0.368 pu/div, Ch2- 0.062 pu/div)*

Fig. 4.71 shows the oscilloscope waveforms of the $i_{sq} - limit$ and ω for a gradual change of speed reference from zero to 0.953 pu. The $i_{sq} - limit$ is constant below the

base speed, increases slightly in the *field weakening region I* and decreases in the *field weakening region II*.

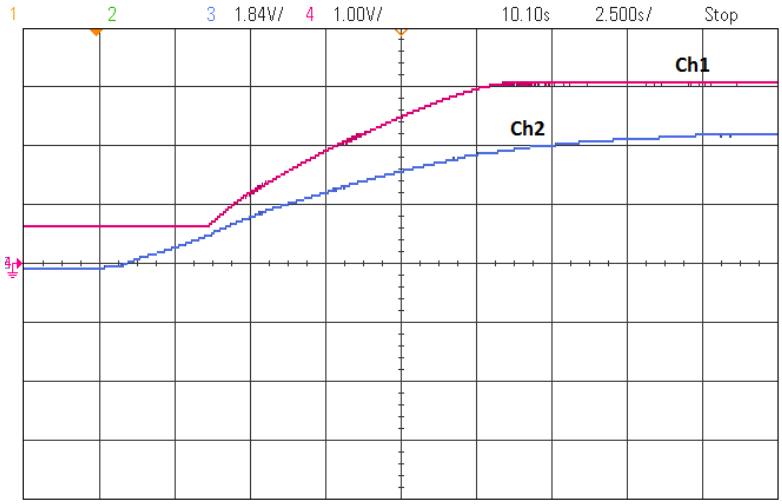

Figure 4.72: *Hardware result*: $v_{sd} - limit$ and ω waveforms for a gradual change of speed reference from zero to 0.953 pu (*Ch1-* $v_{sd} - limit$, *Ch2 -* ω, *Scale: X-axis: 2.5 s/div, Y-axis: Ch1- 0.368 pu/div, Ch2- 0.2 pu/div)*

Fig. 4.72 shows the oscilloscope waveforms of the $v_{sd} - limit$ and ω for a gradual change of speed reference from zero to 0.953 pu. The $v_{sd} - limit$ is constant below the base speed and dynamically varies in field weakening regions. The steady state value of $v_{sd} - limit$ is determined by steady state angular speed of the drive.

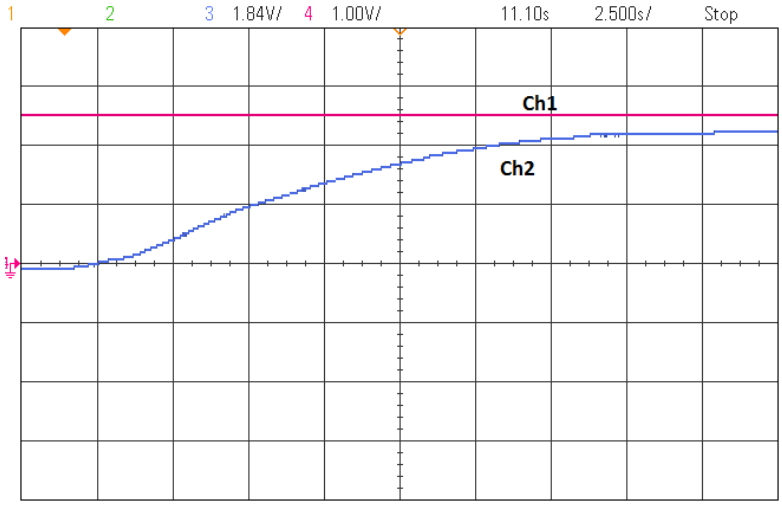

Figure 4.73: *Hardware result*: $v_{sq} - limit$ and ω waveforms for a gradual change of speed reference from zero to 0.953 pu (*Ch1-* $v_{sq} - limit$, *Ch2 -* ω, *Scale: X-axis: 2.5 s/div, Y-axis: Ch1- 0.368 pu/div, Ch2- 0.2 pu/div)*

Fig. 4.73 shows the oscilloscope waveforms of the $v_{sq} - limit$ and ω for a gradual change of speed reference from zero to 0.953 pu. The $v_{sq} - limit$ is constant below the base speed. The variation of $v_{sq} - limit$ is very small in field weakening regions.

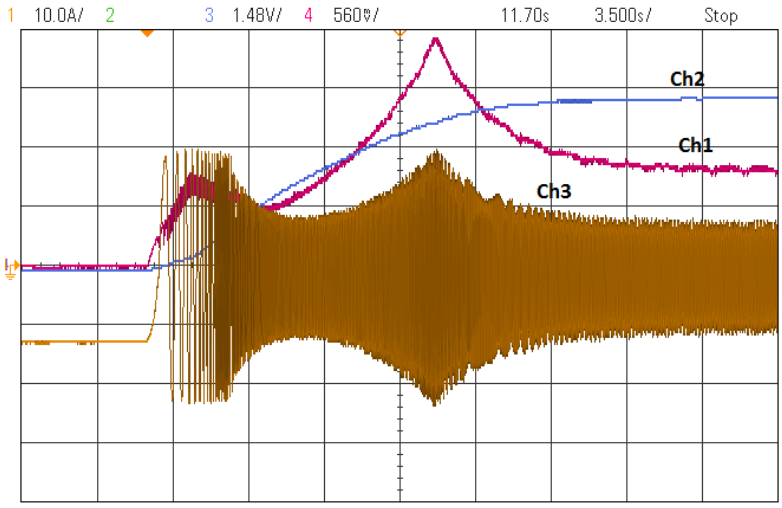

Figure 4.74: *Hardware result*: $i_{sq} - limit$, ω and phase current waveforms for a gradual change of speed reference from zero to 0.953 pu. (*Ch1-* $i_{sq} - limit$, *Ch-2 -* ω, *Ch3-* phase current. *Scale: X-axis: 3.5 s/div, Y-axis: Ch1- 0.1192 pu/div, Ch2- 0.296 V/div, Ch3- 10A/div)*

Fig. 4.74 shows the oscilloscope waveforms of the $i_{sq} - limit$, ω and phase current for a gradual change of speed reference from zero to 0.953 pu. The phase current drawn is very high during the acceleration region and once the motor reaches the steady state, the current drawn will reduced to small value since the machine operates at no load.

4.3 Conclusion

The simulated waveform results of field weakening method for 630 kW and 30 kW FOC based induction machine drive and the experimental results from the actual implementation on the 30 kW motor were presented in this chapter. The experimental results are in close agreement with 30 kW induction machine's simulated results, thus validating the control strategy. The fundamental current estimation of a 630 kW induction machine is presented in this chapter. The harmonic content in estimated fundamental component of current is very less which validates the algorithm of fundamental current estimation.

CHAPTER 5

CONCLUSION

5.1 Summary of the Present Work

The FOC based field weakening scheme was successfully implemented in a 30 KW induction machine. The performance of the drive in the above base speed regions was evaluated up to 5 times the base speed at no load, and satisfactory results were obtained. The transition between the below base speed region and the *field weakening region I* (at ω_{base}), *field weakening region I* and *field weakening region II* (at ω_1) occurred in a smooth manner. Variation of controller limits and flux reference in the field weakening regions were observed as expected. Simulation of field weakening algorithm and overmodulation scheme of the inverter was done with 630 KW induction machine and 30 KW induction machine. All the test cases taken for the simulation of 30 KW machine were verified experimentally in the 30 KW laboratory model machine. The fundamental current estimation algorithm was simulated on a 630 KW induction machine and the results were satisfactory. The hardware implementation of overmodulation scheme of the inverter and the fundamental current estimation algorithm were not done owing to time constraints.

5.2 Future Scope of Work

In this project the performance of the drive in field weakening region was analysed in no load condition only. The load performance of the drive in field weakening region can be analysed in future. The overmodulation operation of the inverter at high speed regions of the drive can be implemented in hardware for maximum dc-bus utilisation. An FPGA based system can be used for implementing the fundamental current estimation algorithm for faster response. The stability of the drive can be improved by online adaptation of sensorless control parameters at higher speed of operation.

REFERENCES

[1] S. H. Kim, S. K. Sul, and M. H. Park, "Maximum torque control of an induction machine in the field weakening region," in *Conference Record of the 1993 IEEE Industry Applications Conference Twenty-Eighth IAS Annual Meeting*, Oct 1993, pp. 401–407 vol.1.

[2] S. Venugopal and G. Narayanan, "An overmodulation scheme for vector controlled induction motor drives," in *2006 International Conference on Power Electronic, Drives and Energy Systems*, Dec 2006, pp. 1–6.

[3] K. D. Hurst, T. G. Habetler, G. Griva, and F. Profumo, "Zero-speed tacholess im torque control: simply a matter of stator voltage integration," *IEEE Transactions on Industry Applications*, vol. 34, no. 4, pp. 790–795, Jul 1998.

[4] J. Holtz, W. Lotzkat, and A. Khambadkone, "On continuous control of pwm inverters in the overmodulation range including the six-step mode," in *Proceedings of the 1992 International Conference on Industrial Electronics, Control, Instrumentation, and Automation*, Nov 1992, pp. 307–312 vol.1.

[5] T. Bhattacharya and L. Umanand, "Improved flux estimation and stator-resistance adaptation scheme for sensorless control of induction motor," *IEE Proceedings - Electric Power Applications*, vol. 153, no. 6, pp. 911–920, November 2006.

[6] S. K. Sahoo and T. Bhattacharya, "Field weakening strategy for a vector-controlled induction motor drive near the six-step mode of operation," *IEEE Transactions on Power Electronics*, vol. 31, no. 4, pp. 3043–3051, April 2016.

[7] P. Y. Lin and Y. S. Lai, "Novel voltage trajectory control for field-weakening operation of induction motor drives," *IEEE Transactions on Industry Applications*, vol. 47, no. 1, pp. 122–127, Jan 2011.

[8] W. Qingyi, L. Yang, and L. Hui, "Optimal flux selection of induction machine in the field-weakening region," in *2012 Asia-Pacific Power and Energy Engineering Conference*, March 2012, pp. 1–5.

[9] L. Zarri, M. Mengoni, A. Tani, G. Serra, D. Casadei, and J. O. Ojo, "Control schemes for field weakening of induction machines: A review," in *2015 IEEE Workshop on Electrical Machines Design, Control and Diagnosis (WEMDCD)*, March 2015, pp. 146–155.

[10] G. Gallegos-Lopez, F. S. Gunawan, and J. E. Walters, "Current control of induction machines in the field-weakened region," *IEEE Transactions on Industry Applications*, vol. 43, no. 4, pp. 981–989, July 2007.

[11] Z. Peroutka and K. Zeman, "Robust field weakening algorithm for vector-controlled induction machine traction drives," in *IECON 2006 - 32nd Annual Conference on IEEE Industrial Electronics*, Nov 2006, pp. 856–861.

[12] H. Mahlfeld, T. Schuhmann, R. DÃűbler, and B. Cebulski, “Impact of overmodulation methods on inverter and machine losses in voltage-fed induction motor drives,” in *2016 XXII International Conference on Electrical Machines (ICEM)*, Sept 2016, pp. 1064–1070.

[13] T. H. Nguyen and D. C. Lee, “Improvement of current control in overmodulation range for vector-controlled induction machine drives,” in *8th International Conference on Power Electronics - ECCE Asia*, May 2011, pp. 421–426.

[14] R. Kumar and S. Das, “A modified approach to both conventional and ann based svpwm controllers for voltage fed inverter in sensorless vector control im drive,” in *2014 IEEE International Conference on Power Electronics, Drives and Energy Systems (PEDES)*, Dec 2014, pp. 1–6.

[15] Texas Instruments. TMS320x2833x, 2823x Enhanced Pulse Width Modulator (ePWM) Module. *Texas Instruments Reference Guide, Literature Number:SPRUG04A*, Oct 2008.

[16] Texas Instruments. TMS320x2833x, 2823x System Control and Interrupts. *Texas Instruments Application Note, Literature Number:SPRUFB0D*, Mar 2010.

[17] Lori Heustess, Texas Instruments. Programming TMS320x28xx and 28xx Peripherals in C/C++. *Texas Instruments Application Note, Literature Number:SPRAA85D*, Jan 2013.

[18] Texas Instruments. TMS320F2833x ADC Module. *Texas Instruments Reference Guide, Literature Number:SPRU812A*, Oct 2007.

[19] Pradeep Shinde, Texas Instruments. Designing analog interface with TMS320F28xx/28xxx DSCs. *Texas Instruments Application Note, Literature Number:SPRAAP6A*, May 2008.

[20] Texas Instruments. TMS320x2833x, 2823x Enhanced Capture(eCAP) Module. *Texas Instruments Reference Guide, Literature Number:SPRUFG4A*, Jun 2009.